Ex-ante viability of wonder nanomaterials from waste CO_2

An ex-ante techno-economic and environmental assessment of CO_2 based carbon nanomaterial production and comparison with status quo

MSc Industrial Ecology

Nikhil Reddy Kunati

Leiden University | Delft University of Technology

TU Delft

Universiteit Leiden
The Netherlands

Ex-ante viability of wonder nanomaterials from waste CO_2

An ex-ante techno-economic and environmental assessment of CO_2 based carbon nanomaterial production and comparison with status quo

by

Nikhil Reddy Kunati

to obtain the degree of Master of Science
in Industrial Ecology
at Delft University of Technology and Leiden University,
to be defended publicly on August 16th, 2023

Student number:	3202712 (Leiden) 5662958 (Delft)	
Project duration:	Feb 22, 2023 – August 16, 2023	
Thesis committee:	Dr. Paola Ibarra Gonzalez	TU Delft, First supnervisor
	Dr. Ruud Kortlever	TU Delft, Second supervisor
	Dr. Earl Goetheer	TU Delft, Third supervisor

Cover Image: Photo by Maren Piwnicki.

An electronic version of this thesis is available at http://repository.tudelft.nl/.
Supplementary data files can be found at https:
//drive.google.com/drive/folders/1SMQeQ7t-LTmpRzafImeQ5o6cBtVwEQxW?usp=drive_link

TU Delft

Universiteit Leiden
The Netherlands

Preface

I would like to express my sincere gratitude to my first supervisor Dr. Paola Ibarra Gonzalez. She helped me gain confidence with modelling on Aspen and encouraged me to take up this thesis despite having a non-chemical engineering background. I am very thankful for the kindness and patience she showed me throughout my thesis.

I gratefully acknowledge my second supervisor Dr. Ruud Kortlever for his guidance and expertise in my pursuit of modelling the electrochemical process with limited data. I am thankful for his genuine interest in my thesis and for being accommodating to my requests.

I am deeply grateful to my third supervisor Prof. Earl Goetheer, for providing all the support he could to help with my thesis struggles. I admire his drive to pursue challenging things and am thankful for his enthusiasm for my thesis topic.

I would also like to acknowledge the support provided by my unofficial PhD supervisor James Tonny Manalal, for sharing his expertise on solving Aspen modelling issues. I am also thankful for PhD student Josephine Vos's support in helping me with my thesis.

I would like to extend my gratitude to my parents and my sister for supporting me throughout this master's with all their care and affection. I am grateful for all the support and memorable moments I had with the friends I made throughout this master's, especially Parth, Varsha and Varun for sticking close to me.

Lastly, I would like to express my special gratitude to my life coach - Shivdasini, my girlfriend - Akhila and my best friend - Ashish for their support and affection throughout my master's.

Summary

The primary objective of this study was to address the lack of understanding of the commercial-scale implementation of novel CO_2 based carbon nanomaterial (CNM) production and its comparison with status quo CNM production processes using unsustainable fossil resources. To accomplish this objective, first, a literature review was performed on the status quo commercial-scale CNM production, the lab-scale CO_2 based processes and the CNM market. In regards to the status quo processes, the literature review yielded mainly chemical vapor deposition(CVD) processes of carbon nanotubes (CNTs) and graphene production. With respect to the lab scale CO_2 based processes, the literature review involved categorising the identified processes into four different approaches based on their working principles - CO_2 based CVD, molten salt based electrochemical CO_2 reduction, liquid metal catalyst aided CO_2 reduction and metal reductant enabled CO_2 reduction. With regards to the CNM market, CNT materials were found to have the highest market share followed by that of graphene. Startup spinoffs working on the graphene and CNT production from CO_2 were identified with origins to university-based research groups.

Following such literature review, a framework was developed to select one process each from the status quo CVD processes and the novel CO_2 based processes, which produced comparable CNM. This framework was applied to the processes obtained from the literature review, which led to the selection of a methane-based CVD process and a molten salt-based electrochemical CO_2 reduction process for small-diameter multi-walled (MW) CNT production. The methane-based CVD process involved the use of Ni-Mo catalyst on MgO support and high-temperature operating condition of 975°C. The molten salt-based electrochemical CO_2 reduction process involved the use of Ni and steel electrodes, pure molten Li_2CO_3 electrolyte and high-temperature operating condition of 750°C. These selected processes were designed and simulated in Aspen Plus at a commercial-scale production level of 5000 tonnes per operating year. The mass balance, energy balance, and equipment cost data obtained from the simulations were used to assess the technical, economic, and environmental performance of the ex-ante CO_2 based production process and the status quo CVD production process.

The technical performance assessment involved the estimation of resource intensity and energy efficiency indicators of the two processes, wherein the CVD process outperformed the electrochemical process in both indicators. The economic performance assessment involved the estimation of total capital investment, operational expenditure, net present value, and payback period. The CVD process performed better than the electrochemical process in all the indicators except total capital investment. Both processes indicated positive net present values and short payback periods, indicating the realisation of commercial scale plants of both processes to be profitable. The environmental performance assessment was carried out using the life cycle assessment methodology in the CMLCA software. The climate change impact indicators at scope 1 and 2 levels along with the net avoided impact from using CO_2 were estimated using the CML 2001 impact assessment family. The electrochemical process was shown to perform considerably better than the CVD process in all the climate change impact indicators. Overall, the technical and economic performance of the CVD process was better than that of the electrochemical process. However, the environmental performance of the electrochemical process was shown to outperform that of the CVD process.

The limitations associated with modeling decisions taken in the two processes and with the uncertainty associated with the lack of data were highlighted. Further, the relevance of this study was discussed with respect to the industrial symbiosis potential of using waste CO_2 from industries leading to GHG emission reduction and subsequent deceleration of climate change impacts. Finally, future potential studies were highlighted that could build on the research and insights generated in this study. One of these studies involved a case study on the implementation of a commercial-scale electrochemical process for MWCNT production in Port of Rotterdam region. Another study involved a techno-economic and environmental assessment of atmospheric CO_2 capture and conversion to carbon nanomaterials for applications that can potentially achieve net negative emissions.

Contents

1

Introduction

Climate change is touted as the biggest threat to global safety (Parry, 2007). One of the indicators of climate change that can be quantified is temperature, which is strongly associated with the magnitude of greenhouse gas (GHG) emissions (primarily CO_2) in the atmosphere. For instance, these emissions have demonstrated an increase of 1.1°C in average global temperature from 1850 to the present day (Ritchie et al., 2020). A majority of these emissions originated from human activities during the aforementioned period (Ritchie, 2020). These activities have caused the so-called global warming and a further increase of 1°C can have devastating effects on natural systems globally (Ritchie et al., 2020) from events such as the melting of glaciers that subsequently lead to an increase in sea levels and coastal flooding (Church et al., 2008). Apart from higher temperatures, climate change's effects further encompass storms, droughts, ocean warming, species loss, food scarcity, human health concerns, human poverty, and human displacement of increasing severity and frequency (United Nations, n.d.).

Worsening climate change can be attributed to over 50 billion tonnes of annual GHG emissions into the atmosphere (Ritchie, 2020). These emissions stem from the broad sectors of energy generation, agricultural activities, waste generation, and industrial activities as a result of the growing needs of the global population. For instance, the GHG emissions from industrial and energy sectors constitute 29.4 % of global greenhouse gas emissions, as shown in Figure 1.1 (Ritchie, 2020). Ritchie (2020) further outlines the various gases of CO_2, CH_4, N_2O and F-gases forming part of the GHG emissions. On measuring the global warming contribution of these gases based on their magnitudes of CO_2 equivalent global warming potentials, CO_2 is shown to contribute the highest (74.4%) amongst various the various GHG emissions gases, followed CH_4 and N_2O. The sector-wise CO_2 emissions breakdown is similar to that of GHG emissions as shown in Figure 1.1.

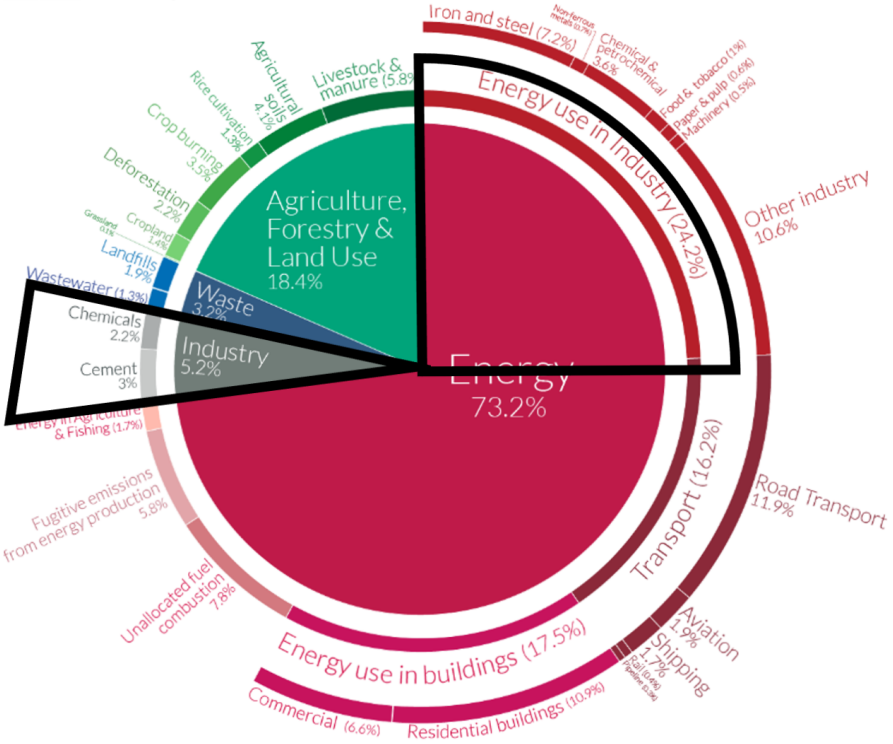

Figure 1.1: GHG Emissions by Sector (Ritchie, 2020)

Reducing GHG emissions to limit global warming and its harmful consequences is imperative for the sustenance of future life on Earth. As shown in 1.1, the industrial sectors and their associated energy use are stationary sources of emissions responsible for more than a quarter of the total emissions. The GHG gases from such sources, which have been described thus far as global warming causing emissions into the atmosphere, can be seen differently as a source of raw materials that can be supplied to other industries which use it to build valuable commodities. Cooperative exchange of waste flows from one industry for use as a feedstock resource for another industry forms the basis for Industrial symbiosis, which takes inspiration from ecological and biological systems and applies the concepts of complex systems and organizations (Chertouw and Ehrenfield, 2012). The GHG gases when used as an input feedstock resource help achieve a circular economy by avoiding waste disposal of these flue gases into the atmosphere and enabling its re-entry to the industrial system thus contributing to sustainable development that fosters "environmental quality, economic prosperity and social equity" (Kirchherr et al., 2017). The re-entry of GHG emissions back into the industrial system would entail the isolation of industrial emissions into different usable constituent gasses for various industrial purposes. CO_2 gas forms the majority of these gases and contributes the highest to global warming, as mentioned earlier, thus making it a significant gas to recover from industrial GHG emissions and limit from entering the atmosphere.

The need to recover CO_2 and curtail its atmospheric emission from industrial GHG emissions, also known as flue gases, has stimulated significant research in CO_2 capture technologies. W. Hong (2022) and X. Wang and Song (2020) described the status quo wherein industries capture CO2 from stationary sources of flue gas streams primarily through post-combustion, pre-combustion and oxyfuel combustion approaches. A promising fourth approach called

chemical looping combustion was also described, however, it is yet to reach technology maturity levels for commercial deployment. Alternatively, CO2 can also be captured from the air directly, which is particularly beneficial in compensating for the non-stationary sources of CO_2 emissions such as fossil-based modes of transport. One instance of large-scale synergy between industries in capturing CO2 from their industrial flue gases within the Netherlands is the Port of Rotterdam CO_2 Transport Hub and Offshore Storage (PORTHOS) project(Porthos, 2023). The PORTHOS project (Fig. 1.2) aims to develop the transportation infrastructure for collecting CO_2 from various industries. The industries that have agreed to participate in and supply their CO_2 emission to the PORTHOS project include large industries operating in the Port of Rotterdam region - Air Liquide, Air Products, ExxonMobil and Shell. The CO_2 collected is however for storage in depleted gas fields under the North Sea rather than for usage in other industries. The captured CO_2 pumped into such gas fields does not create any added value and in turn, requires the mobilisation of economic resources. This draws the need to look into CO_2 utilisation possibilities that have the potential to consume such large quantities of CO_2 while creating added value from it.

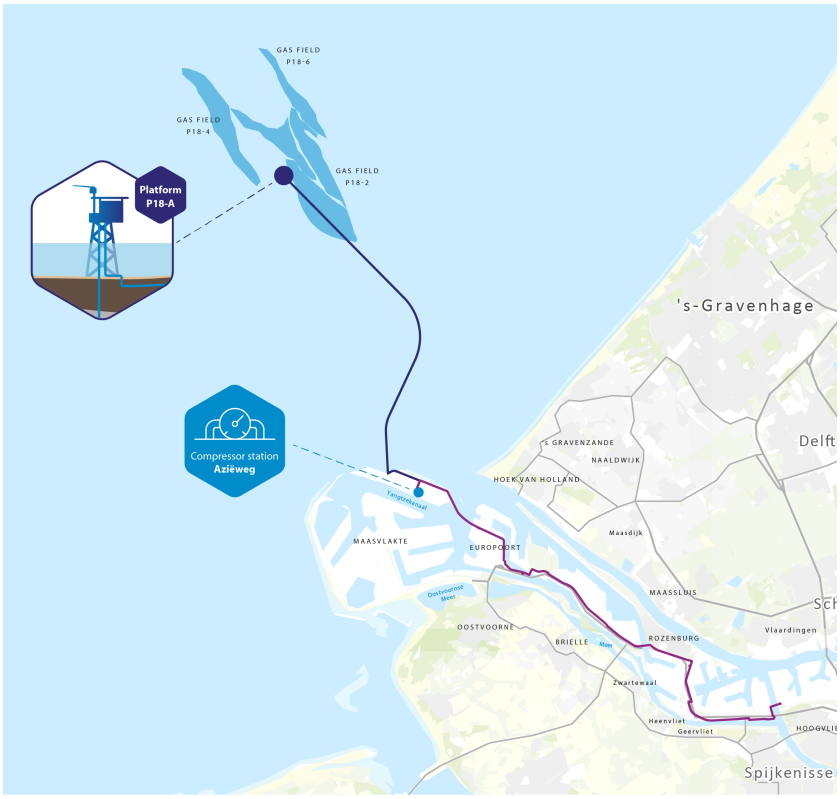

Figure 1.2: PORTHOS project map for CO_2 transport and storage

The captured CO_2 can be utilised for a wide variety of applications involving the use of CO_2 as is, for instance in greenhouses, or by converting it into other commodities such as fuels, chemicals and building materials (IEA, 2019). CO_2 conversion to chemical commodities and fuels, that are conventionally fossil-based, can prove to be effective in reducing fossil fuel usage and its associated GHG emissions given their large-scale global consumption. Kamkeng et al. (2021) outlines the research on CO_2 emission conversion into such commodities that

include methanol, urea and methane. Certain technologies such as CO_2 hydrogenation to methane and carboxylation were shown to achieve significant traction with a Technology Readiness Level of(TRL) 7-9 and certain other electrochemical technologies, at comparatively lower TRL levels, were demonstrated to be up and coming with growing research (Kamkeng et al., 2021). Such CO_2 conversion technologies are also struggling with high costs of operation coupled with a low economic value of the chemical feedstocks (Douglas & Pint, 2017). For instance, the cost to capture one ton of CO_2 from industrial emissions is USD (United States Dollar) 120 (IEA, 2021) and converting such CO_2 into methanol, which retails at USD 555/ton (Methanex, 2023), in a financially viable manner is difficult with only ≈ USD 430 remaining for its electrochemical conversion. Nyári et al. (2020) shows that converting CO_2 to methanol, even at a large scale of 5000 tons/day, is not feasible. This draws the interest to look into other potential applications of CO_2 that can help realize high economic value and scalability.

One such application is the conversion of CO_2 to high value carbon nanomaterials, such as carbon nanotubes and graphene (Fig. 1.3) whose market prices go upto USD 200,000/ton (Azonano, 2020; OCSiAl, 2014). Carbon nanomaterials (CNM) constitute a category of carbon-based materials, occupying a smaller number of spatial dimensions, that began with the discovery of fullerenes and subsequently followed by the discovery of two other carbon allotropes - carbon nanotubes and graphene(G. Hong et al., 2015). Carbon nanotubes and graphene-based CNM form the focus of this study. Carbon nanotubes are one-dimensional CNM in the form of one or more concentric tubes of hexagonally connected carbon atoms whereas graphene is a two-dimensional carbon nanomaterial of carbon atoms connected in similar hexagonal arrangement(G. Hong et al., 2015). Both these materials are known to have unique properties of mechanical strength, electrical and thermal conductivity and optical benefits (Choudhary et al., 2014; Maduraiveeran & Jin, 2021). These carbon nanomaterials can be used in a variety of applications ranging from batteries, supercapacitors, composites, concrete, and filtration membranes, among several others (Dimov et al., 2018; Douglas & Pint, 2017; Manchester, n.d.). These materials thus provide benefits to multiple sectors of construction, energy, wastewater treatment, electrical and electronics, health, and gas separation among several others (Bleu et al., 2018; Jain et al., 2021).

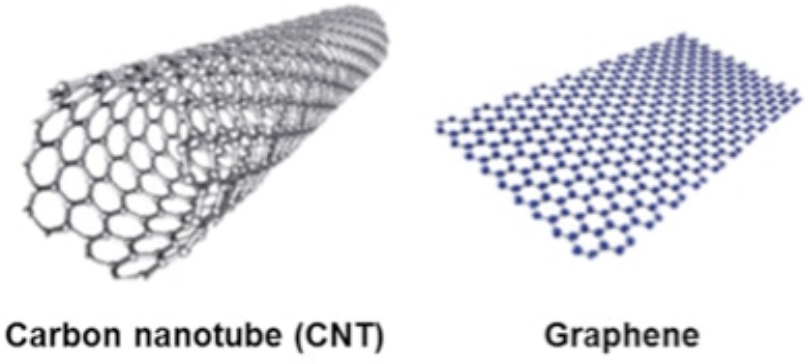

Figure 1.3: Structures of CNT and Graphene

The current status quo for producing high-quality carbon nanomaterials of graphene and carbon nanotubes at an industrial scale is via a process called chemical vapor deposition (CVD)

that involves the breakdown of a vapor phase precursor material and its subsequent deposition as a solid material on a substrate (Carlsson & Martin, 2010; Deng et al., 2019; Mubarak et al., 2014). Deng et al. (2019) and Mubarak et al. (2014), illustrate the usage of fossil based precursors such as CH_4,CO,C_2H_2 and high-temperature operating conditions of upto 1200°C in such CVD processes. These are considerable drawbacks given the environmental impact associated with using fossil resources for high-temperature heating and as precursor materials. Such drawbacks further demonstrate the need to look into novel CO_2 based alternative processes. The research on CO_2 reduction to carbon nanomaterials is in a nascent stage, with most of the literature search revealing lab or pilot experiments. On the other hand, there are also startups such as Carbon Corp, from Canada, that developed processes involving electrolysis of CO_2 based molten carbonate electrolytes with steel and nickel electrodes to form carbon nanotubes for potential applications in batteries (Licht et al., 2016; Ren et al., 2015). Another startup called UP Catalyst, from Estonia, has made considerable strides in commercially developing carbon nanotubes, graphite and other products also from an electrolytic process also involving CO_2 based molten carbonate electrolytes (UP Catalyst, n.d.), albeit at a small scale of 1ton per year (Karu, n.d.) LM Plus, an Australian startup, developed a triboelectrochemical process involving liquid metals to produce graphene for potential use in batteries, construction and aircraft manufacturing (Tang et al., 2021; UNSW, 2021).

The carbon nanomaterials (CNMs) of carbon nanotubes (CNTs) and graphene have market values of USD 0.8 Billion (B) (Global Market Insights, 2023)and USD 0.34 B (Fortune Business Insights, 2022) respectively. Out of the USD 1B+ combined market value of these CNMs, CNTs are evident to have greater applicability with potential uses in various industrial, medical and environmental fields (Farmand et al., 2022). These CNMs are however currently expensive, as demonstrated earlier, making them unviable for adoption in mainstream applications. Cost-effective production of such CNM from CO_2 emissions at a large scale can help achieve dual objectives simultaneously - a) prevent CO_2 emissions into the atmosphere through its usage as a raw material for CNM production, b) increase supply and accessibility of CNM for its widespread adoption. However, such large-scale cost-effective production of CO_2 based CNM is yet to be realized and compared with current CNM production processes, which are predominantly based on fossil-based commodities. In light of this problem, this research intends to understand the comparative technical, economic and environmental implications of large-scale CNM production through novel CO_2-based and conventional fossil-based processes. The insights from this research intend to serve as a practical basis for future developments in cost-effective and sustainable CO_2 based CNM production that can potentially replace conventional fossil-based CNM production and increase CNM adoption. Large-scale usage of CO_2 for its conversion to high-value CNM creates value for captured CO_2 and accelerates its large-scale removal from industrial flue gas emissions and from the atmosphere, thereby helping decelerate climate change.

2

Research

In this chapter, the research involved in this study is explained in further detail. Firstly, the state-of-the-art literature on CNM production through both status quo processes and CO_2 based processes is described. Secondly, the knowledge gaps discovered from this literature study are highlighted. Thirdly, the research questions addressing these knowledge gaps are outlined. Finally, the study's scope is established to highlight what is included and excluded.

2.1. State of the Art

The current prevalent processes for the production of the high market value CNMs of CNT and graphene are through the chemical vapor deposition process. In a review study of CNT production processes,Mubarak et al. (2014) describes CVD as a process involving the break-down and dehydrogenation of a gaseous hydrocarbon, such as methane, at high temperatures and in the presence of catalysts to deposit carbon (nanotubes) on a heated surface. Iron, Cobalt and Nickel were found to be the common catalysts present in the processes studied in the research. Another study by Deng et al. (2019), that summarized the research progress on CVD-based mass production of graphene, describes the CVD growth of graphene through the decomposition of a volatile precursor gas, such as methane, on a substrate surface at high temperatures in two reaction pathways: a homogenous reaction in gas -phase followed by physical deposition on the surface of a substrate, and chemical reaction of heterogenous nature taking place on the catalyst's surface itself. The study further elaborates on the growth of graphene primarily on Nickel and Copper substrates. CNTs are produced as varieties with a single wall of thin diameter (SWCNT) or with multiple walls larger diameter (MWCNT) (Zhu, 2017). Similarly, graphene develops in various physical forms such as very few-layer graphene (VFLG,1-3 sheets of carbon), few-layer graphene (FLG,2-5 carbon sheets), multi-layer graphene (MLG,2-10 carbon sheets) and graphene nanoplatelets (GNP,>5 carbon sheets) (Mason, 2020).

Given the high market value commanded by CNTs, in comparison to that by graphene, CNT mass production has become attractive leading to the development of various CNT mass production processes. Two prominent processes that are widely known for high yield production of SWCNT are HiPCO process, developed at Rice University and CoMoCat process, developed at the University of Oklahoma (Rafique & Iqbal, 2011; F. Wei et al., 2008). The HiPCO

process involved the usage of CO gas as the carbon precursor and $Fe(CO)_5$ at high pressures of 30-50 atm and high temperatures of 90-1100°C (Bronikowski et al., 2001). The CoMoCat process also similarly used CO as the carbon precursor however with Co-Mo catalyst supported on SiO_2 at 700-950°C and 1-10 atm pressure (Resasco et al., 2002). A. E. Agboola et al. (2007) further developed conceptual industrial process design of the HiPCO and CoMoCat processes with 5000 tons annual production capacities and demonstrated their economic feasibility, showing that the CoMoCat commercial scale process was 10% more profitable than that of HiPCO. Pirard et al. (2017) elaborates on their research group's work on the continuous production of MWCNT using methane or ethylene and on their progress from laboratory scale, based in Leige University (Belgium), to commercial scale, as a Belgian-based company called Nanocyl. The study demonstrated the advantage of using industrial natural gas, which is widely available through existing gas pipelines, as the carbon precursor material with a Ni-Mo catalyst on MgO support for commercial scale production of 400 tons of MWCNT annually. The MWCNTs produced at such commercial scale are shown to be of 90% purity (Douven et al., 2012) and are commercially retailed as NC7000 (NANOCYL, n.d.).

The CVD based production processes elaborated thus far in the production of the CNM are at high temperatures of up to 1000°, C which is a considerable drawback. The hydrocarbon-based methane precursor used further makes the process questionable in an environmental sense, as methane and other hydrocarbons are fossil-based resources extracted from nature. Additionally, in a resource supply sense, it is important to decouple from methane use given how events such as Russia – Ukraine war has created a supply scare for Europe which is heavily reliant on Russian gas (World Economic Forum, 2022). This creates a motivation to explore alternative processes of producing such CNMs from CO2, which is an abundant waste resource emitted by industries.

A large number of CO2 to CNM approaches have been tried and performed over the last 10 years with one of the earliest processes involving the combustion of magnesium in CO2 constituting dry ice for graphene production (Chakrabarti et al., 2011). One of the most studied approaches was an electrolytic process in which molten salts are used to both capture carbon and electrochemically transform (MSCC-ET) CO2 to CNTs, graphene and various other CNM such as carbon nanoparticles, carbon nanofibers and hollow carbon spheres at temperature ranges of 450-950°C (Jiang et al., 2019). Stuart Licht's research group initially proposed Li_2CO_3 based molten salt based method to capture and convert CO2 to CNMs in 2010 (Licht et al., 2010) and has since then pioneered the development of the MSCC-ET process to develop carbon nanofibers (Ren et al., 2015), CNT(Licht et al., 2016; Ren et al., 2017; Wang et al., 2020; Liu et al., 2022) , carbon nanotube wools (Johnson et al., 2017), carbon nano-onions (Liu et al, 2019) , graphene (Liu et al., 2020) and carbon fullerene allotropes (Liu et al., 2022). The research group has mostly incorporated Ni-based materials for anodes and steel and brass constituting cathodes in their 700-800°high-temperature electrolytic processes. A university dissertation study by Srininvasan (2018) detailed on the costs and carbon emissions of the scaled MSCC-ET process developed by Stuart Licht's research group, albeit at a surface level without delving into the process design aspects for a commercial scale plant. Several other studies tested various combinations of Li_2Co_3 based electrolytes withK_2CO_3, Na_2CO_3, $BaCO_3$ and $CaCO_3$ at 500-800°C with Ni, Fe and graphite-based electrodes for developing CNMs such as carbon rings, MWCNTs, carbon spheres and honeycomb carbon(Ijije et al., 2014; Jiang et al., 2017; Z. Li et al.,

2018; Ratso et al., 2021; Remmel et al., 2022; P. Wang et al., 2021). A group of studies performed by Hu et al. tested the use of $CaCl_2$-NaCl-CaO electrolytic combination using RuO_2-TiO_2, Ni, Cu and graphite electrodes at 650-850°C temperatures to produce graphene, MWCNTs based CNM (Hu et al., 2017; Hu et al., 2016; Hu et al., 2019).Y. Chen et al. (2020) performed MSCC-ET using an electrolytic mixture of Na_2CO_3-K_2CO_3 with $NaVO_3$ and electrode materials of SnO_2 and Ni to produce MWCNT and carbon sheets. Thin-walled MWCNT (27nm diameter), which can potentially rival CVD-produced CNT in quality, was demonstrated in Douglas et al. (2018) and Douglas et al. (2017) using alumina-coated Ni anode and Fe cathodes. A unique type of electrolytic system different from MSCC-ET processes mentioned thus far was developed by Joongjai's research group, as demonstrated in Pinthong et al. (2022) and Nganglumpoon et al. (2022), that involved an H-Cell type reactor with a ternary electrolyte system that produced polycrystalline varieties of graphene, graphite and diamond.

A catalytic approach for CO_2 transformation to CNM using liquid metals such as Ce, Ga, In and Sn was pioneered by Kourosh Kalanter's research group from Australia. These catalysts reduced CO2 to graphene-like CNM at room temperatures, unlike the high-temperature MSCC-ET processes, using current or mechanical energy in Dimethylformamide and Ethanolamine solutions (Esrafilzadeh et al., 2019 ; Tang et al., 2021). A similar liquid metal catalytic approach, albeit involving heating to temperatures of 200°C, was developed by Zuraiqi et al. (2022) that used a eutectic Ga-In liquid metal alloy to convert CO_2 to graphene-like carbon nanosheets.

A CO_2 transformation approach inspired from metallurgy industries involves the use of metals as reductants for CO_2 reduction to CNM (C. Li et al., 2021). This approach included some processes that uniquely involved the usage of CO_2 constituting solid dry ice, rather than the gaseous co_2 used in the studies discussed thus far, to produce graphene using Mg, Li and Ni-Si metals as reductants (Chakrabarti et al., 2011; Cunning et al., 2014; Poh et al., 2014; Zhou et al., 2020). The majority of the processes in this approach involved reduction of CO_2 at high temperatures of 500-900°C to various varieties of graphene such as FLG, 3D cauliflower fungus like graphene, and 3D honeycomb graphene among others, using K, Na, Mg, Fe, Ni, Ca and Zn reducant mixtures (Baik et al., 2020; Chang et al., 2017; Giannakopoulou et al., 2022; Jo et al., 2019; X. Li et al., 2022a, 2022b; S. Liu et al., 2020; J. Wang et al., 2015; S. Wei et al., 2022; W. Wei, Stacchiola, et al., 2017; W. Wei et al., 2014, 2016, 2017; Xing et al., 2016; Xing et al., 2015). This approach also involved lower temperature (upto 90°C) CO_2 reduction processes that are self-sustaining, have low reaction times ranging from a few seconds to around 10 minutes and used Mg and MgO as reductants (C. Li et al., 2017; Xu et al., 2019; Xu et al., 2018).

Based on the existing status quo CVD approach, which use fossil-based carbon precursors, CO2 precursor-based CVD processes have been developed that use Cu, Cu-Pd and Ni catalysts to reduce CO_2 to graphene (Gong et al., 2022; Luo et al., 2013; Molina-Jirón et al., 2019; Seekaew et al., 2022) and CNT (Kim, Choi, et al., 2020; Kim, Lim, et al., 2020; C. Wang et al., 2015) at high temperatures of 500-1000°C.

The various CO_2 based processes discussed thus far can be categorized into four approaches:

- CO_2 based CVD
- Molten salt based electrochemical CO_2 reduction

- Liquid Metal Catalyst aided CO_2 reduction
- Metal reductant enabled CO_2 reduction

The technical and economic aspects of these CO_2 processes are compiled and shared in the Appendix - A Excel sheet.

Regarding the efforts to commercialise such path-breaking processes, Stuart Licht's research group was one of the first to do so with their MSCC-ET approach which led to the formation of a North American spinoff company called Carbon Corp that also received the prestigious XPRIZE (XPRIZE, n.d.). Two other spinoff companies, based on MSCC-ET research, have been created in recent years - 1) SkyNano (SkyNano, n.d.), from North America, based on the research from Douglas et al. (2018), Douglas et al. (2017) ; 2) Upcatalyst (UpCatalyst, n.d.), from Estonia, based on research from Ratso et al. (2021) and Remmel et al. (2022). These spinoff companies primarily focused on the commercialisation of CNT production along with other CNM, such as graphene. The liquid metal catalytic approach by Kourosh Kalanter's research group is also in the process of commercialization by an Australian spinoff company called LM Plus (LM Plus, n.d.). This approach is particularly promising given the edge it has over the other CO_2 based approaches due to its room temperature-based processes. The details on the CNM produced are not explicitly mentioned, however the research from Esrafilzadeh et al. (2019) and Tang et al. (2021) suggests the production of graphene-like carbon. Regarding the metal reductant-based CO_2 transformation approach, no spinoff companies were identified to the author's best knowledge. The commercialisation of research on electrolytic and catalytic CO_2 transformation thus far indicates the potential to realise significant economic gains. However, it is imperative first to understand how such CO_2 based processes fare against status quo CVD processes for CNM production on a commercial scale based on their technical, economic and environmental aspects for sustainable CNM production.

2.2. Knowledge Gaps

The status quo fossil carbon precursor-based CVD processes detailed in 2.1 discuss lab-scale and commercial-scale production of SWCNTs, MWCNTs and graphene. A. E. Agboola et al. (2007) dives deep into the techno-economics of SWCNT production the techno-economic details on SWCNT production. However, similar insights on the techno-economics of commercial-scale MWCNT and graphene production are lacking. Further, the significant environmental externality of GHG emissions from such fossil-based and high-temperature CVD production of CNM is not discussed.

Wickramasinghe et al. (2021) reviewed approaches, as of 2021, pertaining to the transformation of CO_2 to organic and inorganic CNMs while emphasizing on the operational conditions and problems along with their application in biomedical and energy sectors. Park et al., 2022 similarly provided a comprehensive review of various processes for CO_2 to carbon materials as outlined in published literature and covered in Section 2.1. The CO_2 based processes in Section 2.1 describe the lab-scale production of various types of CNMs and each approach has its unique technical attributes in the form of materials used such as catalysts, electrodes, substrates and electrolytes or reaction conditions such as pressure, temperature and voltage among several

others. However, these approaches fail to include information on their potential scalability, process design, techno-economic viability and GHG emissions avoided in comparison to the status quo CVD alternatives.

A keyword search with the combination of phrases: ex-ante, techno-economic analysis, environmental analysis, emissions, life cycle analysis, chemical vapor deposition, CO_2, reduction, transformation, conversion, direct conversion, indirect conversion, graphene, carbon nanomaterials and carbon nanotubes in leading scientific databases of Web of Science and Scopus yields research specific to various processes for lab scale CO_2 reduction to CNMs and status quo fossil-carbon precursor based CVD production of CNMs. However, this search does not provide research on ex-ante techno-economic and environmental analyses of CO_2 based CNM production and its comparative assessment with commercial scale, status quo CVD-based CNM production processes, thus highlighting a research gap to be covered. Such analyses can help valorise the usage of waste CO_2 feedstock for large-scale CNM production. These knowledge gaps are therefore addressed in this study through the research questions outlined in Section 2.3

2.3. Research Questions

Building on the state of the art and the knowledge gaps, the following main research question has been theorised. Requisite sub-questions have been formulated that will help answer the main research question.

- How to assess ex-ante CO_2 based CNM production, considering its technical, economical and environmental aspects for its commercial implementation, and how does it compare against the status quo CNM production?
  - What are the status quo commercial scale processes and CO_2 based lab scale processes available to produce CNMs?
  - How to develop comparable process simulations of commercial-scale CNM production through such status quo and CO_2-based processes?
  - How do the process simulations of status quo and CO_2 based processes compare in their techno-economic and environmental performances?

2.4. Scope

This study focuses primarily on the transformation of input feestocks to CNMs that are ready for commercial use, thus making it a 'gate to gate' process. The 'gate to gate' processes compared involve mainly the production of CNM from input feedstock, the purification process for making them eligible for commercial use and any potential reuse of input feedstock. This implies that the production and purification of the carbon precursor feedstocks, such as CO_2 from industrial emissions, its subsequent transport and the final use of CNMs do not form part of the system. Similarly, any production and transport of other commodities used in the status quo and CO_2 based production processes are not considered in the study. The handling of wastes and by-products produced in this study is also considered out of scope. The geographical scope of the Netherlands and the time scale of 2022 -2023 for technology implementation are considered while taking necessary assumptions, design decisions, and

costs into account in the rest of the study. The environmental assessment referred to in this study involves the assessment of climate change impact from the Scope 1, Scope 2 and avoided GHG emissions in the whole life cycle of the considered 'gate to gate' processes.

3

Methodology

This chapter describes the methodology followed in this study to answer the research questions highlighted in 2.3. The first section describes the underlying design model that directs the overall approach and goal of this study. The second section establishes the assessment of emerging processes using techno-economic and environmental assessment methods and its relevance with respect to status quo processes. The last section elaborates on the approach of this study that details the framework for applying these methods and their implementation to help answer the various research questions.

3.1. Multilevel Design Model

This study is based on the multilevel design model (MDM), as described by Joore and Brezet (2015). MDM involves performing different steps that constitute a repetitive cyclic design approach, as shown in Fig.3.1. The starting step involves a 'reflection' on the status quo situation that is perceived negatively or is non-desirable. The second step involves the 'analysis' phase of brainstorming on the requirements of a new desirable situation in an abstract manner. The third step of 'synthesis' build on the perceived desirable situation through the design and development of solutions that can help achieve it. The fourth step is the 'experience' phase of putting the new solution into application and evaluating if this new experience is desirable or not. If this experience is perceived as desirable, the design process comes to an end. Otherwise, the design process is repeated until a desirable experience is perceived.

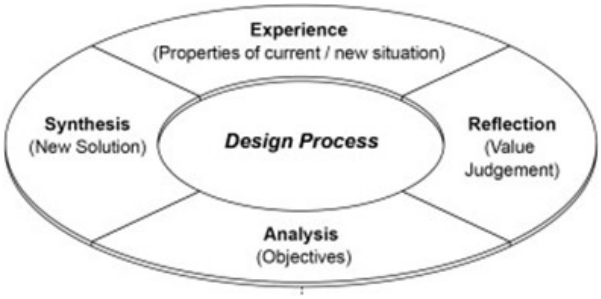

Figure 3.1: 4 cyclic steps of MDM (Joore & Brezet, 2015)

This repetitive cyclic design process takes place at four different system hierarchies of

product technology system, product service system, socio-technical system and societal system, as shown in Fig.3.2. This hierarchical systems approach of the MDM allows its user to ascertain the impact at a higher level system due to a change in a lower level system, thus enabling the use of MDM for bottom-up traceability of impacts. Similarly, the MDM can also be used for top-down traceability of impacts on lower-level systems by changes in higher system levels. This study applies a bottom-up approach starting at the product-technology system level and primarily focuses on the realization of a desirable situation at this level.

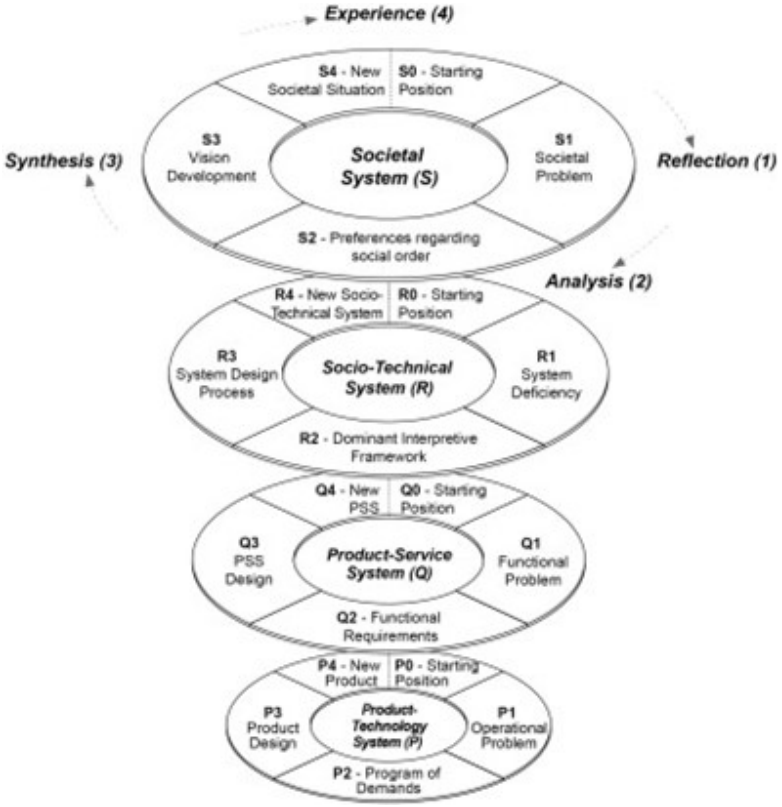

Figure 3.2: 4 system hierarchies of MDM (Joore & Brezet, 2015)

MDM is particularly interesting for this study as it helps bring context to current undesirable situations at different system hierarchies and helps link these different hierarchies of systems bottom-up from the product-technology system of CNM production, that is being researched in this study. Its cyclic and hierarchical design helps design the roadmap for possible future studies at various system levels to realize the commercial-scale implementation of sustainable CNM production using CO_2 that can ultimately help tackle climate change.

Table 3.1 highlights the MDM developed in context to the sustainable CNM production researched in this study. Chapters 1 and 2 discuss in greater detail on the reflection and analysis steps of the product-technical system. Going forward in this study, the synthesis and experience steps of this system are developed. With respect to the experience step, the following section introduces the assessment methodology for emerging processes of CO_2 based CNM production which helps evaluate if the situation resulting from such CNM production is desirable or not compared to the status quo CVD product technical system of CNM production.

Table 3.1: MDM for sustainable CNM production

	Initial situation	**Reflection**	**Analysis**	**Synthesis**	**Experience**
Societal system	Increasing global warming	Increasing global warming is worsening climate change across the world leading to extreme weather events such as droughts and hurricanes and is affecting biological life on earth adversely	Limiting global warming to 1.5°C above pre-industrial levels according to Paris Climate accord	Reduction of GHG emissions which are responsible for global warming	Global warming and climate change related events are in control thereby ensuring a safe and sustainable earth for future generations
Socio-technical system	High GHG emissions	High GHG emissions from human activities resulting in increasing global warming and worsening climate change	Reduction in emissions of GHG gases from large industrial sources	Reduction in GHG emissions from industrial sources of flue gases through its recycle and reuse by other industries, thus facilitating Industrial symbiosis	Reduced GHG emissions which limit global warming and climate change
Product-service system	Minimal industrial symbiosis of waste flue gases between industries	Low levels of industrial symbiosis between industries leads to the emission of waste flue gases into the atmosphere that contributes to the GHG emissions	Improved industrial symbiosis through the novel use of waste flue gases that are not conventionally used in large amounts	Industrial symbiosis through CO_2 capture from flue gases and use as a raw material for high-value commodity production that makes it economically viable and attractive	High levels of industrial symbiosis resulting in decrease of waste flue gas emissions and subsequently lower GHG emissions
Product-Technical System	Production of high-value CNM from fossil-based precursor materials through status quo CVD processes	High-value CNM are produced unsustainably from fossil based carbon precursors and at high temperatures fuelled by fossil fuels leading to high GHG emissions through the status quo CVD process	Sustainable production of CNM that results in lower GHG emissions	Production of CNM through alternative CO_2 feedstocks from waste industrial flue gases using renewable energy based novel processes at lower temperatures	Sustainable production of high-value CNM that helps make use of waste CO_2 from industrial flue gases and achieve industrial symbiosis

3.2. Assessment for Emerging processes

CO_2 based CNM production processes are lab scale CO_2 utilisation processes that have been gradually emerging over the past 10 years, as discussed in section 2.1. The viability of scaling up such lab scale emerging processes to commercial scales can be assessed through ex-ante techno-economic assessments, that involve detailed analysis of process implementation and economic quantification for market competitiveness of final products (Zimmermann et al., 2020). Such ex-ante techno-economic assessments require the creation of process designs and

simulations comprising various sub-process units to process raw material to marketable goods. An environmental assessment, such as quanitification of GHG emissions and global warming potential , complements this analysis further to establish the environmental benefits of an emerging process over the status quo (Thomassen et al., 2019).

The technological maturity of various emerging CO_2 utilisation processes is assessed using the process readiness level (TRL). TRL helps outline the current status of a particular process, ranging from an initial concept stage to a commercially operational stage, as shown in Figure 3.3. processes gradually jump to higher TRL levels through research, validation, prototype development, scaling up and commercialisation activities.

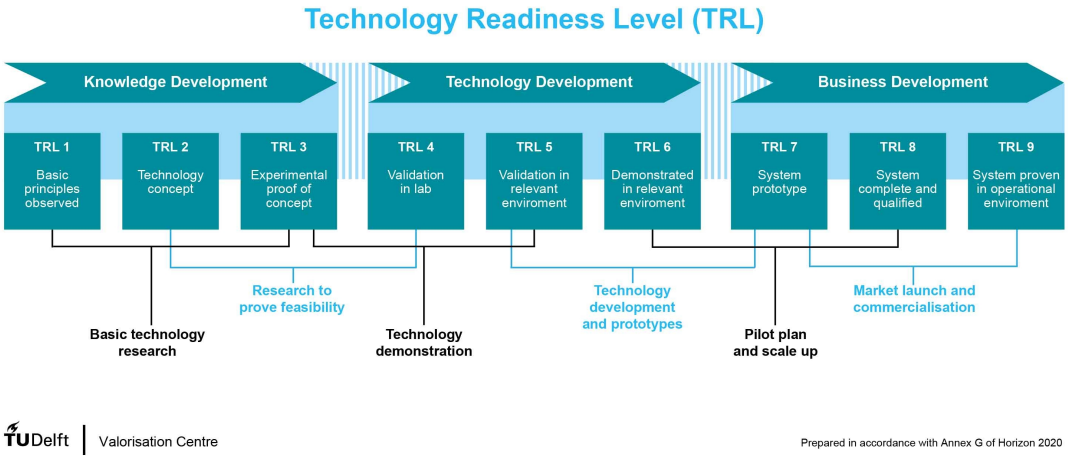

Figure 3.3: Technology Readiness Level (TU Delft, 2022)

The processes described in section 2.1 can be classified to TRL 3-4, given their lab scale status. A majority of the production costs and environmental impact are based on the decisions of process design taken at the early stages of process development, thus making it difficult to improve the techno-economic and environmental aspects of the process when it is fully developed (Thomassen et al., 2019) This highlights the importance of ex-ante assessment of processes for improving environmental effectiveness and cost-efficiency during the research and development process (Faber et al., 2021). Further, a benchmark status quo process is necessary for low TRL processes to put their techno-economic performance into context(Spek et al., 2017). However, it is important to note that techno-economic and environmental analysis (TEEA) at early stages are commonly plagued with problems of data uncertainty, thus limiting the depth of detail the analysis can reach compared to the TEEA of status quo processes. It is also important to note that the TEEA comparison of low TRL CO_2 based processes with that of mature status quo processes can result in an apple-to-orange comparison (Zimmermann et al., 2021).

As discussed in Section 2.2, there is a lack of research on ex-ante TEEA development of CNM production from CO_2 and its comparative assessment with status quo CVD processes. Therefore, this study performs an ex-ante TEEA of CO_2 based CNM production and compares it with status quo CVD production by developing and implementing a requisite framework

that helps factor the differences in TRL. This framework is further elaborated in Section 3.3 in the broader context of answering this study's research questions.

3.3. Approach

In this section, the framework to develop ex-ante TEEA for the CO_2 based method and its comparative assessment with status quo method for commercial scale CNM production, through process design and simulation, is described. The low TRL CO_2 process is designed and modelled assuming that the lab-scale process performance is achieved when scaled up to commercial production quantities. The uncertainties in data, put forth in section 3.2, are addressed through transparency on assumptions and input data used for modelling.

Below, Figure 3.4 showcases the flow diagram of the framework for ex-ante TEEA development and its implementation in the study. This framework is based on the 4 steps of the multilevel design model at a product-technical system level, as described in Section 3.1. It shows the various steps to approach the sub-research questions, from section 2.3, to ultimately answer the main research question. These steps are further explained in the subsequent sections to help understand the overall research approach including the tools used and indicators selected for the TEEA.

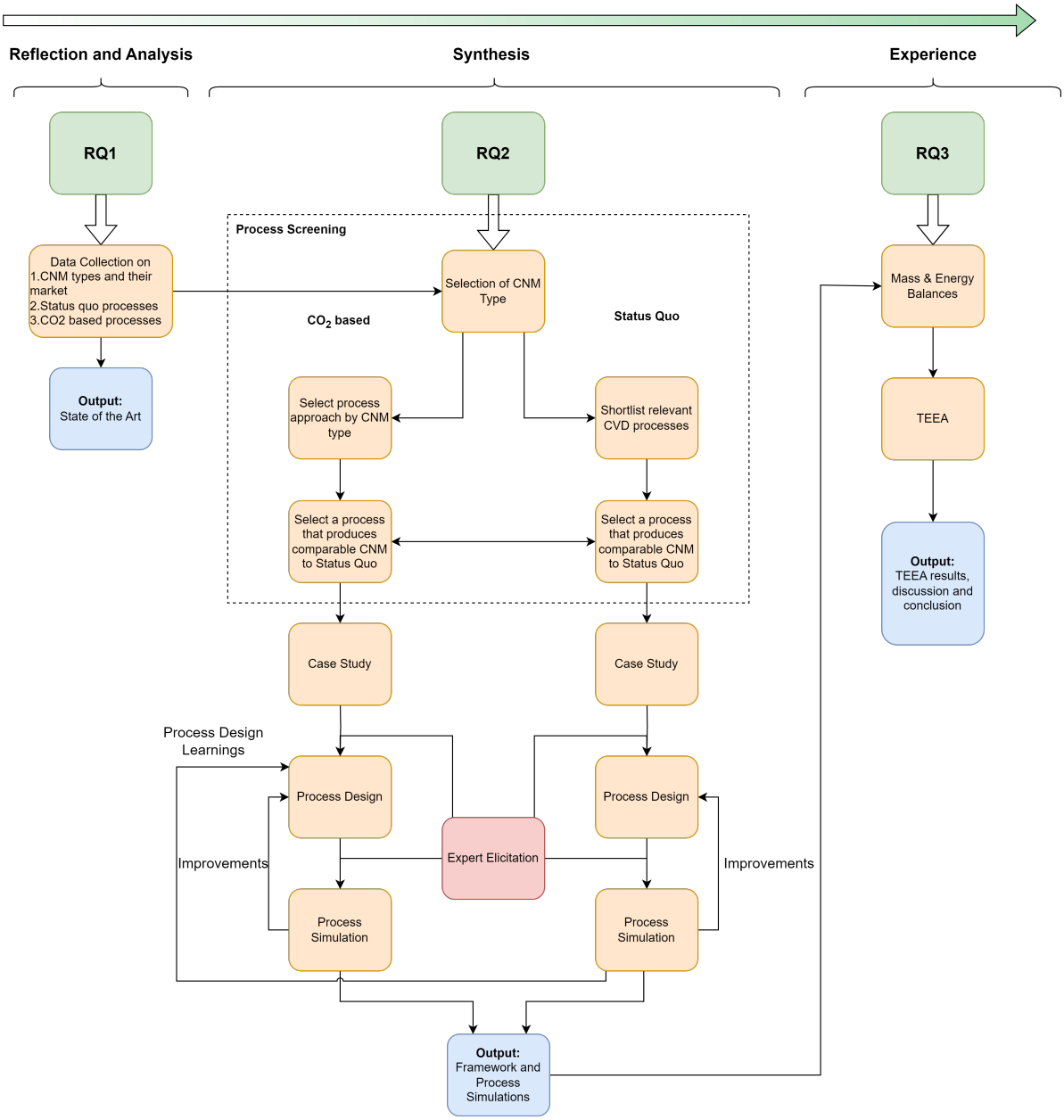

Figure 3.4: Flow diagram of the framework for ex-ante TEEA development contextualised to answering this study's research questions

3.3.1. State of the Art

The first step involved conducting a state-of-the-art research review on status quo processes and CO_2 feedstock-based processes for CNM production, along with obtaining market insights on the types of CNM as shown in Section2.1. The research review on processes involves collecting relevant data on process conditions such as temperature, pressure, feedstock and product specifications, faradaic efficiency, cell voltage, electrodes, etc. and various aspects of the produced CNM such as type, quality, etc. This provides an understanding of the working principles of various process routes along with their advantages and drawbacks, thus facilitating the next step of screening. The market insights involved the commercial market values of CNM and the commercialization efforts of various CO_2 based CNM production

processes.

3.3.2. Screening & Case Studies

A three-step framework is used in this screening process. The market data collected on various CNM and the commercialization of CO_2 based processes are factored to select the type of CNM, whose production will be assessed in the study. Based on the CNM type selected, CO_2 based approaches (as highlighted in Section 2.1) that produce such CNM are selected and accordingly relevant CVD processes are shortlisted. This is followed by a deep dive into the technical aspects of processes of selected CO_2 based approaches and of shortlisted CVD processes, to filter out one promising process each of the twot types that produce CNM of comparable quality. This filtering is carried out based on the process aspects temperature, pressure, process complexity, materials used, data availability, economics, TRL levels and current commercialisation efforts. Lastly, a detailed case study of the two selected processes is discussed to further elucidate the working principles and relevant data of these processes.

3.3.3. Process design and simulation

Process designs (PDs) of the two screened processes are created that reflect their respective compiled data and working principles. The PDs outline the various process unit operations, their interconnection and relevant information for subsequent modelling and simulation on Aspen Plus software to generate process models. The process design and simulation are first performed for the status quo CVD process with lower data uncertainty and more data availability on commercial-scale CNM production. The process design learnings from the status quo CVD process aid in the process design and simulation of the lab scale CO_2 process, which has minimal data on its scale-up to commercial production levels. Additionally, given the experimental nature of the CO_2 based pathway and potential uncertainties resulting from the data used and assumptions taken for modelling the two processes, both the process models are further validated and improved through expert elicitation. Mass balances are frequently employed to verify stream compositions during the process simulation and modify process units to achieve desired compositions. Energy balances are applied for the various process units to ascertain possibilities of heat integration, which improves the energy efficiency of the process simulation. The equipment configurations for the simulated processes are determined using the Aspen Process Economic Analyzer (APEA), which forms part of the Aspen Plus software. APEA allows the mapping of suitable equipment and accordingly sizing them to the scale of the process flows.

3.3.4. Mass and Energy Balances

The finalised process models on Aspen Plus are used to extract information on the overall input and output mass flows of substances that enter and leave the model. The various utilities, such as steam, and electricity, powering different kinds of unit process operations and any energy generated from the unit operations are mapped from the models on Aspen Plus as energy flows. The information on the mass flows and energy flows helps identify potential hotspots that consume or release such flows in large magnitudes and is used for futher techno-economic and environmental assessment.

3.3.5. Techno-Economic and Environmental Assessment (TEEA)

The information from the mass and energy balances are used to assess the two process models based on various technical, economic and environmental indicators. The technical indicators considered are resource intensity and energy efficiency. The economic indicators considered include capital expenditure, operational expenditure, net present value and payback period. The environmental indicators considered involve the climate change impacts on a Scope 1 and Scope 2 level, along with net impact and the avoided impacts from using waste CO_2.

3.3.6. TEEA Results, Discussion and Conclusion

The results of the technical, economic and environmental assessment calculated from the mass and energy flow data of the two simulated process models are discussed and compared against each other. The limitations of this study with respect to the process modelling are outlined. Recommendations for future studies are made which can build on the results on this study to generate more insightful research. Based on the overall research conducted in this study, the three sub-research questions and main research questions will be concretely answered in the conclusion.

4

Screening and Case Studies

In this chapter, the framework mentioned in Sec 3.3 is used to screen one process each from CO_2 based processes and status quo CVD processes. Following that, the selected processes are elaborated further in detail through individual case studies and the development of corresponding process designs that serve as a basis for the following chapter of process modelling. Finally, the basis of design for modelling these processes is detailed.

4.1. Screening Processes

The first step of screening the processes obtained from state-of-the-art research review involves the selection of CNM type. The decision-making involved in this step is summarized in the flow sheet Fig. 4.1. The CNM types, as discussed in 2.1 from the study of various processes, included CNTs, graphene, carbon nano-fibres, carbon nanoparticles, carbon nano-onions, and several others. Out of these CNM types, CNT and graphene were shown to have very high industrial applicability and a large combined market share of over USD 1B (Fortune Business Insights, 2022; Global Market Insights, 2023). CNTs were shown to have the higher market share among the two, contributing over 70% of the combined market value. Moreover, CO_2 based CNT production from the startups working on molten salt-based electrochemical CO_2 reduction processes indicates potenital for realizing profitable production of CNTs. For this reason, this study chooses CNT as the CNM type for ex-ante TEEA assessment of CNM production.

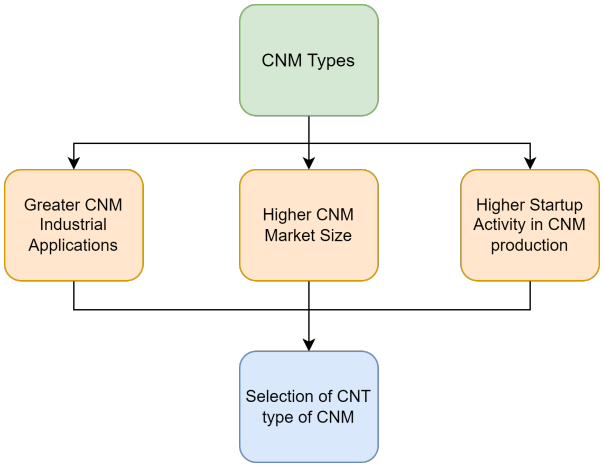

Figure 4.1: Decision-making flow sheet for CNM type selection

The second step involves selecting a range of processes for CNT production from CO_2 carbon precursors and status quo fossil carbon precursors. The decision-making involved in this step is summarized in the flow sheet Fig. 4.2. As outlined in Section2.1, the relevant process for CNT production include - SWCNT (CNT sub type) production from HiPCO process by Bronikowski et al. (2001) and from the CoMoCat process by Resasco et al. (2002), and MWCNT (CNT sub type) production as described by Douven et al. (2012) and Pirard et al. (2017). This MWCNT production is also commercialized by the Belgian Nanocyl company as NC7000((NANOCYL, n.d.) with a 400-ton production capacity. Additionally, a conceptual commercial scale design based on the HiPCo and CoMoCat processes was performed by A. E. Agboola et al. (2007) which elaborated greatly on the techno-economics of both processes. With regards to the CO_2 based CNM production processes, the research covered in Section 2.1 involved the classification of CO_2 based CNM production processes into four approaches. The available technical, economic and environmental details of the various processes categorised into these four approaches were compiled into an Excel sheet in Appendix Appendix A. A deep dive analysis of the CNMs produced by the various processes compiled shows that only processes from CO_2 based CVD approach and molten salt based electrochemical CO_2 reduction approach produced CNT along with other types of CNM. On the other hand, the processes from liquid Metal Catalyst aided CO_2 reduction approach and metal reductant enabled CO_2 reduction approach produced only graphene varieties of CNM and not CNT, thus disregarding these two approaches from further consideration in this study. Of the two approaches that produce CNT, the CO_2 based CVD approach is only slightly different from the status quo approach in terms of the carbon precursor used. The high temperatures of 1000°C are nevertheless highly prevalent in CO_2 based CVD processes as well. Processes based on the molten salt-based electrochemical CO_2 reduction processes with lower operating ranges of upto 800°C and different working principles are thus more attractive to compare with the selected status quo CVD processes.

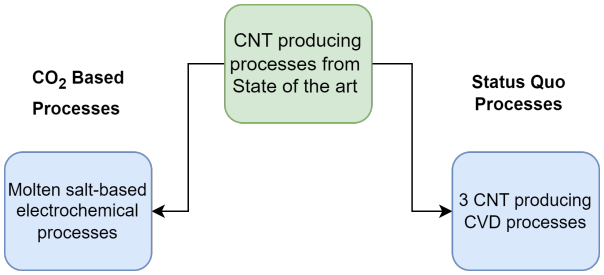

Figure 4.2: Decision-making flow sheet for CNM processes selection

The third step of this screening entails selecting a CO_2 carbon precursor-based process and fossil carbon precursor-based process that produce CNT of comparable quality. The decision-making involved in this step is summarized in the flow sheet Fig. 4.3. The current lab scale nature of most CO_2 production processes shows that these processes are yet to produce CNT of desirable quality consistently at large scales. The status quo CVD processes identified in the second step of this framework involved the production of both SWCNT and MWCNT. SWCNT production is known to be more difficult than MWCNT production for CVD processes (Kumar & Ando, 2010). The same is also evident for molten salt based electrochemical CO_2 reduction processes from the techno-economic details outlined in Appendix A which only describe MWCNT production. For this reason, the MWCNT production from status quo CVD process described by Douven et al. (2012) and Pirard et al. (2017) is considered as the TEEA benchmark process for CNM production. Moreover, the presence of this research's related Nanocyl commercial spinoff in Belgium, which is closer to the geographical scope of Netherlands considered in this study, makes the results from this research more applicable to this study. The MWCNT produced by Nanocyl (NANOCYL, n.d.) and as highlighted in Douven et al. (2012) and Pirard et al. (2017) is of 90 wt.% carbon purity, around 10 nanometers (nm) in diameter and consists of trace impurities of transition metals from the catalyst used. This MWCNT is used as a reference to find a process based on molten salt-based electrochemical CO_2 reduction which produces CNT that is as comparable to the selected MWCNT reference as achievable while ensuring favourable process conditions and sufficient data availability for process simulation.

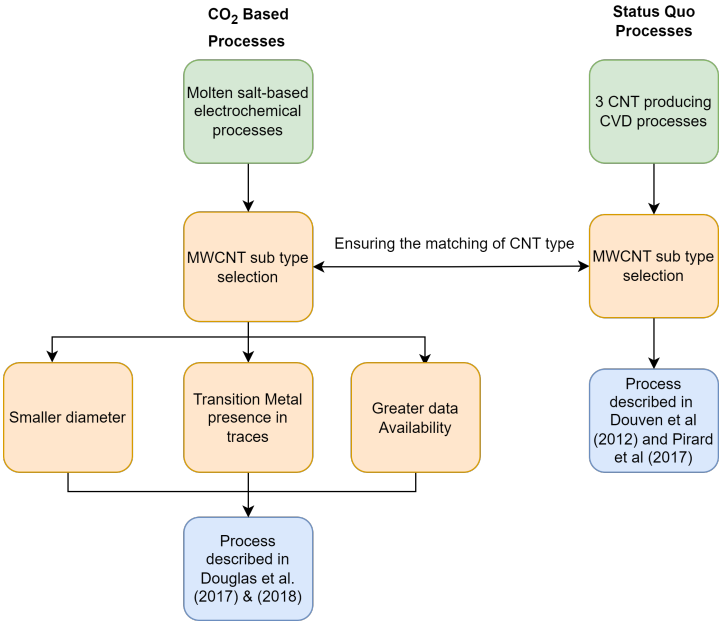

Figure 4.3: Decision-making flow sheet for finalizing one process each for status quo and CO_2 based methods

An analysis of the CNT products produced by molten salt-based electrochemical CO_2 reduction processes, as compiled in Fig. A.1 , reveals that these processes produced CNT of varying diameters, ranging from 10nm(Douglas et al., 2018) to 100 µm(X. Liu et al., 2022), and CNTs doped with various elements such as boron(Ren et al., 2017). With a closer look, four studies were identified that reported small diameter(10-50nm) MWCNT formation with minimal presence of other CNM types. The studies by Douglas et al. (2018), Douglas et al. (2017), that are linked to the SkyNano spinoff, described two of these processes that used pure Li_2CO_3 as the CO_2 based molten salt electrolyte and experimented with the use of different varieties of Ni anodes and Fe cathodes. One of the remaining two studies was by X. Wang et al. (2020), which is linked to Stuart Licht's research group and Carbon Corp spinoff. The process detailed in this study was performed using calcium metaborate dissolved molten Li_2CO_3 electrolyte with Ni anode and Fe cathodes. An earlier study by Ren et al. (2017) from the same research group used lithium metaborate added molten Li_2CO_3 electrolyte that resulted in the production of boron-doped MWCNTs Although no mention of boron doping is made in the X. Wang et al. (2020), which uses the metaborate of calcium in its electrolyte, the boron doping of the resultant small diameter MWCNT cannot be completely ruled out. Any boron (non-metal) doping of the resultant MWCNT would make it non-comparable to the reference MWCNT that is stated to constitute traces of transition metal. As a result, the X. Wang et al. (2020)'s process was not considered for the study. The last of the four identified processes was by Bromberg et al. (2022) which involved the use of molten electrolytic blends of Li, Na and Bo with Ni anode and Fe anode. With respect to data availability, the studies by Douglas et al. (2018), Douglas et al. (2017) divulged more relevant information, that is applicable to the ex-ante TEEA than compared to that divulged by Bromberg et al. (2022). However, the process conditions in the study by Bromberg et al. (2022) involved lower temperatures of 600°C and lower use of Li_2CO_3, which is expensive given the increasing demand for its use in Lithium-ion batteries (Azevedo et al., 2022), compared to higher temperatures of 750 °C and pure LI_2CO_3 usage in the studies by Douglas et al. Owing to better data availability, such as that for yield

and energy consumption, and linked commercialization efforts through the SkyNano spinoff, the process outlined in the studies by Douglas et al. is selected for further ex-ante TEEA of CO_2 based CNM production. The lab-scale process by Douglas et al. involves the use of an electrolyser and the scaling of such an electrolyser based on insights from a benchmark process design of CVD-based CNM production, such as that defined by A. E. Agboola et al. (2007), is difficult given that CVD uses a completely different reactor setup. Srininvasan (2018) developed a conceptual design of an electrolyser for commercial scale CNM production in consultation with Stuart Licht's research group but the author does not provide information on the type of carbon produced which limits its consideration for ex-ante TEEA CO_2 based CNM production to a certain degree. Therefore the process outlined by Douglas et al. (2017) and Douglas et al. (2018) combined with the electrolyser design provided by Srininvasan (2018) is considered for the ex-ante TEEA of CO_2 based CNM production.

4.2. Case Study - Status quo CVD

From section 4.1, the status quo CVD process by Pirard et al. (2017) and Douven et al. (2012) has been selected as the TEEA benchmark process for CNM production in this study.Pirard et al. (2017) discussed the research groups' overall efforts on commercial scale CVD production of different qualities of CNM from methane and ethylene streams which were coupled with various catalysts. Pirard et al. (2017) concluded that the use of widely available methane carbon precursor with Ni-Mo catalyst on MgO support was proven to be the most suitable process for Nanocyl's commercial-scale CNM production. The NC7000 product, sold by Nanocyl in ton scale quantities, is thus assumed to be through such a process. This methane precursor-based CNM production with Ni-Mo/Mgo catalyst is explored in detail by Douven et al. (2012) wherein a continuous reactor setup was developed along with the addition of a few testing equipment to analyse the outflow of this reactor.

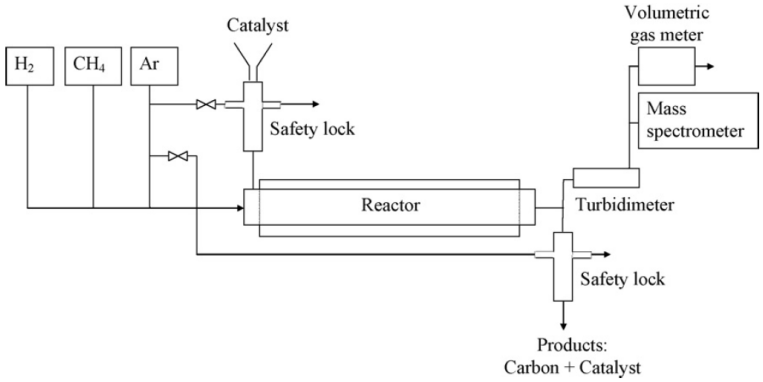

Figure 4.4: CVD reactor setup for testing continuous CNM production Douven et al., 2012

This reactor setup, as shown in figure 4.4, involves the use of an inclined tubular mobile-bed rotating reactor with systems for enabling a continuous flow of Ni-Mo catalyst particles on MgO support (Ni-Mo/MgO) and gas flows of CH_4,H_2 and Ar. Mobile bed reactors, also known as moving bed reactors, are reactors in which the catalytic material is introduced into the reactor simultaneously as the reactants flow, leading to the catalyst also exiting the reactor with the output flows and requiring subsequent catalyst separation. The Ar gas depicted is mainly used to create an inert atmosphere before the start of the process and flush out any

impurities present in the reactor. In this process, an input flow mixture of CH_4 and H_2 entering the moving bed reactor in a 9:1 molar ratio at atmospheric pressure and 975°C resulted in the best reaction productivity for the decomposition of input CH_4 flow on the surface of catalyst particles as carbon, mostly in the form of MWCNT, and hydrogen according to the equation 4.1. The H_2 introduced into the input flow and that generated during the decomposition was further hypothesized by Douven et al. (2012) to restrict the formation of amorphous carbon and the subsequent poisoning of metal catalysts from the produced amorphous carbon.

$$CH_4 \longrightarrow C + 2H_2 \tag{4.1}$$

The rotation and inclination of the moving bed reactor governed the residence time for MWCNT formation and its movement along the length of the reactor until the outlet. The residence time, i.e the time allowed for the MWCNT to nucleate and grow on the catalyst inside the reactor, affected the purity level of carbon reached. Thus by controlling the rotation and inclination of the reactor, the residence time was set and accordingly, MWCNTs of requisite purity were developed. The operating condition for 90% and 97.7% carbon purity levels were outlined by Douven et al. (2012). The purity levels stated were without the presence of the catalyst, however, no systems for the removal of catalysts were discussed in this study. Additionally, the product data-sheet of NC7000 (NANOCYL, n.d.) also describes the scarce presence of amorphous carbon which is not discussed by Douven et al. (2012).

A. E. Agboola et al. (2007) outlines a complete process design based on the lab scale literature data of the HiPCo and CoMoCat processes involving not only the CNT generation process in the reactor but also the subsequent purification processes of the produced CNT, which achieves >90% purity, along with the recovery and reuse of the unreacted fossil carbon precursor flows. Elements of process design from A. E. Agboola et al. (2007) shall be similarly used in this study to purify CNTs and reuse unreacted CH_4.

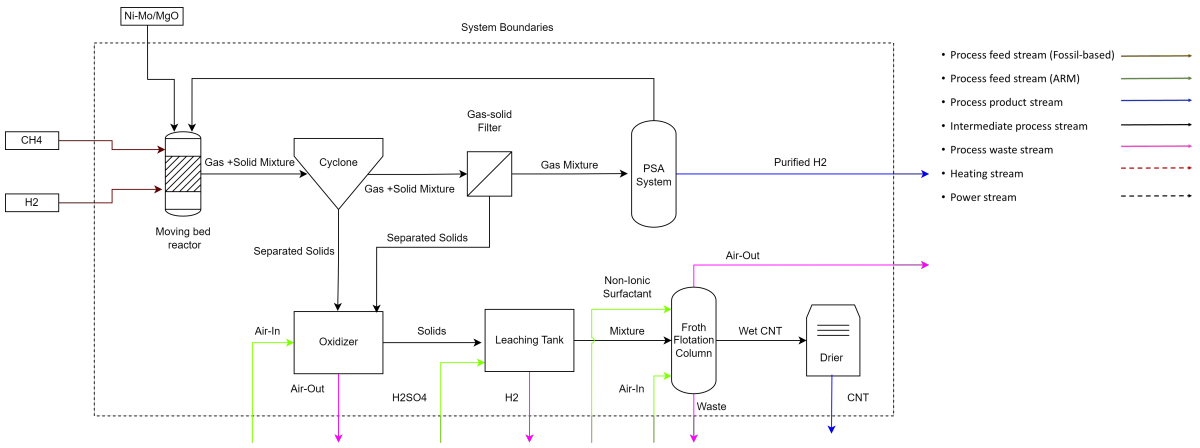

Figure 4.5: CVD PD developed based on A. E. Agboola et al. (2007) and Douven et al. (2012)

Figure 4.5 shows a process design comprising only the main components and excluding the utilities. This process design constitutes the status quo CVD production of the 90% purity MWCNT produced by the moving bed reactor described in Douven et al. (2012) along with adapted CNT purification and feedstock reuse process operations from A. E. Agboola et al.

(2007). The black dotted line represents the system boundary, highlighting the processes that form part of the scope of this study. The various material streams of this process are assigned different colours: predominantly fossil origin input streams - brown, other material based input streams - green, waste output streams - pink, marketable product output streams - blue and intermediate material streams - black. Large-scale implementation of MWCNT production through the moving bed reactor results in large-volume reactor outflows of unreacted CH_4, H_2 and solids of amorphous carbon and MWCNT that are attached to the catalyst particles. Such large outflows require dedicated separation systems to prevent the loss of precious MWCNT. The Ni-Mo/Mgo catalyst used in this study based on Douven et al. (2012) is similar to the Co-Mo/SiO_2 catalyst used by the CoMoCat process as described in A. E. Agboola et al. (2007) and Resasco et al. (2002). Thus, the two-stage solid filtration involving an initial passage through a cyclone separator and subsequent filtration by a gas-solid filter, as described inA. E. Agboola et al. (2007)'s conceptual design of CoMoCat process, is applied in this study. Further, the carbon content formed from the CVD reaction in the moving bed reactor is assumed to comprise 80% MWCNT and 20% amorphous carbon, similar to that considered for the CoMoCat process by A. E. Agboola et al. (2007).

The amorphous carbon formed is purified out of this solids mixture using the oxidizer unit operation. The oxidizer involves passing a pre-heated air gas stream over the CNT product held together between a vacuum-compressed filter while ensuring that the structural integrity of MWCNT is intact (A. E. Agboola et al., 2007; Chiang et al., 2001). The amorphous carbon undergoes oxidation at temperatures of 250°C to form CO_2 according to Eq. 4.2 (Lertrojanachusit et al., 2013). It is important to note that passing air at such temperatures oxidizes neither the CNTs, which show resistance to oxidation up to temperatures of 700°C (Terrones, 2003), nor the Ni-Mo/Mgo catalyst particles, which are also known to be resistant to oxidation at 250°C (Patnaik, 2003).

$$C + O_2 \longrightarrow CO_2 \tag{4.2}$$

Upon completion of the oxidation process, the resulting solids mixture contains the MWCNT attached to the Ni-Mo catalyst particles that are supported by MgO particles. The Ni-Mo/Mgo catalyst considered in this study comprises 30% of Ni-Mo catalyst particles and 70% of MgO support particles (Saconsint et al., 2022). The MgO support particles form the majority of the remaining impurities in the MWCNT solid mixture. Based on the alkali leaching process used by A. E. Agboola et al. (2007) to leach the SiO_2 catalyst support, this study incorporates a requisite 5 Molar (M)H_2SO_4 based acid leaching process (Mortazavi et al., 2010) to primarily leach the MgO catalyst support according to the Eq. 4.3 that readily forms $MgSO_4$ salt (Patnaik, 2003). This acid also dissolves Ni catalyst present in the mixture at a slow pace and releases H_2 as well according to Eq. 4.4 (Patnaik, 2003).

$$MgO + H_2SO_4 \longrightarrow MgSO_4 + H_2O \tag{4.3}$$

$$Ni + H_2SO_4 \longrightarrow NiSO_4 + H_2 \tag{4.4}$$

This resultant mixture of acid salt aqueous solution and MWCNT-catalyst solids is then designed to pass through a froth flotation column based on A. E. Agboola et al. (2007) and Lertrojanachusit et al. (2013). This froth flotation column comprises a non-ionic surfactant,i.e

Surfonic L24-7 (Huntsman, n.d.), through which air is bubbled to generate froth that brings the hydrophobic MWCNT solids to the surface for extraction while the acid salt solution with some amount of Ni catalyst dissolved and all of the MgO catalyst support dissolved lies at the bottom of the column for removal as shown in Fig 4.6. Based on A. Agboola (2005), A. E. Agboola et al. (2007), Chungchamroenkit et al. (2004), and Pornsunthorntawee et al. (2011) the MWCNT are assumed to be still weakly attached to the dissolved catalyst support thus requiring the additional push from froth flotation wherein the force of the airflow enables the froth to break them apart and bring the MWCNTs to the surface. Yianatos et al. (2008) demonstrates the mean residence time for solids to be 9-24 seconds based on their floatability which can be applicable for the MWCNT's froth flotation process as well. The MWCNT obtained from the froth is washed with demineralised water several times to flush out the surfactant until a neutral pH is observed, after which it undergoes centrifugation to remove most of the water. Post centrifugation, the MWCNT is placed in a dryer for removing any leftover moisture content and thus producing the market-ready MWCNTs for various applications.

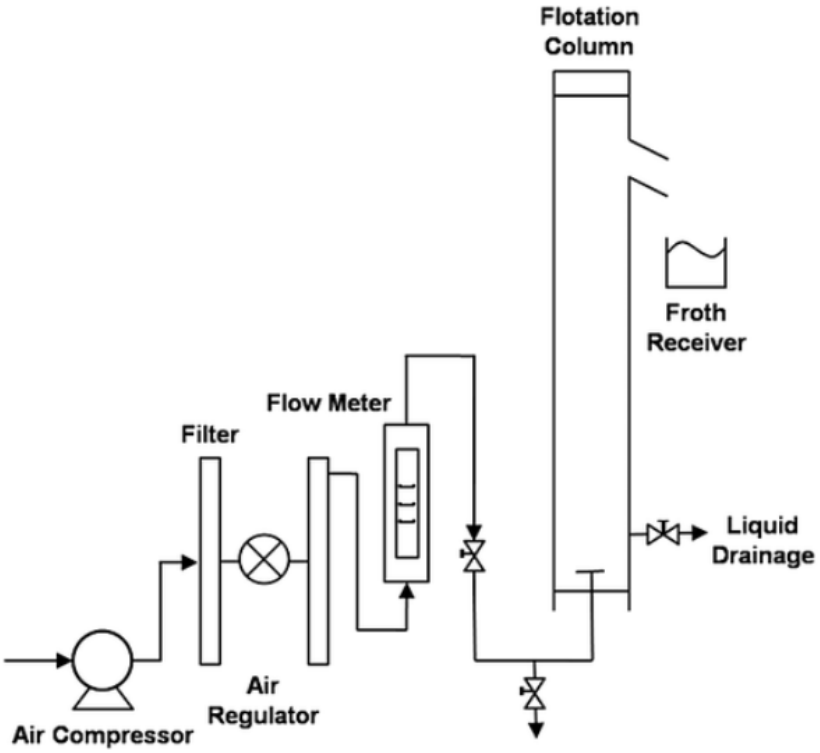

Figure 4.6: Froth flotation experimental apparatus as shown in Lertrojanachusit et al. (2013)

The gaseous outflows from the moving bed CVD reactor constitute unreacted CH_4, H_2 from the input feedstock and additional H_2 generated from the CH_4 breakdown. This gaseous mixture cannot be reused directly for the next reaction as the CH_4 to H_2 molar ratio has changed due to the additional H_2 generated. Therefore this study incorporates a pressure swing adsorption (PSA) system that can separate out the excess H_2 in the gaseous mixture which can subsequently be marketed and sold or reused within the plant for heating. PSA's primary function is to separate or purify gasses within a mixture by adsorbing different gasses through the exertion of different partial pressures on their respective adsorption beds (Ruthven et al., 1993). The adsorbed gases are renewed through the reduction of partial pressure. The

PSA system used in this study is based on the study from Burgers (2020) that developed a 6-bed system that separates H_2 at high purities of 98.8 mol% from a natural gas input feed of 10 vol% H_2 at 20 bar pressure. The recovered natural gas, which is stripped of the excess H_2, is routed back to the moving bed CVD reactor with a 9:1 molar ratio of CH_4 to H_2 as required to achieve the best reaction productivity.

4.3. Case Study - Electrochemical CO_2 reduction

The process outlined in the studies by Douglas et al. (2018), Douglas et al. (2017) were selected in Section 4 as the ex-ante CO_2 based processes for CNM production. Douglas et al. (2017) demonstrated an electrolysis process involving ambient CO_2 dissolved in molten Li_2CO_3 electrolytes for MWCNT formation with average diameters of 27.5nm. In this study, electrode combinations involving three types of Ni anode - 99% Ni, oxidized Ni and Ni wire coated with 50nm of Al_2O_3 - and three types of Fe cathodes - ZnO coated Fe (galvanized steel), Cr_2O_3 coated Fe (stainless steel) and 99% Fe - were tested for electrolysis in pure molten Li_2CO_3 at 750/degree C at 100mA/cm2 and with 1-hour duration, as depicted in Figure 4.7. The electrolytic process involved the breakdown of Li_2CO_3 electrolyte, as shown in Eq. 4.5 into carbon, in the form of MWCNT and amorphous carbon which deposit on the cathode surface, Li_2O and O_2, which gets liberated into the atmosphere at the anode. CO_2 presesnt in ambient air is stated to regenerate Li_2CO_3 by reacting with Li_2O according to Eq. 4.6. In an overall sense, this results in CO_2 breakdown to carbon and oxygen as shown in Eq. 4.7.

$$Li_2CO_3 + 4e^- \longrightarrow Li_2O + C + O_2 \tag{4.5}$$

$$Li_2O + CO_2 \longrightarrow Li_2CO_3 \tag{4.6}$$

$$CO_2 + 4e^- \longrightarrow C + O_2 \tag{4.7}$$

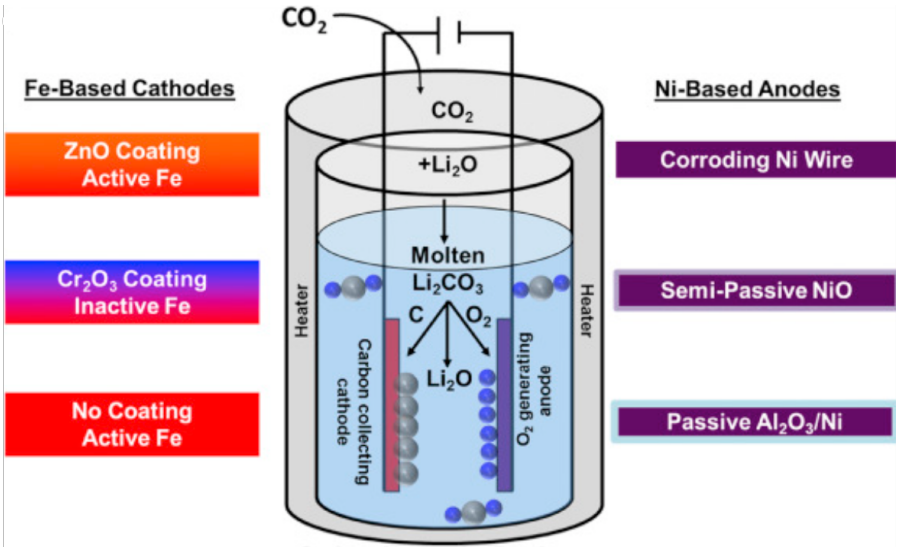

Figure 4.7: Electrolytic setup used in Douglas et al. (2017)

The Al_2O_3 coated Ni anode along with galvanized steel cathode were realised to be the most effective electrode combination resulting in 99% MWCNT formation, unlike the other combinations that involved higher amorphous carbon formation. The Al_2O_3 coating on the

Ni was shown to restrict Ni from taking part in the catalytic process and allow Fe-catalysed MWCNT growth. The MWCNT diameter distribution, as shown in Figure 4.8 was stated to be similar to the distribution of CNT grown from status quo CVD processes.

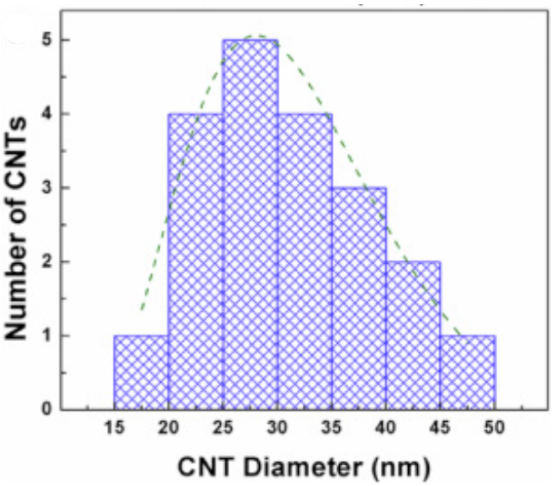

Figure 4.8: MWCNT diameter distribution from Douglas et al. (2017)'s study

Douglas et al. (2018) demonstrated a similar study with a specific focus on creating smaller diameter MWCNT. The study involved the use of an Al_2O_3 coated Ni anode, as used in Douglas et al. (2017), and a stainless steel cathode, with electon beam deposition of Fe in layers of 0.5-5nm thicknesses, in a pure molten Li_2CO_3 at 750/degree C at 100mA/cm2 with durations ranging from 3-60 minutes, as shown in Figure 4.9. Lowest MWCNT diameter of 10nm was achieved with 3min electrolysis duration, albeit at a lower yield, and the CNT diameters were observed to grow larger with a further increase in electrolysis duration. MWCNT median diameters of 33nm and 23 nm were achieved with cathodes of 5 nm and 0.5 nm Fe layer thickness. A 60 min duration growth was shown to produce 50mg of MWCNT on a cathode surface area of 2.5 cm2 at a current efficiency of 90 %. Further, an absence of amorphous carbon was concluded based on a detailed imaging analysis of the produced MWCNT. An energy consumption of 54kWh/kg MWCNT , for both electricity and heating, was estimated in this study and thus was highlighted to be cost competitive with status quo CVD-based MWCNT production.

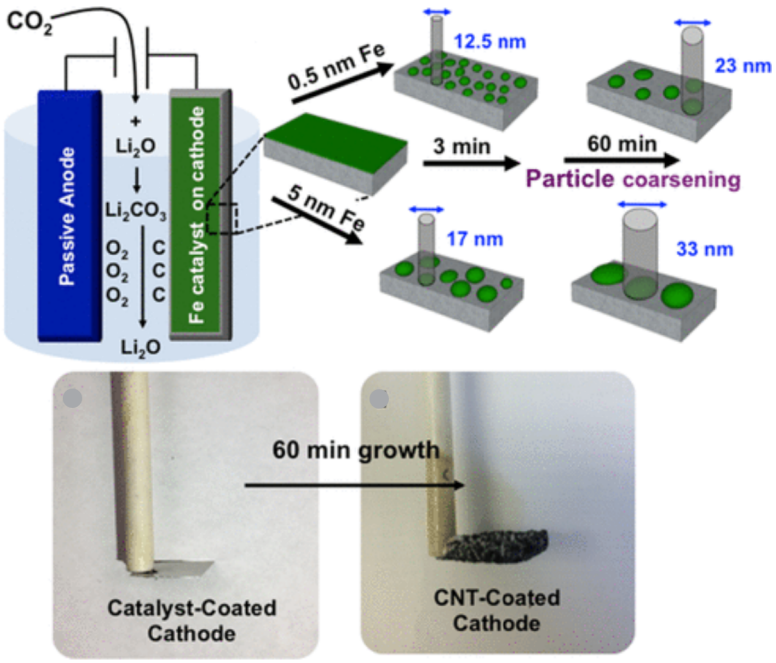

Figure 4.9: Top - Electrochemical cell setup, Bottom - Catalytic growth of MWCNT on cathode (Douglas et al., 2018)

Section 4.1 concluded on the use of Sriniinvasan (2018)'s study as a reference for the visualisation of a commercial scale electrolyser required for the ex-ante commercial scale process design of MWCNT production. In her study,Sriniinvasan (2018) reported on the lifecycle CO_2 emissions and cost aspects of a conceptual commercial scale plant with 540,000 tonne annual capacity of solid carbon production, in the form of CNT and carbon nano-fibres. This conceptual plant was based on the MSCC-ET process developed by Stuart Licht's research group and was theoretically designed to process 2 million tonnes of high temperature CO_2 emissions from a cement industry flue gas stream. The study developed a conceptual design for a commercial scale electrolyser, as shown in Fig. 4.10, for continuous production of solid carbon through a peculiar steel cathode roller and Ni anode plate electrode setup in pure molten Li_2CO_3 electrolyte. Such a setup innovatively makes use of both sides of the cathode and thus increases its productivity. The cathode is mechanically scraped to remove the carbon formed and subsequently allowed to reimmerse into the electrolyte. The scraped carbon was received on a conveyor belt, that further dropped it into a collection vessel. The material footprint of such electrolyser, for its subsequent use in lifecycle carbon emission calculation, was calculated in consultation with Stuart Licht's research group who estimated 114 nickel anode and 114 steel cathode roller plates of dimensions 10.0m x 10.0m x 0.05m (length x width x thickness) along with a conservative estimation of 16,880 tonnes/8000 m3 of lithium carbonate requirement. The continuous operation of such a plant was assumed to entail a yearly replacement of the cathode, a 5-year replacement of the anode, and an electrolyte loss of 50 kg per tonne of solid carbon produced. The flue gas CO_2 feedstock from the cement plant was assumed to be entering the process at a temperature of 800-900 °C and was assumed to sustain the electrochemical reaction without an additional heat source. The electricity consumed by the electrochemical process was calculated using the 4.8

$$Electricity = n_m \times n_e \times F \times V \times \frac{1}{3600x1000} \frac{kWh}{tonne CO_2} \tag{4.8}$$

n_m = no of moles of CO_2 reacting
n_e = no of electrons to convert 1 mol of CO_2 to 1 mol of C
F = Faraday's constant = 96, 485 Amps-sec

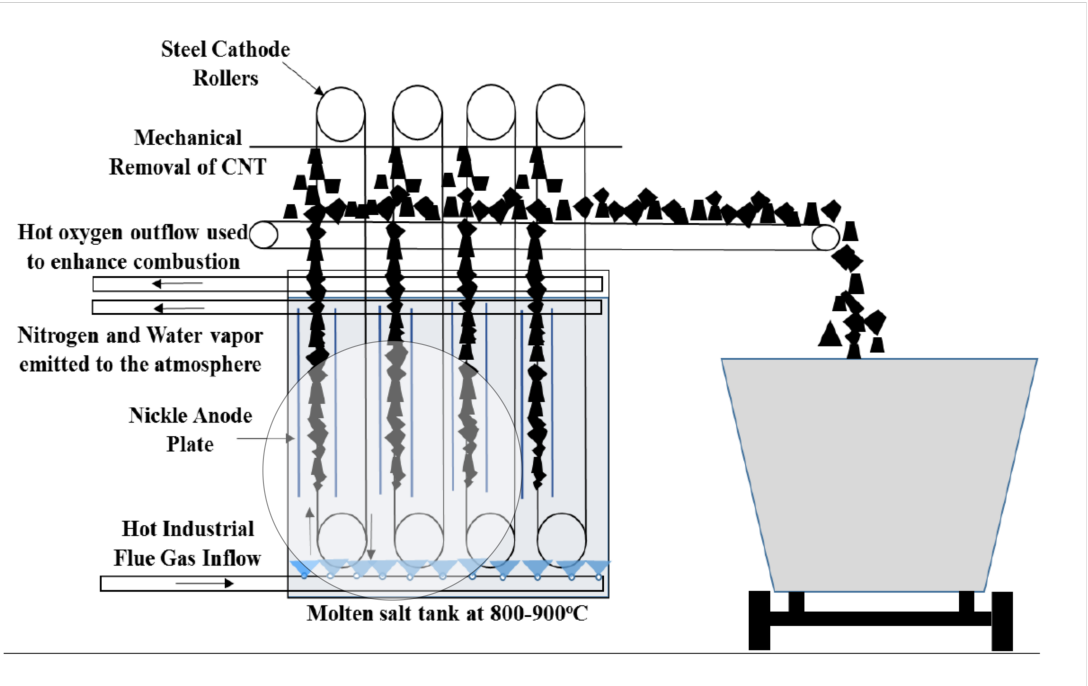

Figure 4.10: Commercial scale electrolyzer as conceptualized by Srininvasan (2018)

The circular highlighted region in Figure 4.10 is further contextualised to the requirements of this study in Figure 4.11, taking into account the data from Douglas et al. (2018), Douglas et al. (2017). 80% of the electrode surface area was assumed to stay immersed into the electrolyte to maximize their productivity while leaving enough space for the MWCNT to be scraped, based on discussions with Prof. Ruud Kortlever. Galvanized steel cathode, based on the study Douglas et al. (2017), is considered in the electrolyser given that it is stated to form 99% MWCNT and that it is a simpler and more easily available cathode than compared to the nm thickness Fe layer electron beam deposited stainless steel cathodes from Douglas et al. (2018). The cathode steel roller is assumed to roll slowly such that 80% of its length rolls through the electrolyte for an hour, which is the time duration considered in Douglas et al. (2017). The cathode productivity, calculated in terms of the MWCNT produced from unit cathode surface area, as provided in Douglas et al. (2018) is considered for estimating the total cathode surface area and an equivalent anode surface area required. CO_2 stream from the Porthos is shown to be bubbled from the base of the electrolyzer for diffusion into the molten liquid electrolyte and regeneration of Li_2CO_3 through reaction with Li_2O, as shown in

Eq.4.6. The MWCNT is shown to form on both sides of the cathode throughout its passage within the electrolyte. The described electrode and electrolyte setup is assumed to be housed in jacketed vessel equipment capable of maintaining 750°C high-temperature conditions and with openings in the top for the rolling steel cathode to pass through and undergo scraping. Douglas et al. (2018) provides an overall energy consumption figure - 54 kWh/kg MWCNT -of the experimental electrolytic reactor that is electrically heated via a ceramic heater, as shown in Figure.4.7. The details on the energy consumption breakdown by heat and electricity are unfortunately not provided. Considering the data unavailability and preference for maximizing the possibility of sustainable renewable energy use, this study assumes the heat stream passing through the jacketed vessel to be generated from electric heating equipment. One such electric heating equipment, identified for use in this study, is the RotoDynamic Heater from Coolbrook (n.d.). The 90% claimed energy efficiency of the RotoDynamic heater makes such an electric heating system favourable for application in this study as it allows for scaling of the 54 kWh/kg MWCNT energy consumption figure, from Douglas et al. (2018), to a figure proportionate to the commercial-scale production capacity considered in this study without the risks of overstating or understating this scaled value by a large amount.

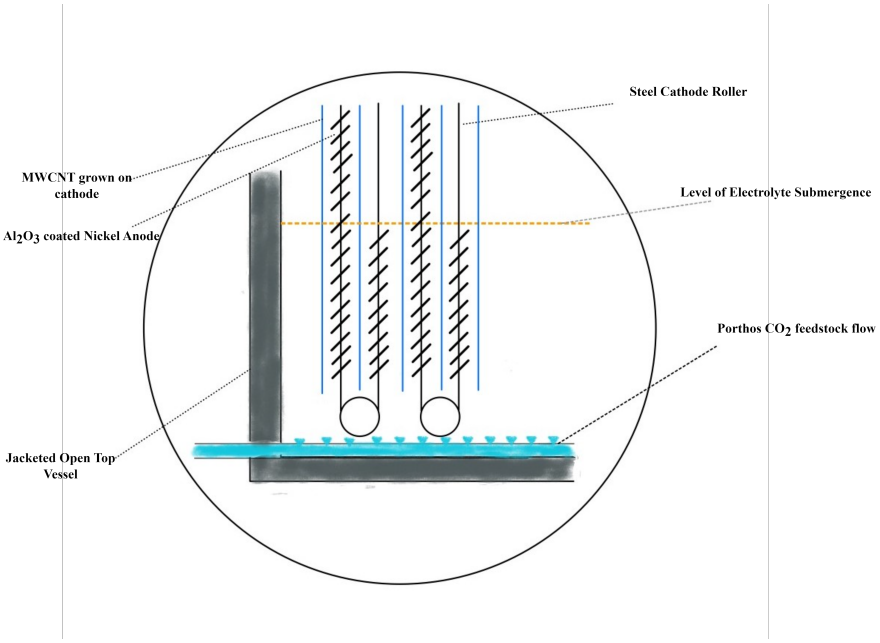

Figure 4.11: Re-visualised electrolyser

Commercial scale MWCNT produced from such electrolyser requires post-processing steps to remove any impurities present and deliver market-ready MWCNT. Based on the PD developed for status quo CVD process, as shown in Figure 4.5 and adapting it to the specifications suitable for the 99% MWCNT , as produced in Douglas et al. (2017), the PD for the ex-ante CO2 based MWCNT production methods is developed, as shown in Fig.4.12, highlighting its main process components excluding the utilities.

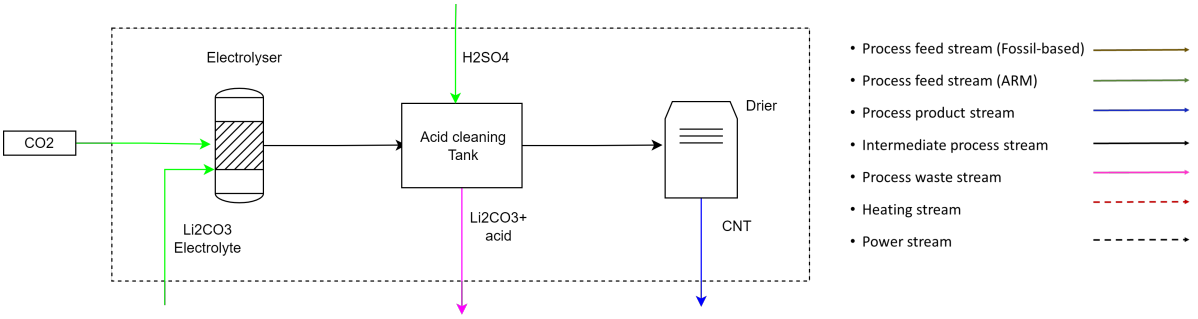

Figure 4.12: PD for ex-ante CO_2 based MWCNT production

The MWCNT produced from the electrolyser is based on Douglas et al. (2017) and is assumed to be of 99% purity with the presence of negligible amorphous carbon thus not requiring an oxidizer, as demonstrated in CVD PD in Figure 4.5. Further, the scraping of the cathode for the MWCNT collection potentially results in small quantities of Fe forming part of the MWCNT, although no mention of it was made in either Douglas et al. (2017) or Douglas et al. (2018). As mentioned in Sriniinvasan (2018), around 50 kgs of Li_2CO_3 electrolyte is thought to leave the electrolyser along with the MWCNT, necessitating its removal. This removal is assumed to be facilitated by the treatment of produced MWCNT with H_2SO_4 solution (Patnaik, 2003) of 5M, basing on the acid treatment demonstrated in section 4.2, in the acid leaching tank according to the Eq. 4.9. Although, Douglas et al. (2018), Douglas et al. (2017) use HCL acid for washing, H_2SO_4 is used in this study since it is known to be less corrosive than HCl, and thus making it easier to handle at an industrial scale, based on discussions with Prof. Earl Goetheer. The MWCNT is easily separated from the resulting solution using a centrifuge and is subsequently washed with demineralised water multiple times until a neutral pH is observed. The cleaned MWCNT is then placed in a dryer to remove any moisture content, resulting in market-ready MWCNTs. The ex-ante CO_2 based MWCNT production process is thus evident to have lesser unit operations than compared to that of status quo CVD process

$$Li_2CO_3 + H_2SO_4 \longrightarrow CO_2 + H_2O + Li_2SO_4 \tag{4.9}$$

4.4. Basis of Design

The scale of the novel CO_2 based process and status quo CVD process for MWCNT production is decided on the factors of data availability and geographical relevance. The conceptual process designs on HiPCO and CoMoCat processes by A. E. Agboola et al. (2007) were scaled to an annual capacity of 5-kilo tonne SWCNT. On the other hand, the Belgian Nanocyl company, whose moving bed reactor design is selected as this study's status quo CVD process, had an annual production capacity of 400 tons of MWCNT. Subject experts - Prof. Earl Goetheer and Prof. Paola Ibarra Gonzalez - consulted in this study suggested that the ex-anteCO_2-based CNM production process be such that it can process CO_2 flows in kilo-tonne scales, which is compatible with the scale of CO_2 emissions from individual plants in the Port of Rotterdam region that contribute to the PORTHOS CO_2 stream. Considering the aforementioned factors and suggestions, a 5 kilo-tonne scale of annual MWCNT production, similar to that from A. E. Agboola et al. (2007) is considered in this study.

The process designs for the CO_2-based process and the status quo CVD process are made with the aim of producing commercial MWCNT specification of CNM with >90 wt.% carbon purity of diameter 10-50nm.

Process simulation guidelines from NWO VICI project - 'Unravelling the impacts of using alternative raw materials in industrial clusters' are utilised in this study, as advised by Prof. Paola Ibarra Gonzalez. These process guidelines include the colour coding of streams applied in Fig. 4.5 and 4.12, nomenclature for identifying streams and equipment, and involve standards on the process conditions of various hot and cold utilities involved in the high-temperature operating conditions of the selected processes, as outlined in Figure 4.13. An operational year is considered to have 800 operational hours. The guidelines include the consideration of no pressure drops in the process simulation. Further, the natural gas input feedstock of the status quo CVD process for CNM production and the composition of air stream used in both processes is according to the VICI specifications highlighted in Figure 4.14.

Cooling type	Inlet Temperature (C)/Vapour fraction	Pressure (bar)	Outlet temperature (C)/vapour fraction	Minimum Delta T (Utility temperature with process fluid)	Process fluid temperature range (C) For reference
Chilled water	5	1.02	7,5	5	10-30
Cooling water	25	1.02	40	5	152-30
LLP steam generation	0	3.9	1	10	164-153
LP steam generation		5.5		10	224-165
MP steam generation		21		10	274-225
HP steam generation		51		10	450-275

Steam type	Inlet vapour fraction/ Temperature (C)	Steam pressure (bar)	Outlet vapour fraction/ Temperature (C)	Minimum Delta T (Condensation temperature with process fluid) (K)	Steam Temperature for reference (°C) (in/out)
LLP steam	1	3.9	0	10	143-142
LP steam		5.5		10	155.5-154.4
MP steam		21		10	215-214
HP steam		51		10	265-264
VHP steam	500 C	100	0	10	500-311
Fired heat	1000	2	750		1000-750

Figure 4.13: VICI guidelines on cooling (left) and heating(right) utilities

Natural Gas Component	Process air Mole fraction	Combustion air Mole fraction
N2	0,777	0,79
O2	0,209	0,21
Ar	0,0093	-
H2O	0,0044	-
CO2	0,0003	-

Air Component	Mole fraction
CH4	0,814
C2H6	0,03
C3H8	0,002
N2	0,144
CO2	0,01

Figure 4.14: VICI air(left) and natural gas(right)specifications

For the CO_2 based process, the 'gate to gate' scope assumes the use of 95 mol% purity CO_2 from the Port of Rotterdam CO Transport Hub and Offshore Storage (PORTHOS) as input

feedstock (Porthos, 2021). The composition of the PORTHOS supplied CO_2 stream is as shown in Fig. 4.15. The input CO_2 feedstock stream's operating conditions include 4°C temperature (NOGEPA, 2008) and 35 bar pressure (Porthos, 2023).

PORTHOS Stream Components	Mole Fraction
CO2	0,95300
H2O	0,00007
H2	0,00750
N2	0,02400
AR	0,00400
CH4	0,01000
CO	0,00075
O2	0,00004
ETHANOL	0,00002
METHANOL	0,00062

Figure 4.15: PORTHOS CO_2 feed compositions

5

Process Modelling

This chapter builds on the PDs developed in Sections 4.3 and 4.2 further by first discussing the use of aspen, followed by stating the general assumptions considered and lastly describing the Aspen modelling and simulation of the two PDs consecutively.

5.1. Using Aspen

This study uses Aspen Plus V12 process simulation software from AspenTech to develop the process models based on the PDs shown in Fig. 4.5 and 4.12. Using Aspen Plus enables high flexibility in terms of the diverse process configurations, which allows for the optimisation of varying operational conditions, and determination of limitations of processes subject to the various operating conditions (Mutlu & Zeng, 2020). The Aspen simulation software however also has limitations with respect to modelling certain process units. Novel technologies such as CO_2 electrolyser, currently cannot be modelled solely using Aspen.

The process simulations from Aspen Plus provide information on the mass magnitudes of various inflow and outflow substances along with the consumption and generation of different forms of energy by various unit process operations. The economic costs are further calculated using the Aspen Process Economic Analyser (APEA) software, which is included in the aspen plus software. The APEA maps and sizes the various equipment required based on its function, its operating conditions and the mass and energy flows associated with it, to ultimately evaluate the individual equipment cost. Such information helps users evaluate the process models on their technical, economic and environmental performance to understand the feasibility of their real-world implementation.

5.2. General Assumptions

This study involved the following general assumptions :

1. The performances as outlined in the studies of the processes selected are assumed to be achievable for the scaled-up processes developed in this study for commercial MWCNT production

2. The general temperature and pressure conditions of the inlet flows and process units are assumed to be ambient operating conditions of 15°C and 1.02 bar, in accordance with the VICI guidelines
3. Components other than the main carbon precursor, in the inlet flows to the CVD reactor/electrolyzers modelled in this study, are assumed to be inert and not take part in the process
4. The solids thermodynamic property method is assumed to be applicable for the modelling of both processes, given that solid MWCNT is the resultant product
5. The equipment used in various units operations is assumed to be capable of handling nanometre-sized MWCNT
6. Particle size distribution (PSD) is assumed to be applicable to the produced MWCNT along with the other solid substances. The stream class - 'MIXCIPSD' is used to reflect the PSD of the solid products
7. The material components used in the Aspen model are of conventional type unless explicitly specified otherwise
8. The processes are modelled as steady-state continuous processes that produce 625 kg/hr of MWCNT resulting in a 5-kilo tonne annual production capacity with 8000 operational hours
9. The natural gas and air steams are as shown in Fig. 4.14
10. Temperatures for various equipment and streams, unless explicitly specified by the modeller, are assumed to be estimated by Aspen during the simulation
11. Default equipment automatically mapped and sized by APEA are assumed unless explicitly specified by the modeller
12. The types of heat exchanger equipment used in the process simulation varied with their operating temperature conditions and hence, are manually selected by the modeller, in accordance with the Aspen ICARUS handbook
13. The heating and cooling heat exchanger process units with varying temperature steps are modelled considering the temperature limits of the various utility streams described in Fig. 4.13

5.3. Status Quo CVD

Based on the PD portrayed in Fig.4.5 , a corresponding Aspen process simulation has been developed as shown in Fig.5.1 . The guidelines on the nomenclature for streams and equipment, as mentioned in Section4.4, are used in this process diagram. The Aspen process diagram constitutes various unit process operations, represented by icons designated by Aspen. It incorporates the crude process flow shown in Fig. 4.5 by detailing the requisite equipment, such as reactors, and supplementing it with auxiliary equipment, such as heat exchangers, to best represent a real-world industrial-scale process for MWCNT production. This Aspen process diagram is broadly separated into three process blocks:

1. MWCNT production through the CVD reaction of CH_4 on the catalyst followed by the separation of the MWCNT, amorphous carbon and catalyst solid substances from the unreacted input gas feedstock

2. The purification of produced MWCNT from the CVD reactor to >90 wt% MWCNT content through the removal of other impurities of amorphous carbon and catalyst particles
3. The separation of excess H_2 produced from the CVD decomposition of CH_4 in the exit gas stream of the CVD reactor for further reuse in the system.

The following subsections describe the streams and unit process operations of the three process blocks individually in detail by traversing from the starting (leftmost) stream to the ending (rightmost) stream of each process block. The calculations and data for this process simulation can be referred to from Appendix B -1,2 and 3.

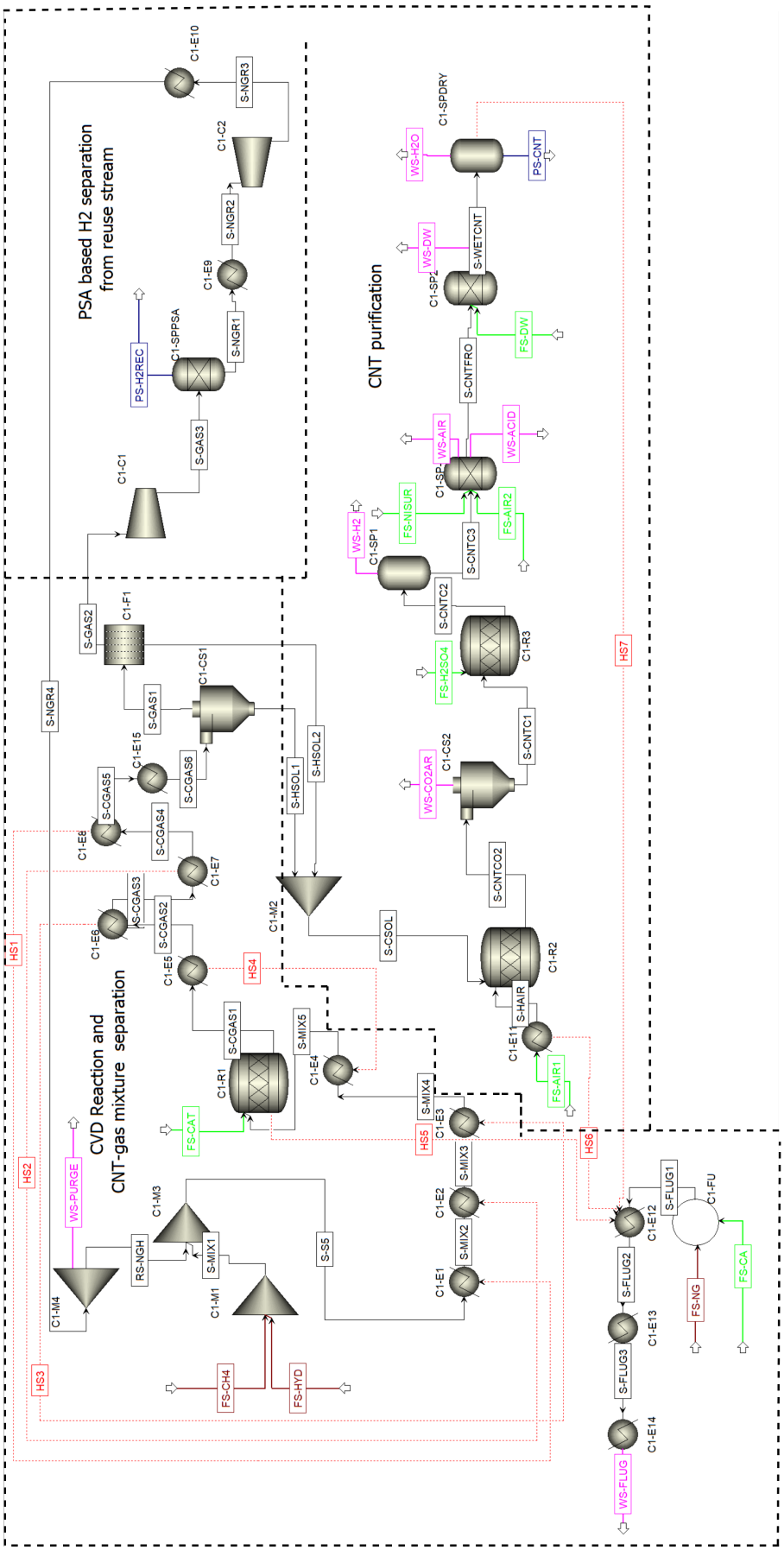

Figure 5.1: Aspen process diagram of status quo CVD process segregated into three process blocks

5.3.1. CVD Reaction and CNT-Gas Separation

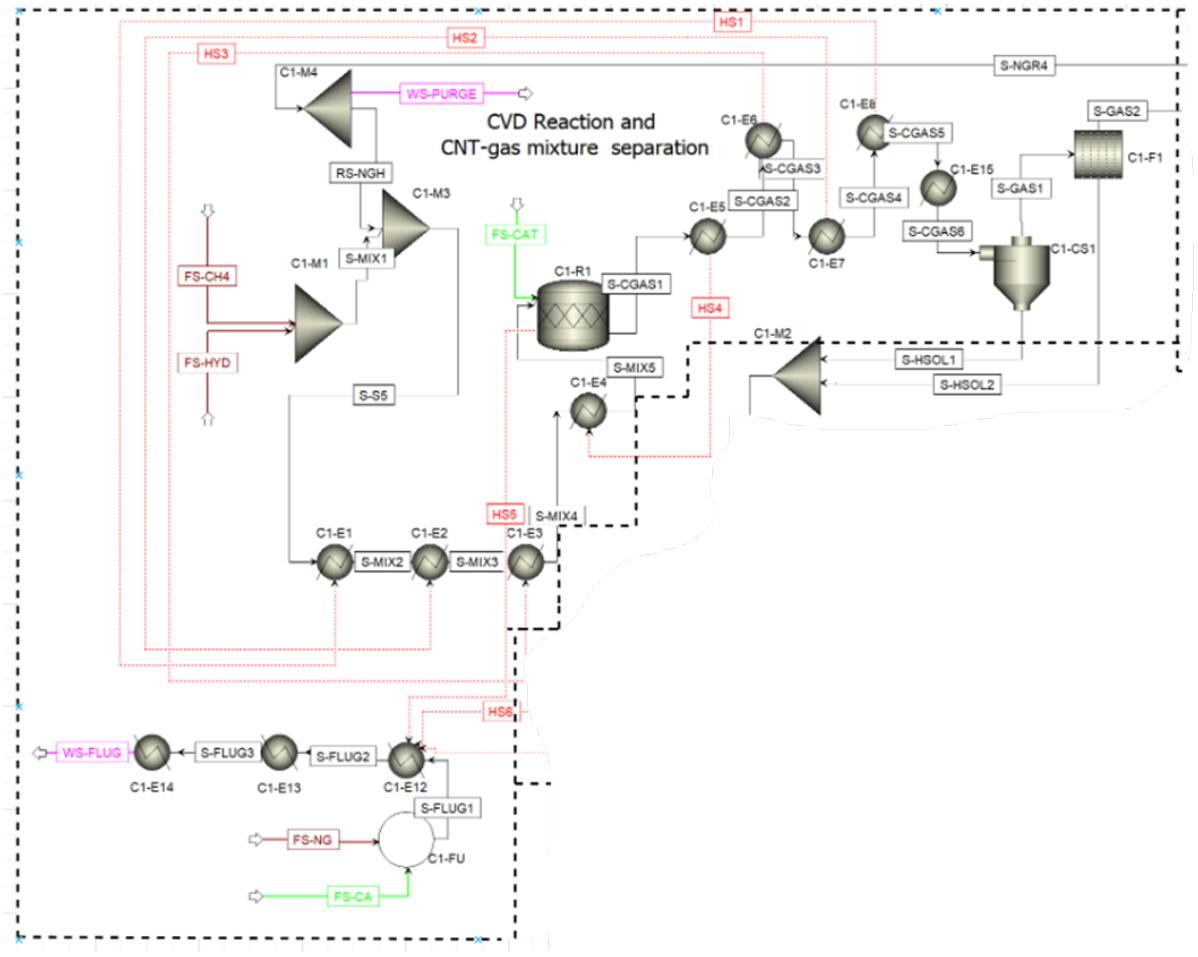

Figure 5.2: CVD Process Block 1

The CVD reaction involves the use of CH_4 as the carbon precursor that decomposes into carbon, in the form of MWCNT and amorphous carbon, and H_2. The modeller assumes the CH_4 entering the system to be sourced from the industrial natural gas streams from the pipelines operating within the Netherlands, with a composition indicated in Fig. 4.11 and with operating conditions of 15°C and 1.02 bar. It can be observed that this natural gas stream consists mainly of CH_4 (81.4%), followed by N_2 (14.4 %) and CO_2 (1%) along with traces of C_2H_6 and C_3H_8. This input feed stream of natural gas (FS-CH_4) is supplemented with a H_2 stream (FS-HYD) of 99.8% purity, with 0.2% contaminant being CH_4, also at 15°C and 1.02 bar. This H_2 stream is sourced from the H_2 separated from the PSA system that is described further in detail in Section 5.3.3. Fig.5.2 shows these two streams entering the system and together forming a single stream via a mixer (C1-M1). The unused input stream (S-NGR4) from the previous cycles is recycled into the system. Prior to being introduced into the reactor, this recycled stream goes through a purge (C1-M4) of 6% of its original mass based on discussions on best industrial practices and resource efficiency optimization with Prof. Paola Ibarra Gonzalez and PhD. supervisor James Tonny Manalal. Such a purge limits the accumulation of impurities present in the input feed streams - such as those of nitrogen, carbon dioxide, C_2H_6 and C_3H_8 - thus preventing the dilution of the main reactant - CH_4. Upon purging, the recycled stream

(RS-NGH) is shown to combine with the stream of new feedstock through a mixer (C1-M3). Through trial and error, the input streams of FS-CH_4 and FS-HYD are manipulated to achieve an overall CH_4-to-H_2 molar ratio of 9:1, as described in Section 4.2, to yield the best reaction productivity. It is important to note that the mixer equipment shown in this process diagram is implemented to prevent Aspen from generating errors, however, they do not exist in the actual plant owing to the highly miscible nature of gases that allows them to freely mix with each other.

The combined feed stream (S-S5) is heated through heat exchangers (C1-E1, C1-E2, C1-E3, C1-E4) in four steps of varying magnitudes of temperature increase ranging from 115 to 338 °C to ultimately reach a temperature of 956°C. This heated stream (S-MIX5) enters the moving bed reactor (C1-R1) to undergo chemical vapour deposition in the presence of the Ni-Mo/MgO catalyst (FS-CAT). Ni-Mo/MgO catalyst comprising 15 wt% Ni-solid type, 15 wt% Mo-solid type, and 70 wt% MgO-solid type is considered in this study based on Saconsint et al. (2022), owing to its similarity to this study with respect to the use of CH_4-based biogas to produce MWCNT and lack of sufficient data on the catalyst preparation from Douven et al. (2012) . The operating conditions for a 90% purity level of MWCNTs based on Douven et al. are used in this study. The calculation based on the data from these operating conditions, as shown in Appendix B1, shows that approximately 16% of the input methane converts into carbon, according to Eq.4.1 .As described in Section 4.2, 80% of this carbon is assumed to be MWCNT and the remaining 20% comprises of amorphous carbon. The other carbon precursor gases such as CO_2, C_2H_6 and C_3H_8, which form part of the reactor's input stream, are assumed to not take part in the reaction and stay inert owing to their low concentrations and the lack of data on their CVD mechanisms in the presence of a dominant CH_4 stream supply considered in this study. The N_2 gas in the input reactor stream, however, is generally known to be inert and is thus assumed to not play any role in this CVD process. Factoring this information into the Aspen model, a stoichiometry-based Aspen reactor unit is implemented for C1-R1 that comprises two reactions in which 12.8% and 3.2% of input methane break down to form MWCNT-solid type, with an Aspen component id C, and amorphous carbon-solid type, with an Aspen component id AC, respectively. The reactor is assumed to operate at 975°C and an atmospheric pressure of 1.02 bar based on Douven et al. (2012). Based on the 450s mean residence time of the reaction(Douven et al., 2012), the required reactor volume for the production of 625 kg/hr of MWCNT is estimated as 210 m^3, as calculated in Appendix B3. A generic PSD mesh based on two intervals - 5 to 20nm and 20 to 100nm - is considered in this study based on the MWCNT diameter sizes of 5 to 20nm (Douven et al., 2012). and an assumption that the amorphous carbon particles have a diameter of up to 100nm. Such PSD has been applied to the input catalyst feedstocks with weight fractions of 0.9 and 0.1 for the smaller and larger diameter distribution interval respectively, assuming that 90% of the catalyst size particles belong to the smaller diameter distribution interval. For the MWCNT and amorphous carbon solids produced from the CVD reaction, the weight fractions of 0.8 and 0.2 for the smaller and larger diameter distribution interval respectively are assumed based on the 80% and 20% proportions of MWCNT and amorphous carbon formation respectively.

The heat required to maintain the 975 °C temperature condition of C1-R1 is provided by the fired heat furnace modelled as C1-FU. The C1-FU is modelled in Aspen as a reactor with input natural gas (FS-NG) and air (FS-CA) stream with compositions, as shown in Fig. 4.11, and at

operating conditions of 15°C and 1.02 bar. The reactor is modelled as a combustion chamber wherein the primary constituent methane along with the other hydrocarbons exothermically react with air generating flue gas stream (S-FLUG1) at high temperatures. A design specification was also applied to the air stream (FS-CA) to estimate its required quantity based on the oxygen required for the combustion reaction to generate heat of the requisite high temperature. The heat from this high-temperature flue gas stream is captured from the heat exchanger C1-E12 which transfers the requisite heat via the heat stream HS-5 to the CVD moving bed reactor(C1-R1). It is important to note that the icon representing C1-FU by Aspen is that of a calculator block and not a reactor owing to an unresolvable error. From C1-E12, the exiting flue gas stream is passed through two more heat exchangers- C1-E13 and C1-E14 - that generate saleable MP steam and LP steam respectively before the flue gas stream(WS-FLUG) is released into the atmosphere. This waste flue gas stream is modelled to be liberated into the atmosphere at a temperature of 200°C based on the maximum safe temperature limits for the release of flue gases into the atmosphere, realized from a discussion with PhD. supervisor James Tonny Manalal.

The outlet stream (S-CGAS1) of C1-R1 constitutes the unreacted input gas stream, H_2, MWCNT, amorphous carbon and catalyst particles at a high temperature of 975°C. This mixture of gas and solids is cooled down through five heat exchangers, in five steps of varying magnitudes of temperature decrease ranging from 85 to 325°C, to a final stream temperature of 15°C from the heat exchanger C1-E15. Simultaneously, the heat captured from the preceding four heat exchangers (C1-E5, C1-E6, C1-E7 and C1-E8)) is transferred to heat exchangers (C1-E1, C1-E2, C1-E3 and C1-E4) with comparable heating and temperature requirements that collectively heat the input feed stream of C1-R1 reactor from 15°C to 956°C. This heat integration ensures that no temperature cross occurs and thus allows the optimisation of heat energy usage. The two-stage solid filtration described in Section 4.2 is carried out first through a cyclone separator that is assumed to separate 96% of the solids into the solids stream(S-HSOL1) and the remaining 4% of the solids enter the gas stream(S-GAS1). The second filtration of the solids is carried out by the fabric filter that is assumed to separate the entirety of the solids in the input gas stream (S-GAS1) into a separate solid outlet stream (S-HSOL2), leaving a pure gas outlet stream (S-GAS2).

5.3.2. CNT Purification

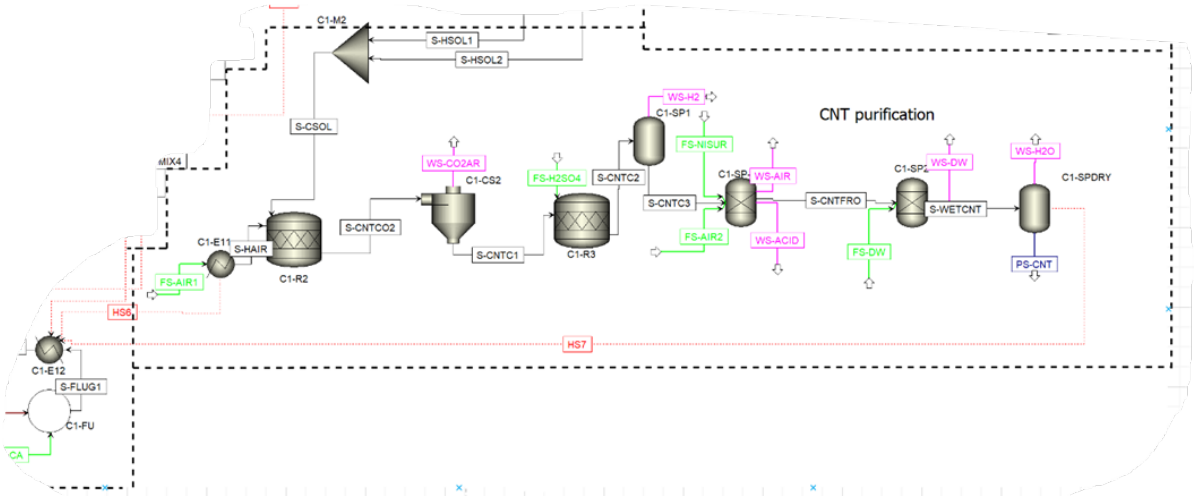

Figure 5.3: CVD Process Block 2

The separated solid streams of S-HSOL1 and S-HSOL2 are shown in Fig. 5.3 as being sent to the mixer C1-M2, for combining them into a single stream (S-CSOL). In the actual plant however, these solids are assumed to be collected together in a container and do not require a mixer. The solids stream (S-CSOL) undergoes oxidation in C1-R2, as described in Section 4.2, with operating conditions of 250°C and 1.02 bar. The air stream (FS-AIR1), which acts as the source of oxygen for the oxidation reaction, is first heated through a heat exchanger at 250°C given that the oxidation in C1-R2 occurs at 250 °C. This heat exchanger derives the requisite heat from C1-E12 , as outlined in Section5.3.1, through the heat stream HS6. The quantity of air required is estimated through a design specification incorporated into the model that calculates the oxygen content of air needed for the oxidation of the amorphous carbon present in S-CSOL. The reactor equipment used for this oxidation is sized to require $8m^3$ of volume (Appendix B) based on the combined volume of air and solids entering the reactor in an hour and the residence time data applied in C1-R1 due to lack of relevant data for the oxidation process unit. Due to a lack of data on the vacuum-compressed filter mechanism and the air-blowing equipment required, they are not considered in this model. In C1-R2, 100% of the amorphous carbon present in S-CSOL is assumed to undergo oxidation to formCO_2 according to Eq.4.2. Further, the oxidation reaction is understood to be exothermic upon simulation of the aspen model due to which the modeller has connected a low-pressure steam generation utility to C1-R2 for the valorisation of the heat generated.

The resulting gas-solid stream consisting of unused components of air,CO_2, MWCNT and catalyst particles are sent to a cyclone (C1-CS2) for separation into solid(S-CNT1) and gas(WS-CO2AR) streams. These separated solid and gas streams are assumed to comprise purely of solids and gases. The gas stream is released into the atmosphere as a waste emission that comprises significant CO_2 amounts.

The oxidized solid stream(S-CNTC1), which comprises the MWCNT and the Ni-Mo catalyst particles with MgO support, is transferred to C1-R3 for the acid-leaching process to enhance the

MWCNT purity of the final product. An acid feed stream (FS-H2SO4) of sulphuric acid, with composition as calculated in Appendix B2 based on quantities of Ni-Mo/Mgo catalyst present in S-CNTC1, is introduced into C1-R3 to carry out the acid leaching. The acid leaching in C1-R3 assumes 100% of MgO (Eq 4.3) and 20% of Ni (Eq4.4) to be consumed, as described in Section 4.2. Acid leaching in C1-R3 is assumed to take place in an agitated reactor, as mapped and sized by APEA, for a time period of 1 hour at operating conditions of 50°C and 1.02 bar. The heat duty required by C1-R3, as estimated by Aspen, is supplied through low-pressure steam utility. The resulting stream (S-CNTC2) of the acid salt aqueous solution, MWCNT-catalyst solids, and H_2 gas is passed through a flash separator (C1-SP1) to release the H_2 gas, generated from the acid leaching process in C1-R3, leaving behind the liquid stream of S-CNTC3. This H_2gas is assumed to be emitted into the atmosphere as a waste stream owing to its low quantities of less than 1 kg/hr of production.

The S-CNTC3 stream is passed through a froth flotation process in C1-SP-FF. The froth flotation process as described in Section 4.2, requires input feedstocks of non-ionic surfactant solution of Surfonic L24-7 and air stream to initiate the separation of undissolved solids from the aqueous solution in the froth flotation column. Based on surfactant concentration data from Lertrojanachusit et al. (2013) and the quantity of solids in S-CNTC3 stream entering C1-SP-FF, the quantity of surfactant solution is estimated as shown in Appendix B1. The quantity of air entering the reactor is assumed to be 1kg/hr by the modeller to be realistic and considerable given that the geometrically scaled value from Lertrojanachusit et al. (2013) is too high, whereas the value from A. E. Agboola et al. (2007) is too low (Appendix B1). It is assumed that the input feed streams of C1-SP-FF, mentioned thus far, gradually enter the column over a period of one hour. During this one hour, the froth stream (S-CNTFRO) dropping into the froth receiver, as shown in Fig. 4.6 is assumed to separate out 100% of MWCNT, 95% of the surfactant and 5% of water in the assumed mean residence time of 24s (Yianatos et al., 2008). The Ni-Mo catalyst particles are assumed to be separated from the CNT completely through the force of air-bubbled froth, thus leading to pure MWCNT output. This assumption was taken to make this pure CNT comparable to that produced from the electrochemical process. The % separation of other components was done arbitrarily based on discussion with the thesis supervisors. The air stream (WS-AIR) bubbled exits the column from the top and the leftover aqueous solution (WS-ACID) exits from the bottom, as shown in Fig. 4.6. Aspen lacks provision for such a froth flotation column due to which a separator block is incorporated in this study. Due to scarce data on the equipment of the froth flotation column required for this scale and the lack of relevant data on APEA, this equipment is not mapped or sized, however, its costs are sourced from A. Agboola (2005). The utilities associated with driving the airflow of 1kg/hr are assumed to be minimal and hence not considered in this study.

The S-CNTFRO stream, constituting majorly the surfactant froth and MWCNT, is assumed to undergo several rounds of washing with demineralized water (FS-DW) and subsequent centrifugation, all in the separator block modelled as C1-SP2. The C1-SP2 has an input stream of demineralized water which is arbitrarily assumed, owing to lack of data, to have roughly a total input equal to half of the CNT produced, as shown in Appendix B1 . A disk centrifuge is mapped for C1-SP2 in Aspen APEA. The equipment required for washing the CNTs is assumed to have minimal impact on the study's results and hence is not considered. The

difficulty stemming from modelling the two processes of washing and centrifugation in one separator process unit makes it difficult to ascertain the utilities associated with this process unit. Therefore, the utilities for this process unit are also disregarded assuming that they have a minimal impact on the results of the study. C1-SP2 is assumed to separate 99.95% of MWCNT and remaining catalyst solids, and 20% of the water as S-WETCNT. This leaves 0.05% of MWCNT and catalyst solid for spillage into the waste stream (WS-DW) along with the waste liquid solution of surfactant and water.

S-WETCNT stream undergoes drying in the C1-SPDRY process unit which is modelled as a separator flash in Aspen for ease of simulation, based on advice from PhD supervisor James Tonny Manalal. However, on APEA, C1-SPDRY is mapped and sized as a single atmospheric drum dryer. C1-SPDRY is assumed to operate at 200°C based on observation from studies - A. E. Agboola et al. (2007), Lertrojanachusit et al. (2013), and Pornsunthorntawee et al. (2011) - yielding the dry MWCNT final product (PS-CNT). Steam generated from the liberation of moisture present in the input wet MWCNT stream is released into the atmosphere as waste emissions (WS-H2O). The heat energy for the drying of MWCNTs at 200°C in C1-SPDRY is provided through the heat stream HS7 connected to the heat exchanger C1-E12, as described in Section 5.3.1.

5.3.3. PSA based H_2 separation

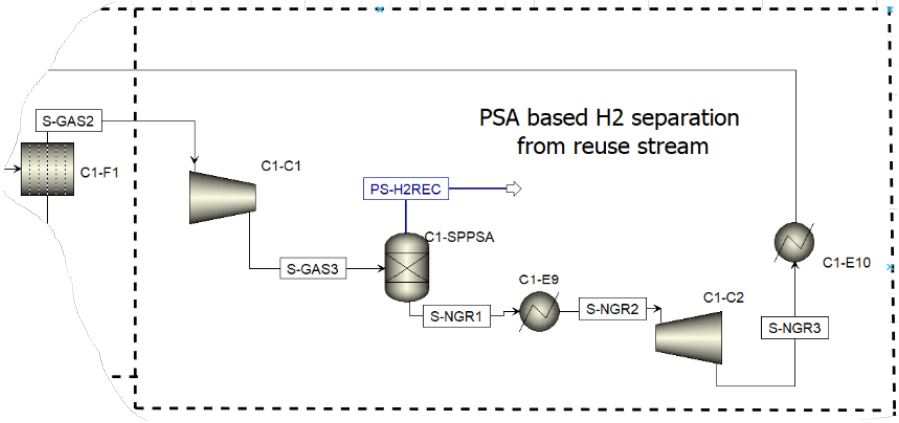

Figure 5.4: CVD Process Block 3

The S-GAS2 stream leaving the fabric filter, as described in Section 5.3.1 and shown in Fig.5.4, comprises the unreacted carbon precursor CH_4, CVD generated and pre-existing H_2, and the accumulated non-CH_4 constituents of the natural gas stream - N_2, C_2H_6, C_3H_8 and CO2. The S-GAS2 stream, which is operating at 1.02 bar pressure, undergoes compression in the compressor process unit (C1-C1) to achieve a 20 bar pressure stream(S-CGAS3) for subsequent PSA based separation(Burgers, 2020) into a saleable 99.8% H_2 stream (PS-H2REC) and CH_4 constituting reuse stream (S-NGR1), as described in Section 4.2.

The PSA system is assumed to separate out 80mol% of the H_2 and 0.082mol% of CH_4 in S-GAS3 as 99.8mol% outlet H_2 stream (PS-H2REC), based on Burgers (2020). The input gas mixture concentrations and output gas flow concentrations, as shown in Burgers (2020). are

different compared to those of this study. As opposed to the 10 mol% H_2 concentration of PSA input stream in Burgers (2020), the S-GAS3 input stream in this study has approximately 20mol% H_2. Thus, this study assumes that the PSA system from Burgers (2020) is applicable to the steam compositions of this study as well. Therefore C1-SPPSA separates 80% of the 20 mol% H_2 present in the inlet stream along with methane separation of 0.082mol% resulting in PS-H2TREC with 99.8% H_2 and 0.2% CH_4.

The PSA process unit (C1-SPPSA) is shown on Aspen as a separator block due to the non-availability of a pre-defined Aspen process unit for PSA. In addition, due to limited data on the equipment of the PSA system applicable to the scale required for this study and the lack of requisite data on APEA, this equipment is neither mapped nor size. However, the capital costs outlined by Burgers (2020) are geometrically scaled to the requirements of this study for its subsequent use in capital expenditure estimation. The utilities associated with the PSA process unit of this study are assumed to be minimal, based on Burgers (2020) and are hence not considered in this study. The mentioned PSA system is assumed to be tolerable to high temperatures of the input gas stream (S-GAS3), resulting from its compression to 20 bar from 1.02 bar, which is a limitation given that the PSA system in Burgers (2020) operates at 25°C.

The S-NGR1 stream generated from C1-SPPSA, at 20 bar pressure and 380°C,is cooled down in the heat exchanger C1-E9 to a lower temperature stream (S-NGR2) of 280°C, which is the maximum operable temperature range for subsequent decompression in the turbine C1-C2. The cooling is achieved in C1-E9 by means of high-pressure steam generation through the heat extracted from the S-NGR3 stream. C1-C2 turbine decompresses the S-NGR2 stream to the ambient pressure of 1.02 bar from 20 bar. The resulting depressurised stream (S-NGR3) is still at a high temperature of 99°C, due to which it is passed through the heat exchanger C1-E10 to achieve an ambient temperature condition of 15°C. Chilled water utility is connected to C1-E10 to meet the cooling requirements. The requirement of cooling S-NGR3 to the ambient temperature of 15°C is considered in this study assuming that it is necessary for subsequent mixing with streams of S-MIX1, as described in Section5.3.1 comprising the fresh input streams of natural gas and hydrogen.

5.4. Electrochemical CO_2 reduction

An aspen process simulation is developed based on the PD portrayed in Fig 5.5 and Section 4.3. The guidelines on nomenclature for streams and equipment, as mentioned in Section 4.4 , are implemented in the aspen process diagram Fig.5.5 . Similar to the aspen process diagram of the status quo CVD process, as shown in Fig. 5.1, the aspen process diagram for the electrochemical CO_2 reduction process is categorized into three blocks:

1. Handling of input CO_2 feedstock and outletO_2 emission gases
2. CO_2 electrolysis process resulting in MWCNT formation andO_2 liberation
3. Purification and process of MWCNT to >90 wt % to remove the electrolyte

These three process blocks are individually described in detail, with respect to their streams and unit process operations, in the following subsections. The descriptions of these process blocks begin with the material streams entering their boundaries, progress through the various

streams and process units along the course of the process and end with the final stream exiting their boundaries. The calculations and data for this process simulation can be referred to from Appendix C -1,2 and 3.

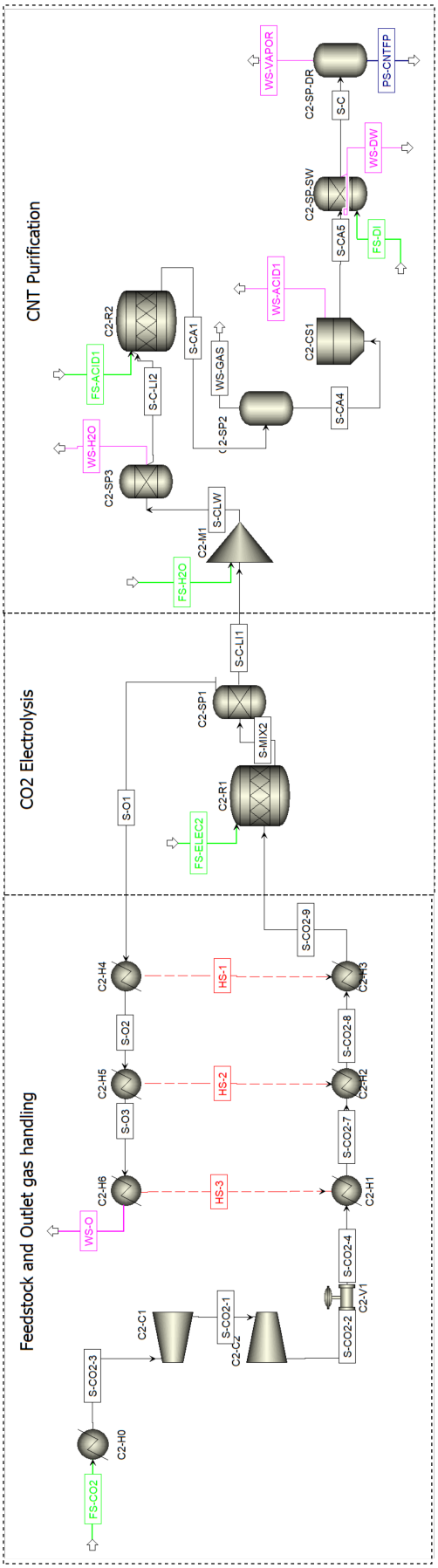

Figure 5.5: Aspen process diagram of electrochemical CO_2 reduction process segregated into three process blocks

5.4.1. Handling of Input Feedstock and Outlet gases

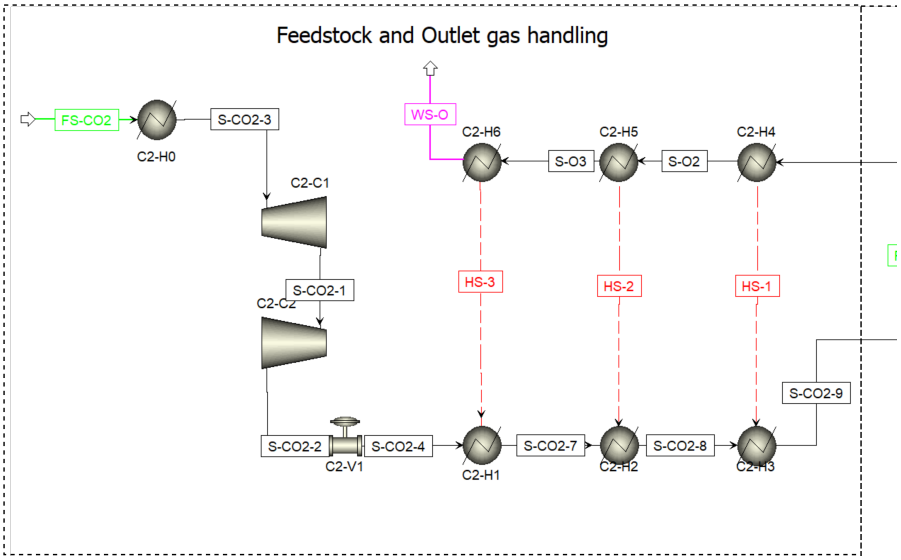

Figure 5.6: Electrochemcial CO_2 reduction - Process Block 1

The electrochemical CO_2 reduction process simulation, as shown in Fig5.6, considers the input feedstock of industrial flue gas origin CO_2, from Porthos with composition as shown in Fig. 4.15. The usage of such CO_2 aids in realising industrial symbiosis and circular economy within the Port of Rotterdam region. The CO_2 feedstocks stream (FS-CO2) enters the process system at 4°C and 35 bar pressure, as described in Section4.4. The electrolysis process considered in this study is assumed to operate at atmospheric/ambient pressure based on observations from molten salt based electrochemical CO_2 processes identified in the state of the art - Section 2.1, and discussions with Prof. Ruud Kortlever. Therefore, it is necessary to decrease the pressure to 1.02 bar of ambient pressure condition. The process of such depressurisation also results in a rapid temperature decrease of the CO_2 stream that would result in its condensation from a gas state to a liquid state. Also, the depressurisation turbine process units function only with gas state streams. For these reasons, the FS-CO2 stream first undergoes heating to 80°C in the heat exchanger C2-H0. Subsequently, the stream undergoes depressurisation in 2 steps of 10 bar and 15 bar in turbine process units C2-C1 and C2-C2 respectively, which also. The saleable electric utility is selected for these process units to valorise the power generated by them during depressurization. The resulting stream S-CO2-2 from C2-C2 is further depressurized by controlling its flow through the valve C2-V1, as a way to minimize the use of expensive turbine process equipment. The resulting stream (S-CO2-4) exiting C2-V1 achieves ambient pressure of 1.02 bar and a low temperature of 3°C.

Further heating of the S-CO2-4 streams, for use in the 750°C high-temperature electrolysis process (Section 4.3), is carried out through the heat exchangers C2-H0, C2-H1, and C2-H3 with temperature increase steps of varying magnitudes ranging from 137 to 178 °C. Such heating through multiple heat exchangers eventually results in S-CO2-9 stream with 470°C temperature. Further heating of this CO_2 feed stream to 750°C for the electrolysis process in C2-R1 is assumed to take place within the reactor equipment itself by the modeller to minimise the use of heat exchanger equipment used and improve the process economics. The

electrolysis process in C1-R1 results in the formation of MWCNT solids and the liberation ofO_2, in accordance with Eq. 4.7 in Section 4.3. The 750°C high-temperature stream (S-O1), which constitutes majorly electrolysis liberatedO_2 and unused CO_2 feed, is passed through three heat exchangers C2-H4, C2-H5 and C2-H6 with varying magnitudes of temperature decrease ranging from 175-215°C to capture the waste heat. The waste heat captured from those heat exchangers is transferred accordingly to C2-H3, C2-H2 and C2-H1 for heating of the input CO_2 feed stream, thus enabling efficient energy usage. The 750°C S-O1 stream is eventually cooled down to 160°C for release into the atmosphere as a waste emission steam(WS-O). Unlike the PSA-based H2 and CH_4 separation process utilised in the status quo CVD process, anO_2 and CO_2 separation process is not implemented in the electrochemical CO_2 reduction process as O_2 purification to high purities of >99% was perceived to be expensive, based on discussions with Prof. Earl Goetheer and Prof. Paola Ibarra Gonzalez. Additionally, the emission of such O_2 concentrated stream to the atmosphere would not contribute significantly to GHG emissions, thus making it considerably harmless for climate change.

5.4.2. CO_2 Electrolysis

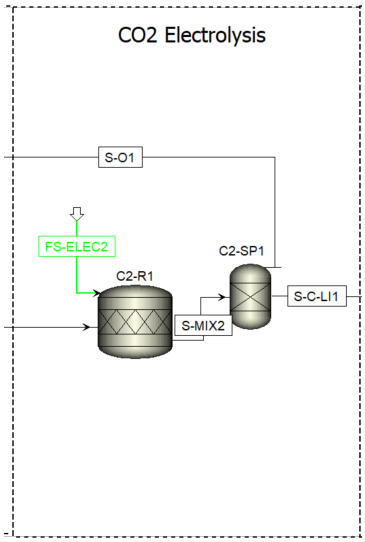

Figure 5.7: Electrochemcial CO_2 reduction - Process Block 2

The S-CO2-9 stream is shown in Fig. 5.7 to enter the electrolysis process unit C2-R1 along with the pure Li_2CO_3 electrolyte stream (FS-ELEC). C2-R1 is modelled in Apen as a stoichiometric reactor due to the unavailability of an electrolyser process unit. This reactor operates at 750°C temperature and 1.02 bar pressure and is modelled to convert 90% of the input CO_2 to C, in the form of MWCNT, and O_2 (Eq. 4.7) based on the 90% yield observed in Douglas et al. (2017). Amorphous carbon formation is not considered in this process based on the 99% MWCNT purity claimed by Douglas et al. (2017). A PSD mesh, based on Fig. 4.8 (Douglas et al., 2017), is modelled into C2-R1 with two intervals of 0-30nm and 30-60nm and each assigned equal weight fractions of 0.5. It is important to note that constituents other than CO_2 in the input S-CO2-9 streams, such as N_2 and CH_4, are assumed to not participate in the electrolysis processes and stay inert based on Douglas et al. (2018) and Douglas et al. (2017), Srininvasan (2018) which do not report on the electrolytic participation of non-CO2 gases.

The electrolyser process unit, as described in Section 4.4, involves a combination of jacketed vessel equipment, galvanized steel cathode rollers, Al_2O_3-coated Ni anode plates and the Li_2CO_3 electrolyte as the major fixed components, along with minor equipment such as MWCNT scraper and collector bin/vessel from the cathode (Fig. 4.10). APEA is used only to size the vessel equipment, given its inability to size the requirements of the other fixed components. The cathode surface's productivity of 50mg MWCNT from 2.5 cm^2 of surface area at 90% current efficiency, as discussed in Section 4.3, is considered in this study. The cathode's surface productivity is used to estimate the number of cathodes and anodes required for producing 625 kg of MWCNT per hr, as shown in Appendix C3 The volume of the vessel equipment is manually calculated by the modeller, as shown in Appendix C3. This volume calculation was made considering the electrolysis setup hypothesized in Fig4.11 with cathode and anode plate dimensions of 10.0m x 10.0m x 0.05m (length x width x thickness), a separation distance of 0.05m between the electrodes and the estimated 41 electrode plates (cathodes and anodes). Further estimations of the electrode materials and the electrolytes were made in Appendix C3 for subsequent use in cost estimation of the electrolyser setup. The amount of Li_2CO_3 electrolyte required is estimated considering 120% of the requisite amount for 625 kg/hr production of MWCNT, according to Eq.4.5 and as calculated in Appendix C3. The costs of all the electrolyser components estimated thus far are calculated to obtain the total electrolyser costs, as shown in Appendix C4, by combining the costs of these components and multiplying them by a factor of 4 to account for the extra costs arising from the overall fabrication, based on suggestions from Prof. Earl Goetheer. The total heat required for driving the 750°C electrolysis process in C2-R1 is assumed to be provided by a RotoDynamic Heater, as described in Section 4.3, that uses electrical energy to generate the high-temperature heat with 90% efficiency. The total electrical energy requirement for powering such electrical heating equipment and driving the electrolytic process is estimated using the energy consumption figure of 54kWh/kg MWCNT, based on Douglas et al. (2018), assuming that scales of economy and improved heat insulation shall help overcome the 10% loss of efficiency in the RotoDynamic Heater. Additionally, the electrical energy required solely for driving the electrolytic process of CO_2 dissociation is theoretically estimated to be 14.7 kWh/kg MWCNT using Eq.4.8 and accounting for 90% current efficiency (Douglas et al., 2018), as calculated in Appendix C3. Based on this theoretical estimation and the total electrical energy requirement figure, the energy required for heating is estimated to be 39.3 kWh/kg MWCNT.

The stream(S-MIX2) exiting C2-R1 in Fig. 5.7 comprises the cathode-scraped MWCNT solids, Li_2CO_3 electrolyte absorbed by the MWCNTs (Srininvasan, 2018) and O_2 constituting gas. The S-MIX2 steam is shown to go through a separator block (C2-SP1) in the Aspen process diagram to separate the gases from the MWCNT and Li_2CO_3 solid-liquid mixture. Such a separator block however does not exist in the actual plant but is modelled in this study for ease of simulation. Further, the limitations of modelling the electrochemical CO_2 reduction process on Aspen include the inability to account for the Fe particles scraped from the cathode along with MWCNT. It is also important to note that the FS-ELEC modelled to enter C2-R1 represents the amount of Li_2CO_3 electrolyte that is replenished due to its loss from MWCNT absorption, as shown in Appendix C3. The S-C-LI1 stream leaving the C2-SP1 separator block thus comprises the MWCNTs and lost Li_2CO_3 electrolyte, which needs to be separated for

producing the final MWCNT product.

5.4.3. CNT purification

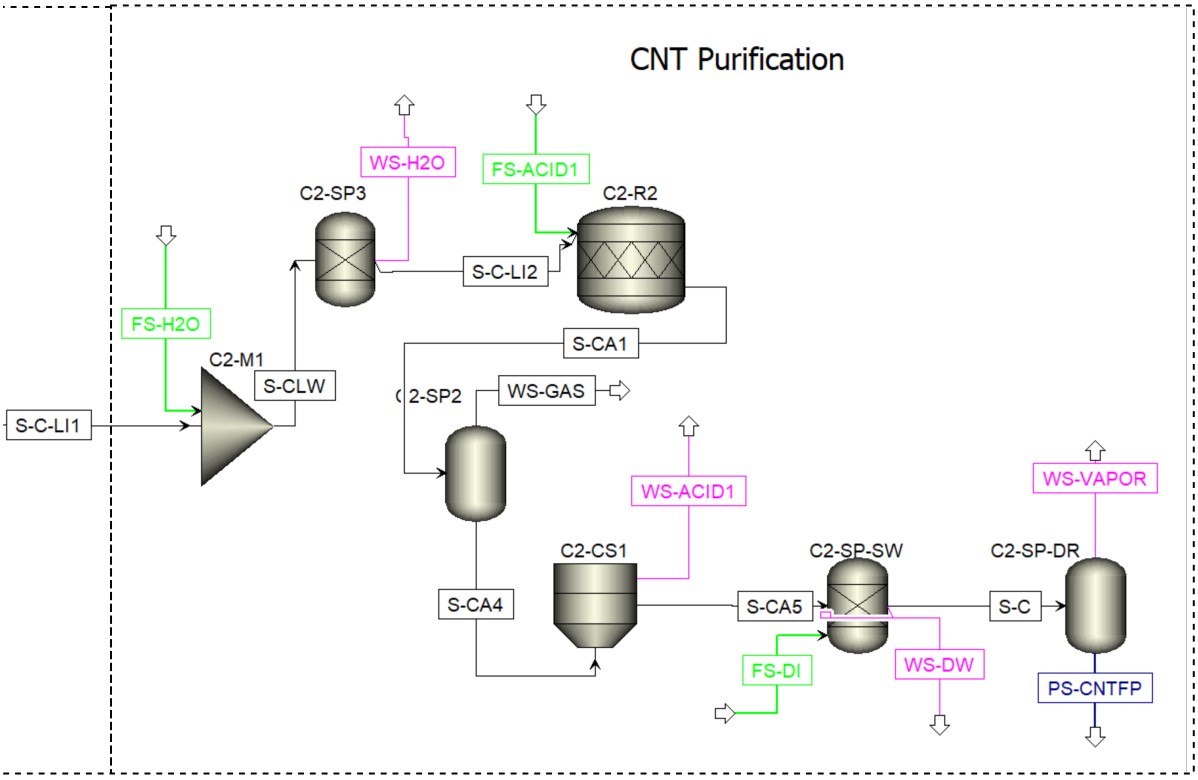

Figure 5.8: Electrochemcial CO_2 reduction - Process Block 3

The S-C-LI1 stream, which constitutes MWCNTs and Li_2CO_3, exits C2-SP1 at a temperature of 750°C. The subsequent removal of Li_2CO_3 through acid treatment however is assumed to take place in C2-R2 at 50°C temperature, similar to the acid treatment of the status quo CVD process Section 5.3.2. In a real plant, the MWCNT- Li_2CO_3 stream collected in a vessel is assumed to lose its high temperature to convective cooling over time, however, the same cannot be reflected on Aspen. For this reason, the cooling of the SC-LI1 stream is shown to undergo cooling to 50°C in the aspen process diagram by mixing with a large quantity of ambient temperature water in C2-M1 followed by the separation of that quantity of water in the C2-SP3 separator block. The mixer (C2-M1) and the separator block (C2-SP3) equipment are accordingly disregarded while mapping and sizing equipment in APEA, due to their irrelevance in the actual plant.

The cooled S-C-LI2 stream from the C2-SP3 separator block enters the stoichiometric reactor unit C2-R2 along with H_2SO_4 stream FS-ACID1, with composition, as calculated in Appendix C3. The reactor unit, operating at 50°C and 1.02 bar, is assumed to transform 100% of the Li_2CO_3 to CO_2, H2O and Li_2SO_4 through its reaction with H_2SO_4, as shown in Eq. 4.9. A chilled water utility is assigned to C2-R2 to provide the negative heat duty required for the modelled process unit. The resultant S-CA1 stream is passed through the flash separator C2-SP2 to release the CO_2 gas formed as waste emission into the atmosphere. The remaining liquid-solid mixture (S-CA4) of MWCNT and Li_2CO_3 from C2-SP2 undergoes centrifugation in C2-CS1 to separate

out the MWCNTs from waste aqueous solution. The centrifuge process unit C2-CS1 is modelled assuming 100% separation of the MWCNT solids and 20% of the aqueous liquid solution as S-CA5 stream. The remaining 80% of the aqueous solution is modelled as a waste stream (WS-ACID1) exiting the system. It is important to note that the froth flotation process unit, as used in the status quo CVD process (Section5.3.2), is not necessary for this process as the MWCNT produced is not attached to any catalyst support particles that require froth to break the attachment.

The S-CA5 stream from C2-CS1 is assumed to undergo several rounds of washing with demineralized water(FS-DI) to achieve a neutral pH sample, followed by centrifugation in the separator block C2-SP-SW. The modelling of this process unit is similar to the washing process in the status quo CVD process (Section 5.3.2) that involves the mapping of disk centrifuge in APEA. The utilities are also similarly disregarded in this process simulation for their perceived minimal impact on the study's results. C2-SP-SW is assumed to separate 100% of the MWCNT solids along with 20 % of the demineralized water as S-C stream. The remaining water solution forms the waste stream WS-DW.

The S-C stream constituting wet MWCNT is modelled in the Aspen process diagram to undergo drying in the flash separator block C2-SP-DR at 200 °C, based on the similar modelling of the drying process unit in the status quo CVD process (Section 5.3.2). The C2-SP-DR is also similarly mapped and sized on APEA as a single atmospheric drum dryer. A medium-pressure steam utility is assigned to C2-SP-DR to satisfy the heating requirements of the drying process. The drying process results in the release of water vapor (WS-VAPOR) as waste emissions into the atmosphere and yields the final saleable products of MWCNT (PS-CNTFP).

6

Mass & Energy Balances

The material and energy flow-related data generated from the modelling and simulation of the two processes compared in this study is extracted and analysed in this chapter. The first section outlines the overall input and output mass flow balance of the streams modelled for the two processes in Chapter 5. The second section similarly outlines the energy flows associated with the different types of process units constituting the two processes and the overall energy balance.

6.1. Mass Balances

The overall mass flows of various components flowing into and out of the status quo CVD process and electrochemical CO_2 reduction process in tonnes per operating(op.) year (yr) are shown in Fig. 6.1. The total inflows and outflows for both processes can be observed to match signalling that a mass balance has been achieved. These components form part of the various feed streams, product streams and waste streams, as explained in Section 5. The detailed component-wise breakdown of these streams can be referred to from Appendix E. There is a difference of an order of magnitude between the overall mass balances of the status quo CVD process and electrochemical CO_2 reduction process, with the former amounting to 170849 tonnes/op. year and the latter amounting to 68642 tonnes/op. year.

CH_4 inlet quantities of 14,365.1 tonnes/op.yr for the status quo CVD process are used in the fired heat process unit (C1-FU) and the CVD reactor unit (C1-R1), with more than two-thirds of this CH_4 being used for CVD reaction (Fig. E.1). However, the overall consumption of CH_4 as a carbon precursor for the status quo CVD process is lower compared to CO_2 as a carbon precursor for the electrochemical reduction process. This is despite a 16% CH_4 utilisation of the CVD reactor (C1-R1) compared to the 90% CO_2 utilisation of the electrolyser (C2-R1). This is because most of the CH_4 input to C1-R1 comprises CH_4 from the recycled stream that has accumulated from multiple cycles of MWCNT production and hence does not reflect in this mass balance. The CH_4 inflow of 77.9 tonnes/op. yr in the electrochemical process is an impurity component present in the PORTHOS CO_2 stream (FS-CO2) which are released as outflows as they do not take part in the electrolyser reaction. The significant amount of 2630.4 tonnes/op.yr of CH_4 outflows from the CVD process result from the purge(WS-PURGE)

operation that prevents the accumulation of gases within the system. Ethane and Propane form the impurities in the input natural gas stream in CVD process and they are released as a waste purge stream (WS-PURGE) in slightly lesser quantities than compared to their inflows. The H_2 generated as a product stream from the PSA process unit (C1-SPPSA) in the CVD process is assumed to satisfy the input H_2 requirements. This is however not modelled into the CVD process, thus showing a H_2 inflow of 196 tonnes/op.yr. The small quantities of 7.3 tonnes/op.yr H_2 entering and leaving the electrochemical process constitute the impurities of the PORTHOS CO_2 stream. Both processes produce approximately 5000 tonnes of MWCNT, which is identified as C in this study. The small difference in quantities is observed due to the absence of a design specification to achieve exactly 5000 tonnes of MWCNT.

CO_2 also forms part of the input natural gas streams as another impurity in the CVD process. Large amounts of 15101.6 tonnes/op.yr CO_2 emissions emitted in the CVD process are primarily from the flu gas (WS-FLUG) generated from the fired heat process(C1-FU) and the waste stream (WS-CO2AR) from the amorphous carbon oxidation process (C1-R2). 2185.8 tonnes/op.yr of CO_2 emissions from the electrochemical process stem from the unused input PORTHOS CO_2 stream to the electrolyser.The small quantities of CO, Ar, Methanol and Ethanol with < 15 tonnes/op.yr also constitute the impurities present in the PORTHOS CO_2 stream The O_2 and N_2 inflow and outflow streams of the CVD process originate from the air streams used in various process units of C1-FU, C1-R1 and C1-SP-FF. For the electrochemical process, a large amount of 13329.6 tonnes/op.yr of O_2 is generated from the electrolysis of CO_2. N_2 forms another major impurity component of the PORTHOS CO_2 stream, resulting in inflow and outflow quantities of 326.5 tonnes/op.yr. Ni, Mo and MgO form part of the Ni-Mo catalyst supported on MgO (FS-CAT) with a combined inflow of 976.2 tonnes/op.yr, out of which 20% of Ni and 100% of the MgO react with H_2SO_4 to form $MgSO_4$ and $NiSO_4$ while Mo stays inert. . Li_2CO_3 inflow stream of 250 tonnes/op.yr is another significant inflow for the electrochemical process.

The H_2SO_4 requirement for the CVD process is 1720 tonnes/op.yr, which is much higher than that of the 334.3 tonnes/op.yr requirement for the electrochemical process. This is because the CVD process involves the leaching/removal of close to 700 tonnes/op.yr of MgO and Ni in comparison to the removal of 250 tonnes/op.yr of Li_2CO_3. Such removal using H_2SO_4 results in the formation of 77.2tonnes/op.yr of $NiSO_4$ and 2041 tonnes/op.yr of $MgSO_4$ in the CVD process and 372 tonnes/op.yr Li_2SO_4 for the electrochemical process. A large amount of 4848 tonnes/op.yr of surfactant is used in the froth flotation process unit(C1-SP-FF) of the CVD process, whereas the electrochemical process does not use any surfactant due to the non-requirement of a froth flotation process unit. The surfactant and H_2SO_4 feed streams also involve dilution with H_2O resulting in its 10,000 tonnes/op.yr quantities in the inflows and outflows of the CVD and electrochemical process. The electrochemical process further models an additional H_2O stream (FS-H2O) (Fig. E.2) for the cooling of the MWCNT produced from the electrolyser for ease of simulation on Aspen, however, it is important to note that such cooling with water does not take place in the actual plant. Comparable amounts of around 2400 tonnes/op.yr of demineralized water are used in both processes given that they involve washing of similar amounts of MWCNT produced.

Overall, it can be observed that the main carbon precursor streams, the MWCNT produced, air constituents - O_2 and N_2 and water contribute 1000 tonnes/op.yr to the mass balances of the CVD and electrochemical CO_2 reduction processes.

Substance	Status Quo CVD		Electrochemical CO2 Reduction	
	Inflows (tonnes/op. year)	Outflows (tonnes/op. year)	Inflows (tonnes/op. year)	Outflows (tonnes/op. year)
METHANE	14365.1	2630.4	77.9	77.9
H2	196.0	2295.6	7.3	7.3
C	0.0	5001.6	0.0	5003.2
ETHANE	992.3	758.3	0.0	0.0
PROPANE	97.0	74.1	0.0	0.0
CO2	484.1	15101.6	20369.1	2185.8
O2	28120.7	10337.9	0.6	13329.6
N2	97049.4	97048.4	326.5	326.5
MGO	683.4	0.0	0.0	0.0
NI	146.4	117.2	0.0	0.0
MO	146.4	146.4	0.0	0.0
CO	0.0	0.0	10.2	10.2
H2O	19584.0	27947.1	44682.3	44743.3
H2SO4	1720.0	8.0	334.3	2.5
MGSO4	0.0	2041.0	0.0	0.0
NISO4	0.0	77.2	0.0	0.0
LI2CO3	0.0	0.0	250.0	0.0
LI2SO4	0.0	0.0	0.0	372.0
ETHANOL	0.0	0.0	0.4	0.4
METHANOL	0.0	0.0	9.6	9.6
AR	0.0	0.0	77.6	77.6
DEMINERALIZED WATER	2416.0	2416.0	2496.0	2496.0
SURFACTANT	4848.0	4848.0	0.0	0.0
Total Mass Flows	170849.0	170849.0	68642.0	68642.0

Figure 6.1: Mass Balance pertaining to 5000-ton annual MWCNT production

6.2. Energy Balances

In this section, the energy consumption by 4 equipment types - Pressure Modifiers, Heat Exchangers, Reactors and Dryer - are outlined and discussed for the two processes consecutively. Following this, the overall net energy balance of the two processes are compared and analysed.

6.2.1. Status Quo CVD

Pressure Modifiers: The pressure modifiers used in the status quo CVD process, as highlighted in Fig. 6.2, include a compressor process unit (C1-C1), which has a positive energy value and consumes energy, and a turbine process unit(C1-C2), which has a negative energy value and generates energy. These pressure modifiers are used in pre-treatment and post-treatment of methane recycle stream undergoing H_2 separation through PSA in the C1-SPPSA process unit. As a result, the electricity generated by the C1-C1 (26728.3MWh), which processes a higher

quantity of recycle stream before H_2 separation, is higher than that generated by the C1-C2 (11514.5MWh), which processes a lower quantity of recycle stream after H_2 separation.

Pressure Modifiers				
ID	Unit Type	Utility Type	Energy (MWh/yr)	Energy (TJ/yr)
C1-C1	COMPRESSOR	ELECTRIC	26728.3	96.2
C1-C2	TURBINE	ELECTRIC	-11514.5	-41.5

Figure 6.2: Pressure modifiers in the status quo CVD process

Heat Exchanger: The various types of heat exchangers used along with their utility types and their heat/energy duty in TJ/yr are shown in Fig. 6.3. In the CVD process, the cooler unit type corresponds to the heat exchanger that reduces the temperature of an input stream using the chilled water utility. The heat generator unit type also reduces the temperature of input streams, but instead through the generation of low-pressure, medium pressure and high-pressure steam from the heat of the input stream. The energy duty of such heat extraction process units is represented with a negative sign. The heat exchanger unit types mentioned in Fig. 6.3 enable the heat transfer to other process units within the system without any external heating/cooling utility, thus helping realise efficient use of heat energy available within the system. In essence, all the process units shown in Fig. 6.3 are heat exchangers as they exchange energy in the form of heat, however those with the unit type 'heat exchanger' are regarded so in the sense that they exchange/transfer heat with the other similar process units within the system itself. The process unit C1-E10 and C1-E15 use chilled water utility procured from external sources, whereas the process units C1-E9, C1-E14 and C1-E13 generate steam of varying pressures which have no use within the system and are hence sold to external sources. The process unit C1-E13 has the highest cooling energy duty of 69.3 TJ/yr as it reduces the temperature of a flue gas stream of $\approx$ 16000 kg/hr mass flow rate from a temperature of $\approx$ 900°C to $\approx$ 400°C. The heat exchanger process unit C1-E12 has the next highest cooling energy duty of 65.4 TJ/yr as it is used to provide heat for the high-temperature CVD reactor C1-R1, for the heat exchanger C1-E11 that heats the air stream for oxidation in C1-R2 and for the dryer process unit C1-SPDRY. The heat exchangers C1- E1 to C1-E8 are all mutually connected to each other such that the heating energy duty for heat exchangers C1-E1 to C1-E4, which heat the input feed stream of the CVD reactor from 15 to $\approx$950°C, match with the cooling energy duty of C1-E5 to C1-E8, which cool the CVD reactor outlet stream from 975 to 100°C.

Heat Exchanger			
ID	**Unit Type**	**Utility Type**	**Energy (TJ/yr)**
C1-E10	COOLER	CHILLED	-16.7
C1-E15	COOLER	CHILLED	-20.3
C1-E9	HEAT GENERATOR	HPSGEN	-26.1
C1-E14	HEAT GENERATOR	LPSGEN	-24.8
C1-E13	HEAT GENERATOR	MPSGEN	-69.3
C1-E12	HEAT EXCHANGER	HEAT TRANSFER	-65.4
C1-E1	HEAT EXCHANGER	HEAT TRANSFER	26.0
C1-E2	HEAT EXCHANGER	HEAT TRANSFER	75.7
C1-E3	HEAT EXCHANGER	HEAT TRANSFER	70.7
C1-E4	HEAT EXCHANGER	HEAT TRANSFER	131.0
C1-E5	HEAT EXCHANGER	HEAT TRANSFER	-131.0
C1-E6	HEAT EXCHANGER	HEAT TRANSFER	-70.7
C1-E7	HEAT EXCHANGER	HEAT TRANSFER	-75.7
C1-E8	HEAT EXCHANGER	HEAT TRANSFER	-26.0
C1-E11	HEAT EXCHANGER	HEAT TRANSFER	3.8

Figure 6.3: Heat Exchangers in the status quo CVD process

Reactors: The reactors used in the CVD process along with their utility type and energy duty are outlined in Fig. 6.4. Stoichiometric reactor unit types are primarily used. The highest heat energy duty (159.5 TJ/yr) generated is from C1-FU process unit that generated fired heat utility representing an industrial furnace. The flu gas generated from this furnace with the generated heat energy duty goes through the heat exchanger C1-E12, which was previously mentioned, which transfers the requisite heat of 58.9 TJ/yr for achieving 975°C high-temperature of the CVD reactor. It can be observed that the heat requirement of CVD reactor C1-R1 constitutes close to 1/3rd of the energy generated by the fired heat furnace C1-FU which is a considerably large amount. C1-R2 reactor that represents the oxidizer process unit for oxidizing amorphous carbon, which is understood to be an exothermic reaction that releases excess heat. The excess heat generated by C1-R2 is thus captured to produce low pressure steam utility for use outside the system. The heating energy duty of C1-R3, which represents the acid leaching process unit, is quite low owing to the 50°C temperature requirement of the reactor and smaller input mass flows, compared to that for C1-R2 and C1-R1.

Reactors			
ID	**Unit Type**	**Utility Type**	**Energy (TJ/yr)**
C1-R3	RSTOIC	LPSSTEAM	4.5
C1-R2	RSTOIC	LPSGEN	-39.3
C1-FU	RSTOIC	FIRED HEAT	159.5
C1-R1	RSTOIC	HEAT TRANSFER	58.9

Figure 6.4: Reactors in the status quo CVD process

Dryer: The details on the utility type and heating energy duty required for the drying process unit of the status quo CVD process are as shown in Fig. 6.5. The dryer process unit C1-SPDRY is connected to the C1-E12, as described earlier in heat exchangers, for meeting its heating energy duties from within the system without relying on external utilities. Compared to the heating energy duties of process units discussed thus far, C1-SPDRY has a low heating

energy duty of 2.7 TJ/yr possibly because of the low input mass flows which constitute only the wet MWCNT stream of around ≈ 1000 kg/hr coupled with the low heating temperature of 200°C.

Dryer			
ID	Unit Type	Utility Type	Energy (TJ/yr)
C1-SPDRY	DRYER	HEAT TRANSFER	2.7

Figure 6.5: Dryers in the status quo CVD process

6.2.2. Electrochemcial CO_2 reduction

Pressure Modifiers: The pressure modifiers used in the electrochemical CO_2 reduction process with information on their utility type and energy duty in MWh/yr and TJ/yr units are shown in Fig. 6.6. The two pressure modifiers in the electrochemical process are of turbine type which decompresses the input stream and generates electrical energy in that process. The input PORTHOS CO_2 stream enters the process system at 35 bar which is first reduced by 10 bar in C2-C1 and then by 15 bar in C2-C2 to a final stream pressure of 10 bar. The higher decompression undergone in C2-C2 thus yields higher electrical energy of 277.1 MWh/yr or 1 TJ/yr compared to that yielded from C2-C1 which is equal to 115.8 MWh/yr or 0.4 TJ/yr.

Pressure Modifiers				
ID	Unit Type	Utility Type	Energy (MWh/yr)	Energy (TJ/yr)
C2-C1	TURBINE	ELECTRIC	-115.8	-0.4
C2-C2	TURBINE	ELECTRIC	-277.1	-1.0

Figure 6.6: Pressure modifiers in the electrochemical CO_2 reduction process

Heat Exchanger: The heat exchangers used in the electrochemical CO_2 reduction process are outlined with their unit types, utility types and energy duty in TJ/yr. The heat exchanger C2-H0 of heater unit type constitutes the only heat exchanger with an externally sourced utility of medium pressure stream which generates a heating energy duty of 1.4 TJ/yr. The process units of heat exchanger unit type, that constitute C2-H1 to C2-H6 process units, are modelled similarly to those in the status quo CVD process with system heat integration involving the transfer of heat from the hot outlet stream of the electrolyser to its colder input stream. The heating energy duty of these heat exchanger-type process units ranges from 3-3.5 TJ/yr.

Heat Exchanger			
ID	Unit Type	Utility Type	Energy (TJ/yr)
C2-H0	Heater	MPSTEAM	1.4
C2-H1	HEAT EXCHANGER	HEAT TRANSFER	3.4
C2-H2	HEAT EXCHANGER	HEAT TRANSFER	3.0
C2-H3	HEAT EXCHANGER	HEAT TRANSFER	3.5
C2-H4	HEAT EXCHANGER	HEAT TRANSFER	-3.5
C2-H5	HEAT EXCHANGER	HEAT TRANSFER	-3.0
C2-H6	HEAT EXCHANGER	HEAT TRANSFER	-3.4

Figure 6.7: Heat exchangers in the electrochemical CO_2 reduction process

Reactors: The reactor process units used in the electrochemical CO_2 reduction process are as

shown in the Fig. 6.8 which outlines their utility types and energy duty in TJ/yr. Stoichiometric reactor unit types are used in process model simulation. The energy calculations of process unit C2-R1 are however calculated manually unlike the C2-R2 whose energy calculations are as calculated from Aspen. The C2-R1 process unit, which represents the electrolyser, has a very large energy consumption figure of 972 TJ/yr or 270 GWh/yr due to the high electrical energy required in the disassociation of CO_2 molecule to C and O_2 and the electrically generated high-temperature heat of 750°C considered in this process. The energy breakdown, which is realised from the theoretical calculation of electricity utilised in C2-R2 (Section 5.4.2), is as shown in Fig. 6.9 . The heat energy duty, amounting to 196.6 GWh/yr, is observed to constitute more than 2/3rds of the 270GWh /yr total consumption while electrical energy constitutes only 73.4 GWh/yr of the total energy. This could be due to the high energy required to maintain the temperatures of 750°C and energy losses resulting from poor insulation. The C2-R2 process unit represents the acid treatment reactor which primarily dissolves the Li_2CO_3 electrolyte present in the MWCNT output stream of the electrolyser. This reaction is understood to be exothermic thus requiring a chilled water utility to cool the reactor process unit and achieve a set temperature of 50°C in the outlet stream of C2-R2.

Reactors			
ID	**Unit Type**	**Utility Type**	**Energy (TJ/yr)**
C2-R2	RSTOIC	CHILLED	-0.2
C2-R1	RSTOIC	ELECTRIC	972.0

Figure 6.8: Reactors in the electrochemical CO_2 reduction process

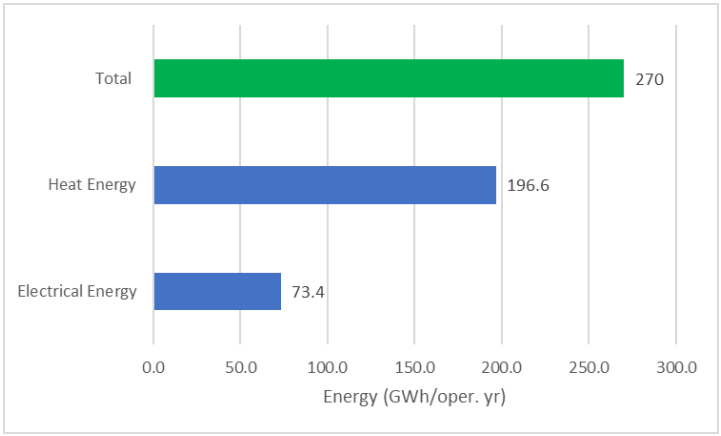

Figure 6.9: Electrolyser energy use breakdown

Dryer: The details on the utility type and energy duty in TJ/yr for the dryer process unit of the electrochemical CO_2 reduction process are shown in Fig. 6.10. The dryer process unit C2-SP-DR is modelled to use the medium pressure steam utility type to achieve an energy duty of 2.2 TJ/yr for drying the wet MWCNT input stream at 200°C.

Dryer			
ID	Unit Type	Utility Type	Energy (TJ/yr)
C2-SP-DR	DRYER	MPSTEAM	2.2

Figure 6.10: Dryers in the electrochemical CO_2 reduction process

6.2.3. Overall Energy Balance

The overall energy balance comparison of the two processes modelled in this study, based on the energy breakdown detailed in Section 6.2.1 and6.2.2, is as shown in the Fig. 6.11. This overall energy balance classifies the various types of utilities, which either generate heat or consume heat or use electricity, in energy duty units of TJ/yr and determines the net total energy duty of the two processes.

Utility type	Electrochemical CO2 Reduction	CVD	Unit
Utilites removing heat			
HEAT TRANSFER	-10.0	-368.8	TJ/yr
LPSGEN	0	-64.1	TJ/yr
MPSGEN	0	-69.3	TJ/yr
HPSGEN	0	-26.1	TJ/yr
CHILLED	-0.2	-37.0	TJ/yr
Total -ve Heat Utilities	-10.2	-565.3	TJ/yr
Utilites consuming heat			
LPSTEAM	0	4.5	TJ/yr
MPSTEAM	3.6	0.0	
FIRED HEAT	0	159.5	TJ/yr
HEAT TRANSFER	10.0	368.8	TJ/yr
Total +ve Heat Utilities	13.6	532.8	TJ/yr
Net Heat Utilites	**3.4**	**-32.5**	**TJ/yr**
Total Electric Utilites	**970.6**	**54.8**	**TJ/yr**
Net Energy	**973.9**	**22.3**	**TJ/yr**

Figure 6.11: Overall Energy Balance comparison of status quo CVD process and electrochemical CO_2 reduction process

The electrochemical CO_2 reduction process has a net energy duty balance of 973.9 TJ/yr out of which electric utilities constitute 970.6 TJ/yr, which forms more than >99% net energy duty, and heat utilities constitute only 3.4 TJ/yr. The electric utilities are majorly used by the electrolysis process unit, as shown in Fig. 6.8 and 6.9. The medium-pressure steam utility of 3.6 TJ/yr contributes majorly to the net heat utilities. The heat transfer utilities, as shown in Fig. 6.7, involve a cumulative exchange of 10 TJ/yr which is a significant amount of energy duty. Given that the processes are modelled as steady-state continuous processes, this energy duty of 10TJ/yr is assumed to be introduced once during the initial start-up phase of the plant and to circulate within the system of interconnected heat exchangers outlined in Fig.6.7. The heat transfer utilities thus enable savings from the consumption of externally sourced utilities.

The status quo CVD production process has a net energy duty balance figure of 22.3 TJ/yr. This net energy duty balance results from a net positive electric duty of 54.8 TJ/y and a net

negative heat duty of -32.5 TJ/yr. The compressor process unit C1-C1, highlighted in Fig. 6.2, contributes to the high electrical energy duty of 54.8TJ/yr. The net negative heat energy duty is achieved as the overall heat removed from the process is greater than the heat consumed by the process. The fired heat utility, which supplies high-temperature heat required for the CVD process unit, consumes the highest heat duty of 159.5 TJ/yr. The low, medium and high-pressure types of steam utilities generated cumulatively extract and generate heat duty of - 159.5 TJ/y, which peculiarly is similar to the heat duty consumed by the fired heat utility. The other major utility that removes heat includes the chilled water utility with a duty of -37 TJ/yr. The heat transfer utilities, as shown in Fig. 6.3, exchange a large energy duty amount of 368.8 TJ/yr. This draws light on the energy efficiency achieved from such heat integration and avoidance of externally sourced utilities.

In an overall sense, it can be observed the net energy duty balance of the electrochemical CO_2 reduction process (973.9 TJ/yr) is more than one order of magnitude higher than that of the status quo CVD process (22.3 TJ/yr). The electric utilities duty constitutes the majority of the electrochemical process net energy duty however for the CVD process both heat and electric utilities contribute significantly to the net energy duty. The heating utility consumption is higher for the CVD process, which uses and generates several types of heat utilities with high energy duties, than the electrochemical process, which consumes only one type of heat utility (MPSTEAM) and does not generate any heating utility. The heat transfer energy duties of the CVD process are also higher by an order of magnitude compared to that of the electrochemical process. From these insights, it can be inferred that the CVD process is heat utility intensive whereas the electrochemical process is electric utility intensive.

7

Results and Discussion

In this chapter, firstly, the results of the comparative technical, economic and environmental assessments of the status quo CVD process and electrochemical CO_2 reduction process conducted according to Section 3.3.5 are consecutively presented and discussed. This is followed by a general discussion on the overall research conducted in this study, outlining the limitations and the relevance of this study. Lastly, further recommendations for improvements and future studies are detailed.

7.1. Technical Assessment

In this section, the technical performance indicators of resource intensity and energy efficiency (EE) are assessed for the two processes and compared.

7.1.1. Resource Intensity

Resource Intensity (RI) is defined in this study as the mass of input feedstock(in tonnes) required to produce one tonne of final product. The usage of such an indicator helps assess the extent to which the input resources are used effectively to produce the maximum quantity of reference product by the two processes. The process with minimal input resource use per tonne of final product produced is favoured. It is calculated according to the Eq 7.1 wherein the input feedstock refers to the main carbon precursor and the output product refers to the CNM produced.

$$RI = \frac{\text{Total mass of input feedstock}}{\text{Total mass of output product}} \tag{7.1}$$

The RI for the two processes is calculated with units of tonne carbon precursor material used per tonne MWCNT produced (t_precursor/t_MWCNT). The carbon precursor material considered for the CVD process involves CH_4 whereas that for the electrochemical process involves CO_2. Two REs are calculated for the CVD process, which involve CH_4 quantities associated with the feed stream (FS-CH4) only and CH_4 quantities associated with both the feed stream(FS-CH4) and recycle stream(RS-NGH). The CVD process involves the recycling of unused CH_4 precursor stream and RI calculated considering this reuse stream can be insightful in understanding the extent of overall CH_4 usage, despite this study being modelled as a steady-state continuous process. For the electrochemical process, the RI is calculated considering the quantity of CO_2

input feed stream. The calculations for the RI of the two processes can be referred to from Appendix B6 andC6.

The REs, as shown in Fig.7.1, show that the highest RI of 10.4 corresponds to that of the CVD process considering both the feed stream and recycle stream. This is because of the fact that only 16% of input CH_4 undergoes chemical vapor deposition in the C1-R1 process unit, which is accurately reflected in the RI result of 10.4. However, the RI of the CVD process considering only the feed stream is only 2.2, which is five times considerably lower than the RI 10.4. The high RI value of 10.4 can be explained by the significant amount of ≈ 5000 kg/hr CH_4 constituting RS-NGH, along with ≈ 1300 kg/hr of CH_4 constituting FS-CH4. The low RI value of 2.2 can be explained the ≈ 1300 kg/hr of CH_4 constituting FS-CH4 considered in the RI calculation.

The 4.1 RI of the electrochemical process is significantly lower than the 10.4 RI of CVD process, which considers both FS-CH4 and RS-NGH, but still higher than the 2.2 RI, which considers only FS-CH4. The electrochemical process considers 90% of the input CO_2 carbon precursor to undergo electrolysis wherein the CO_2 disassociates into atomically lighter carbon and atomically heavier O_2(4.7). The considerably higher RI of 4.1 for the electrochemical process can be attributed to the C constituting a lower mass% of the CO_2 molecule undergoing electrolysis to form C-based MWCNT.

In summary, the RI of the CVD process is shown to be better than that of the electrochemical process when considering a steady-state scenario of only feed streams. Whereas, when considering absolute resource consumption, which also includes the recycle streams, the electrochemical process is shown to have better RI than that of the CVD process.

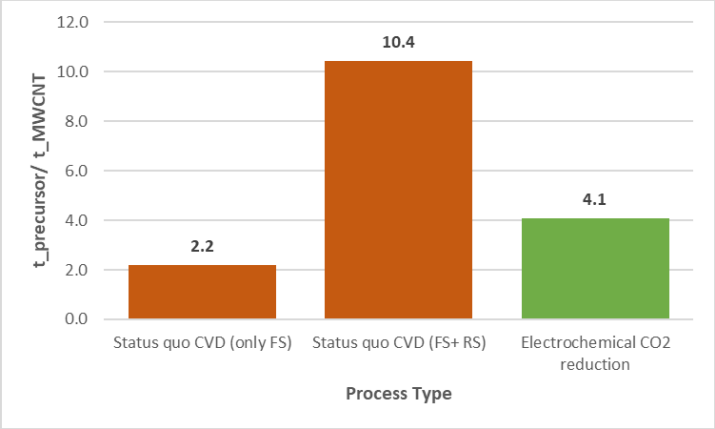

Figure 7.1: Resource Intensity comparison

7.1.2. Energy Efficiency

Energy Efficiency (EE) is defined in this study as the amount of total input energy required by the process to produce one tonne of final product, similar to RI which is instead based on the mass of input resource feedstock. The total input energy can be in the form of electricity or heat. Energy efficiency, as an indicator, helps evaluate how productively the energy is utilised in the production of the final product. The process with minimal energy use per tonne of final

product produced is favoured. EE is calculated as shown in Eq. 7.2

$$EE = \frac{\text{Total Input energy}}{\text{Total Mass of output product}} \tag{7.2}$$

The EE for the two processes is calculated with units of Giga Joule per tonne MWCNT produced (GJ/t). The EE calculation constitutes three categories based on the total heat, total electric and net energy duties of both processes as outlined in Fig. 6.11. The calculations for the EE, as shown in Fig. 7.2, can be referred to from Appendix D4.

The EE of CVD processes is observed to be significantly lower than the EE of electrochemical processes by up to two orders of magnitude. The EE with respect to net energy is 4.5 GJ/t for the CVD process which is ≈ 50 times lower than the 194.8GJ/t net energy EE of the electrochemical process. With regards to heat utilities, the EE of the CVD process is -6.5 GJ/t due to heat removing utilities of steam generation and chilled water, as explained in Section 6.2.3. This negative value however does not indicate energy efficiency in its true sense given that it consumes chilled water to remove heat upon which it is not utilised elsewhere and is hence wasted, unlike the different varieties of steam generated which can be externally used. The heat utility-based EE of the electrochemical process is 0.7 GJ/t owing to the minimal use of heat utilities in the process. The EE associated with electric utilities is 11GJ/t for the CVD process which is an order of magnitude lower than the 194.1 GJ/t EE for the electrochemical process. The higher EE of the electrochemical process is particularly driven by the electrical energy required for the electrically heated 750°C electrolysis process unit C2-R1.

Overall, it can be inferred that the CVD process has better EE than the electrochemical process owing to considerable negative energy duty from the steam generation heat utilities of the CVD process and the exceptionally high duty from the electric utility of the electrochemical process.

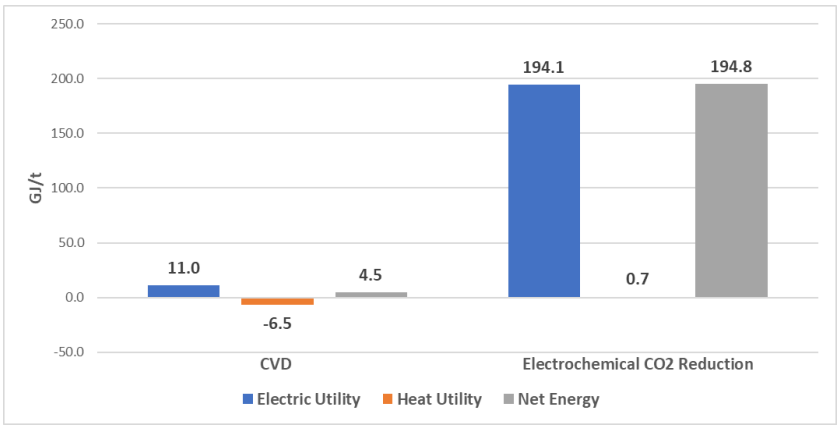

Figure 7.2: Energy Efficiency Comparison

7.2. Economic Assessment

In this section, the economic performance indicators of total capital investment (TCI), operational expenditure (OPEX), net present value, and payback period are assessed and compared for the two processes.

7.2.1. Total Capital Investment

Total Capital Investment (TCI) involves the estimation of the various capital costs incurred for establishing the industrial-scale plant based on the process simulations developed. The primary component of total capital investment involves equipment costs. The equipment costs of the simulated processes in this study are obtained from APEA, which evaluates its costs based on a 2018 database of equipment costs. These costs also include the cost of installation of the equipment. The equipment costs which cannot be estimated by APEA, such as PSA and electrolyser process units, are referred to from the literature or calculated by the modeller. The equipment costs are then adjusted to the 2022-2023 temporal scope of this study using the chemical engineering plant cost index (CEPCI) (Access Intelligence, 2023). The conversion factor of 0.92 is considered for currency conversion of 1 United States Dollar (USD) to Euro (EUR). The details of the various equipment and their cost estimations can be referred to from Appendix C4 and B4. The overall fixed capital investment, which includes several direct and indirect costs, is calculated as a % of the APEA estimated equipment costs, based on the cost estimation method outlined in the textbook 'Plant design and Economics for Chemical Engineers' by Peters et al. (2003). Based on a range of percentages provided for various cost components constituting the direct and indirect costs, an arbitrary % perceived fit for such components is selected by the modeller as shown in Fig 7.3. These % values are then normalised which adds up to 100% of the fixed capital investment (FCI). As shown in Fig 7.3, the purchased equipment costs including installation are equivalent to 31.2 % of the FCI. From this, the FCI is back-calculated and the other cost components are subsequently calculated as a % of the FCI. Based on the FCI, the working capital investment (WCI) is calculated as 18% of the FCI (Peters et al., 2003). The total capital investment constitutes the sum of FCI and WCI.

Cost Components		% selected	Normalized %
Direct Costs	Purchased equipment	34	31,2%
	Instrumentation and controls	7	6,4%
	Piping	8	7,3%
	Electrical systems	5	4,6%
	Buildings	5	4,6%
	Yard improvements	2	1,8%
	Service facilities	14	12,8%
	Land	1	0,9%
Indirect costs	Engineering and supervision	10	9,2%
	Construction expenses	12	11,0%
	Legal expenses	1	0,9%
	Contractor's fee	2	1,8%
	Contingency	8	7,3%
Fixed Capital Investment (FCI)		109	100%
Working Capital Investment (WCI)			18% of FCI
Total Capital Investment (TCI)			FCI+WCI

Figure 7.3: Breakdown of costs comprising the TCI

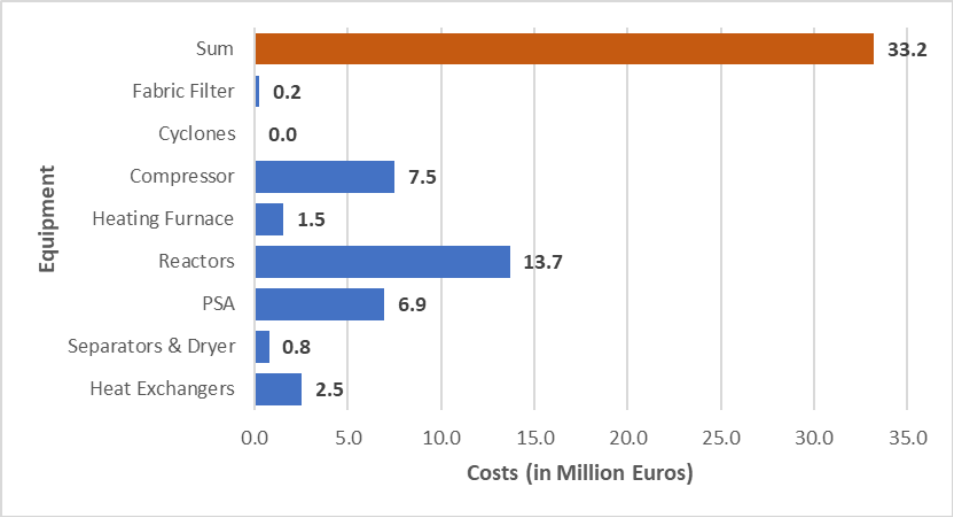

Figure 7.4: Status quo CVD process equipment costs

The various equipment costs of the CVD process are categorized by their equipment types and outlined in Fig. 7.4 in units of Million(M) EUR. The total equipment costs for the CVD process are 33.2M EUR. Of these total costs, the reactors cost the highest amount of 13.7M EUR, out of which the CVD reactor process unit (C1-R1) contributes the greatest amount of ≈ 13.4M EUR. Inconel alloy in C1-R1 process unit is used to help withstand the 1000°C high temperatures (Salomon's Metlanen B.V., n.d.) of the CVD reaction, and the high quantity of ≈ 16,000 kg/hr of input flow. The compressors and the PSA column, which together comprise the PSA system of H_2 separation, comprise 14.4M EUR of the total equipment costs. The high-pressure vessels, adsorbent materials, and pressure-modifying compressor and turbine units are responsible for contributing to the high cost of the PSA system. The heating furnace cost of 1.5M EUR also forms a notable part of the total costs. The large number of heat exchangers utilised in the system, with some of them costing as high as ≈ 0.75M EUR, cumulatively comprise 2.5M EUR equipment cost. Other equipment comprising centrifuge separators, dryer, cyclones, and fabric filters cost ≈ 1M EUR cumulatively. The total installed equipment costs of a similar 5000-tonne annual capacity plant of SWCNT production, as estimated by A. Agboola (2005), is only ≈ 3M USD. The large difference in the equipment costs can be explained by -

- the older 2005 temporal scope wherein prices were lower,
- the consideration of expensive PSA system and Inconel alloy reactor in this study,
- the inclusion of fired heat utility equipment within the scope of the process system,
- the excess heat exchangers utilised in this study to implement heat integration which helps save on operational costs arising from externally sourced utility usage
- the 'CAPCOST ' capital estimation program used by A. Agboola (2005) to estimate costs could be less accurate compared to that estimated from the APEA capital estimation tool of Aspen Plus, given that Aspen is widely used as the industry standard program for techno-economic evaluation

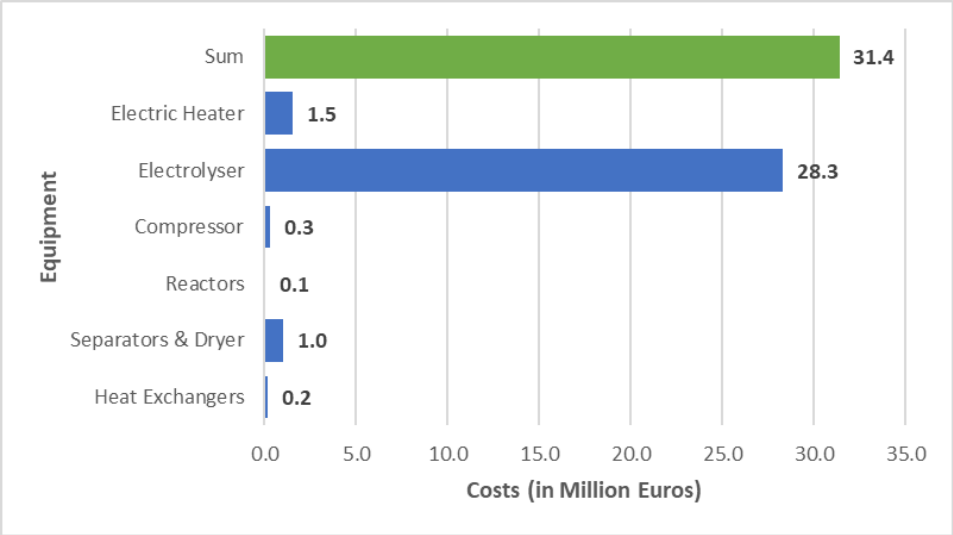

Figure 7.5: Electrochemical CO_2 reduction process equipment costs

The cost of the various equipment comprising the electrochemical process is as shown in Fig. 7.5. It can be observed that the total equipment cost of the electrochemical process (31.4M EUR) is closely comparable to that of the CVD process (33.2 M EUR). The trend of electrolyser dominance in EE of the electrochemical process, as shown in 7.1.2, is also observed here with the electrolyser itself constituting ≈ 90% of the total equipment costs. The electrolyser is comprised of four main components whose cost contribution breakdown is as shown in Fig. 7.6. It is important to note that only the reactor vessel component of the electrolyser is evaluated using APEA and the other components are manually calculated by the modeller based on Douglas et al. (2018) and Douglas et al. (2017), Srininvasan (2018). The electrolyte is shown to form 70% of the total electrolyser cost, given its significant quantity required for the electrolytic production of 625 kg/hr and the high costs of the Li_2CO_3. Using Li_2CO_3 for MWCNT production runs the risk of competing against the use of Li_2CO_3 in batteries, which are currently in great demand (Azevedo et al., 2022) to help decarbonize important sectors such as transport and renewable energy storage. This signals the need to look into other electrolyte alternatives that are cheaper and more widely available. The next highest cost component of 26% is the reactor vessel that is evaluated in APEA assuming an open-top reactor of SS316 material. The cost for the Al_2O_3 coated Ni anode was estimated based on the quantity and density of Ni, and the cost of the galvanized steel cathodes was also similarly estimated. The sum of costs of the electrolyser component was multiplied by a factor of 4, based on expert elicitation with Prof. Earl Goetheer, to account for-

- the fabrication costs of the electrolyser setups shown in Fig. 4.10 and 4.11,
- the Al_2O_3 atomic layer coatings on the Ni electrode (Section 5.4.2)
- the insulated jacketing of the vessel for heating the vessel (Section 5.4.2)

It is important to note that such cost estimation of electrolyser makes it subjective to high uncertainty but provides a basis for further refinement of the cost estimation with improved data. Further, due to a lack of data on the cost of the electric Rotodynamic heater used in this process for 750°C high-temperature heating, the cost of the fired heat utility of the CVD process is assumed to be applicable. The other process equipment including the compressor,

heat exchangers, centrifuges and dryers comprise about 1.6M EUR of the total equipment costs. The costs of the compressors in the electrochemical process are considerably lower than that of the CVD process, as the mass flows being handled in the electrochemical process compressors are an order of magnitude lower than that being handled in the CVD process compressors. The total equipment costs of the electrochemical process are highly concentrated around the electrolyser whereas the total equipment costs of the CVD process are more distributed among different types of equipment.

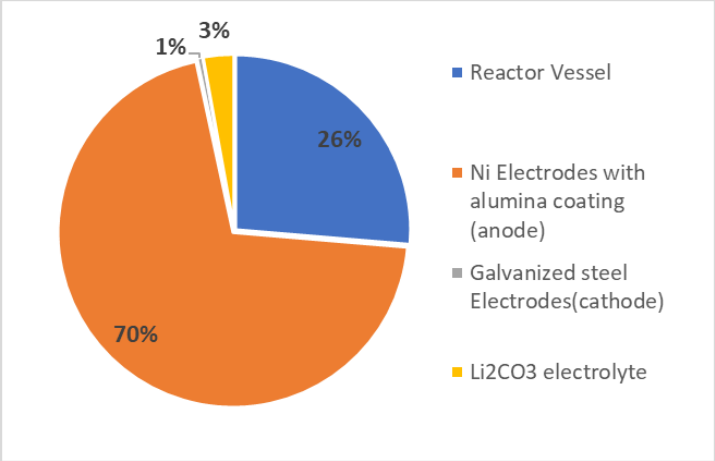

Figure 7.6: Electrolyser cost breakdown

Based on the equipment costs highlighted thus far, Fig. 7.7 has been created for TCI calculation of the two processes in units of M EUR . The CVD process has a TCI of 125.6 M EUR which is slightly higher than the 118.7 M EUR TCI of the electrochemical process. Given that the electrochemical process consists of lesser process units than those of the CVD process, a reduction in the cost of the electrolyser process unit of the electrochemical process can thus help achieve significant reductions in the overall TCI and make it economically more attractive. The usage of a cheaper non-lithiated electrolyte can help realise considerable cost reductions in the electrolyser process unit, and thus improve the overall economic performance of the electrochemical CO_2 reduction process over that of the status quo CVD process. The TCI for a same-scale CVD-based SWCNT production plant, as estimated by A. Agboola (2005) and A. E. Agboola et al. (2007), is shown to be only $\approx$ 4.5M EUR. The 125.6M EUR TCI estimation of the CVD process modelled in this study covers various direct and indirect cost components and is based on a much higher equipment cost, due to which it is two orders of magnitude higher than the 4.5MEUR TCI of SWCNT production.

In conclusion, it can be seen that the distribution of equipment costs between the CVD and electrochemical processes differs significantly, with the reactor and PSA system accounting for the majority of the former's costs and the electrolyser system for the latter. However, the total equipment costs and TCI of the two processes are of the same order of magnitudes with the CVD process being only slightly more expensive than the electrochemical process. Further comparison with the TCI and equipment costs of an SWCNT production plant of the same scale (A. E. Agboola et al., 2007) showed great disparity, stemming from differences in the process modelling and methodology of cost estimation by A. E. Agboola et al. (2007) and this study.

Cost Components		Normalized % of FCI	CVD	Electrochemical CO2 reduction	Unit
Direct Costs	Purchased equipment	31.2%	33.2	31.4	Million Euros
	Instrumentation and controls	6.4%	6.8	6.5	Million Euros
	Piping	7.3%	7.8	7.4	Million Euros
	Electrical systems	4.6%	4.9	4.6	Million Euros
	Buildings	4.6%	4.9	4.6	Million Euros
	Yard improvements	1.8%	2.0	1.8	Million Euros
	Service facilities	12.8%	13.7	12.9	Million Euros
	Land	0.9%	1.0	0.9	Million Euros
Indirect costs	Engineering and supervision	9.2%	9.8	9.2	Million Euros
	Construction expenses	11.0%	11.7	11.1	Million Euros
	Legal expenses	0.9%	1.0	0.9	Million Euros
	Contractor's fee	1.8%	2.0	1.8	Million Euros
	Contingency	7.3%	7.8	7.4	Million Euros
Fixed Capital Investment (FCI)		100.0%	106.4	100.6	Million Euros
Working Capital Investment (WCI)		18% of FCI	19.2	18.1	Million Euros
Total Capital Investment (TCI)		FCI+WCI	125.6	118.7	Million Euros

Figure 7.7: TCI comparison between CVD and Electrochemical processes

7.2.2. Operational Expenditure

The operational expenditure(OPEX) constitutes labor costs, maintenance costs, and fixed costs as shown in Fig 7.8 along with the cost of utilities and feedstocks. The total operating labor cost calculated in this study is based on the textbook 'Plant design and Economics for Chemical Engineers' by Peters et al. (2003). It is calculated as a product of the employee hours(h) required per day, the number of process blocks/steps(s), the number of operational days(d), and the hourly labor costs(c). Based on a 15 tons/day plant capacity of the designed processes, the employee hours were estimated as 33 hrs from Peters et al. (2003). The process models, as described in Section 5.3 and 5.4, were each divided into three process blocks, and the same is considered in this calculation. Based on the VICI stated guideline of 8000 hours of plant operation per year and an assumption that the plant runs for 24 hours/day, the number of operational days was calculated as 333.3 days. The average per-hour labor costs in the Netherlands in 2022 were found to be 40.5 EUR (Eurostat, 2023). From this the total operating labor cost was calculated as 1.3 M EUR, as documented in Appendix B5 and C5 . The calculation basis for the other operational cost components of the two processes is as outlined in Fig. 7.8 . It is important to note that the operating labor costs calculated thus far are associated with a considerable degree of uncertainty as the human resource capacity of the modelled process blocks is not exactly known.

Category	Sub-Category	% value	Basis	CVD	Electrochemical CO2 Reduction	Unit
Labor	Operating labor		hxsxdxc	1.3	1.3	Million Euros
	Operating Supervision	15%	of operating labor	0.2	0.2	Million Euros
	Lab Charges	10%	of operating labor	0.1	0.1	Million Euros
Maintenance	Maintenance	7%	of FCI	7.5	7.0	Million Euros
	Operating Supplies	15%	of maintenance	1.1	1.1	Million Euros
Fixed	Taxes, Insurance and Loan Interest	10%	of FCI	10.6	10.1	Million Euros
	General expenses	20%	of labor, supervision and maintenance	1.8	1.7	Million Euros
	Plant Overhead	50%	of labor, supervision and maintenance	4.5	4.3	Million Euros
Total				27.2	25.8	Million Euros

Figure 7.8: Labor, Maintenance, and Fixed Operational costs

Along with these operational cost components, OPEX, also includes the cost of utilities and input feedstock materials used, whose unit costs are as shown in Fig. 7.9. . The electric

utility can be observed to have the highest price of 0.18 Euros/kWH whereas the low pressure steam and chilled water utilities have the lowest price of 0.03 Euros/kWh. The most expensive feedstock constitutes the PORTHOS CO_2 feedstock owing to the capital-intensive carbon capture and high-pressure pipeline transport involved. The price of the feedstock is however subject to change, with the potential of the industrial flue gas basedCO_2 being offered at a subsidised price or for no cost by the industrial entity generating the flue gas. The next most expensive stream that has to be procured from the market involved the Li_2CO_3 electrolyte at 39 Euros/ton. The sulphuric acid feed stream costs the lowest amount of 0.0426 Euros/kg of all the feed streams. The same natural gas feed stream is considered for the fired heat furnace process unit as well as CVD process unit. The total costs of the utilities and feedstocks consumed in the two processes are obtained by multiplying these unit costs by the corresponding use values from the mass and energy balances.

Feedstock	Price (2022)	Unit	Source
Natural Gas feedstock stream	0.07	Euros/kWh	Eurostat, 2023
Ni-Mo/MgO	7.36	Euros/kg	Alibaba, 2023
De-mineralized Water	0.66	Euros/m3	Intratec, 2018
Sulphuric acid	0.0426	Euros/kg	Intratec, 2018
Non-ionic surfactant	2.58	Euros/kg	Alibaba, 2023
Porthos CO2 stream	80	Euros/ton	Port of Rotterdam, 2021
Li2CO3 electrolyte	39	Euros/ton	Trading Economics, 2023

Utitlity	Price (2022)	Unit	Source
MPSTEAM	0.04	Euros/kg	Intratec, 2018
LPSTEAM	0.03	Euros/kg	Assumption:0.9 x MPSTEAM
HPSTEAM	0.04	Euros/kg	Assumption: 1.1 x MPSTEAM
CHILLED WATER	0.03	Euros/kWh	Intratec, 2018
COOLING WATER	0.07	Euros/m3	Intratec, 2018
ELECTRIC	0.18	Euros/kWh	Eurostat, 2023
NATURAL GAS BASED FIRED HEAT	0.07	Euros/kWh	Eurostat, 2023

Figure 7.9: Feedstock and utility prices

The total OPEX for the CVD process based on the operational costs described thus far is 66.7 M EUR, as shown in Fig.7.10. The natural gas feed stream contributes the highest amount of 14.8M EUR, owing to its use in large quantities for the CVD reaction and fired heat generation. The next highest contributor to the OPEX is the non-ionic surfactant with an operational cost of 12.5 M EUR. The non-ionic surfactant is used in a large quantity $\approx$ 4800 tonnes which is almost equal to the MWCNT produced and is thus responsible for such a high cost. There is however some uncertainty associated with the use of the non-ionic surfactant in such a large quantity leading to $\approx$ 1:1 ratio of surfactant to MWCNT. The surfactant quantity is calculated from geometrical scaling of the reported values from Lertrojanachusit et al. (2013), which might reflect an exceptionally large value than what is actually required for the scale of this study. Further, the recycling of waste surfactant from the froth flotation process can reduce the costs arising from the new surfactant feed. The Ni-Mo/Mgo catalyst comprised another major feedstock that contributes a significant amount of 7.2 M EUR. The catalyst, although used in small amounts of $\approx$ 1000 tonnes/op.yr, has a significantly high unit cost of 7.36 EUR/kg leading to such high overall costs. Additionally, the incorporation of recovery and reuse of the catalyst can potentially help reduce the catalyst feed costs provided that such recovery and reuse do not significantly add to the operational costs further. The other major cost components include the fixed cost components, with a cumulative contribution of $\approx$ 17M EUR, and the maintenance

cost component, with a contribution of 7.5M EUR. The total OPEX for the CVD-based SWCNT production processes modelled by A. E. Agboola et al. (2007) extends to as high as 186 M EUR. This ≈ 3x higher OPEX than that of the CVD process modelled in this study can be explained by the comparatively higher operating labor costs of ≈ 9M EUR and higher catalyst costs of ≈140M EUR. This draws uncertainty to the costs of the Ni-MO/MgO catalyst and the cost of operating labor estimated in this study and calls for further scrutiny to ascertain reliable estimates.

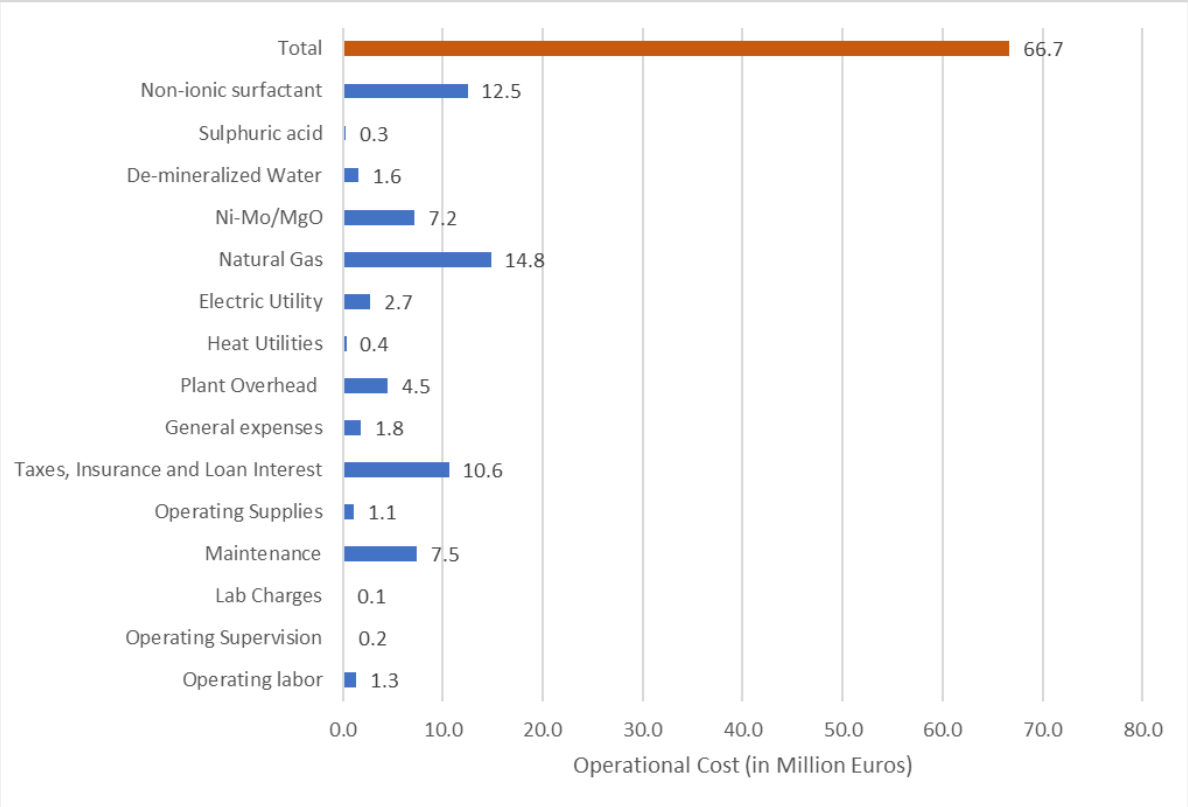

Figure 7.10: Status quo CVD OPEX

The total OPEX for the electrochemical CO_2 reduction process, as shown in Fig. 7.11, is 87.6 M EUR, which is ≈ 20M EUR more than that of the CVD process. Electric utility alone contributes 48.5M EUR, which is more than half of the total OPEX. This is due to the ≈ 270 GWh electricity consumption considered for driving the 750°C high-temperature electrolysis process modelled in this study. Such a high electricity consumption is however associated with a considerable degree of uncertainty, given that it is obtained from geometric scaling of the electricity consumption figure obtained from the lab scale process described by Douglas et al. (2018). This lab-scale electrolysis setup constitutes electrodes with a 2.5 cm^2 surface area and 40g of electrolyte in a ceramically heated crucible which is significantly different compared to the jacketed electrolysis vessel with rolling cathodes of 100 cm^2 surface area and ≈ 5000 tonnes of electrolyte considered in this study. An accurate understanding of the electrolytic disassociation of CO_2 through the electrodes while facilitating a constant electrolyser temperature of 750°C through electric heating utilities for a 5000-tonne scale plant is necessary to further decrease the data uncertainty. Such understanding could help realize potential solutions for optimizing energy use which could in turn improve the economic

performance of this process. The replenishment of the lost Li_2CO_3 during the electrolysis process contributes a considerable amount of 9.8M EUR owing to its high unit costs. The use of cheaper alternative electrolytes and recovery of the spent electrolyte for reuse can potentially reduce these costs. The carbon precursor costs of the PORTHOS CO_2 feed, at 1.7M EUR, is ≈ 10x lower than the natural gas-based carbon precursor feed costs, thus making a case for the electrochemical CO_2 reduction-based MWCNT production. The cost components comprising various labor, maintenance, and fixed costs are considered to be similar to those of the CVD process. However, given the lesser number of process units involved in the electrochemical process compared to that involved in the CVD process, the labor costs could potentially be lower for the electrochemical process. The lack of relevant data on labor requirements for such production processes hinders the accurate estimation of these costs, thus adding to its uncertainty.

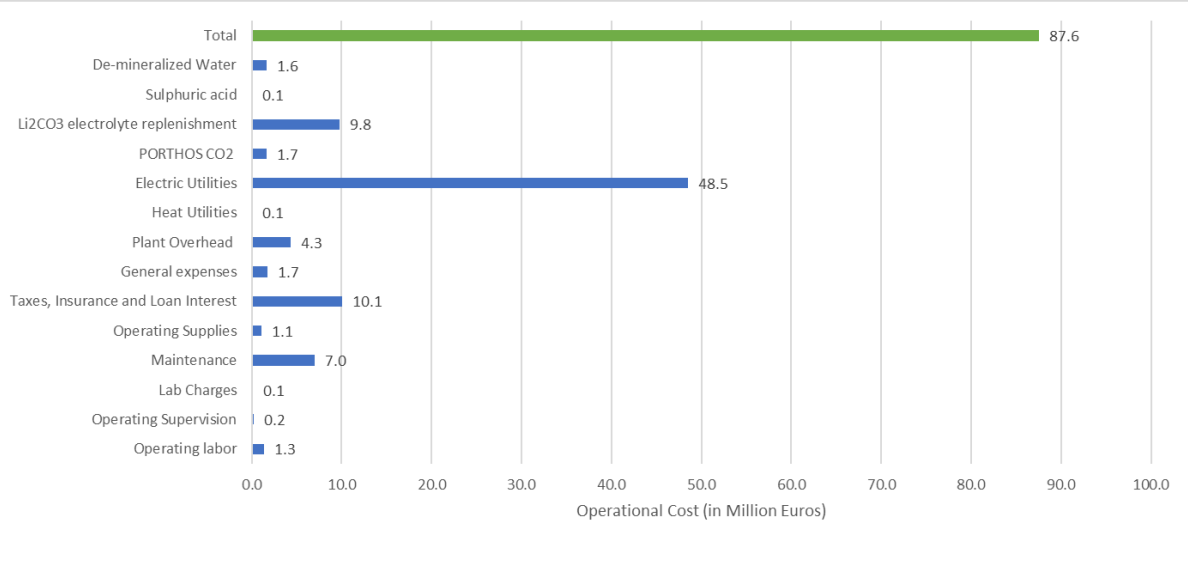

Figure 7.11: Electrochemical CO_2 reduction process OPEX

The sales revenue of the products generated from the two processes is shown in Fig. 7.12. Both processes generate 184M EUR in revenue from the sale of >90% purity MWCNTs produced, based on a unit cost of 36.8 EUR/kg (Made-in-China, 2023). The high unit cost considered may be lower in actuality given the 5000-ton scale considered in this study that enables significant cost reductions through scales of economy. Further, both the processes modelled assume the consistent production of high-quality MWCNTs, as reported by the smaller scale reference studies of Douglas et al. (2018) and Douglas et al. (2017), Douven et al. (2012). The process conditions observed in such smaller-scale processes are however difficult to replicate and maintain in the 5000-tonne scale processes modelled in this study. This may result in greater production of undesirable amorphous carbon and decreased sales revenue, thus attributing uncertainty to the achievability of 184M EUR of sales revenue.

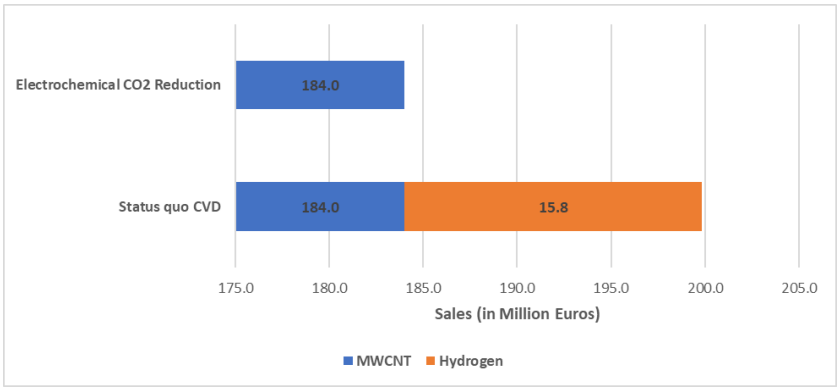

Figure 7.12: Sales revenue generated from the output product streams

The high price of MWCNT is understood to have hindered its large-scale adoption and restricted its market size to less than 800M EUR (Global Market Insights, 2023). The global installed production capacity is estimated to be little over 20,000 tons (Modekwe et al., 2020). Meanwhile, the Netherlands CNT demand is estimated to be just ≈ 40 tonnes (Chemanalyst, 2021). The 5000-tonne MWCNT production processes, which are modelled with respect to a Netherlands geographical scope, can thereby satisfy local and global demands for MWCNT. Additionally, this large scale of MWCNT production was considered to evaluate the potential feasibility of reducing costs through scales of economy. Such cost reduction can accelerate its large-scale adoption and unlock its use in new applications.

Further, the CVD process also generates an additional revenue of 15.8M EUR from the sale of 99.8% purity H_2, with a unit cost of 8.3 EUR/kg (Chemanalyst, 2023). The unit price considered is however for 99.9% pure H_2 streams whereas the H_2 generated by the CVD process modelled in this study consists of 0.2% impurity of CH_4. This limits the use of such H_2 stream from high-purity applications such as fuel cells (Gasunie, 2023).

7.2.3. Net Present Value & Payback Period

Net Present Value (NPV) calculation facilitates the evaluation of the overall economic performance and profitability of the plant throughout its lifetime considering the various costs incurred, the revenue generated from the plant's operation, the depreciation undergone, and the taxes levied. The economic performance throughout the lifetime of the plant depends on the cashflows generated each year. NPV of a plant is estimated by the summation of cashflows generated over the lifetime of the plant while discounting such cash flows (CF) at a fixed discount rate(r), as shown in Eq. 7.3 (Towler & Sinnott, 2012). A process plant with a higher NPV is preferred as it reflects the generation of greater economic value over the lifetime of the plant.

$$NPV = \sum_{n=1}^{n=t} \frac{CF_n}{(1+r)^n} \tag{7.3}$$

A discounted cash flow spreadsheet for the 20-year operational plant life is generated, as shown in Appendix F, based on the book 'Chemical Engineering Design: Principles, Practice and Economics of Plant and Process Design' (Towler & Sinnott, 2012). A modified accelerated cost recovery system(MACRS) for 5 years, as explained in Towler and Sinnott (2012), is assumed to

be applicable in this study for factoring the capital depreciation. The Netherlands corporate tax rate of 25.8% is considered for the tax deductions (PWC, 2023). A discount rate of 10% is assumed to be applicable in this study. The plant construction is assumed to be completed in year zero and the production of CNM is assumed to start from year 1 itself. Further, the costs of yearly replacement of cathode and 5-year anode replacement for the electrochemical process and the 10-year CVD reactor replacement for the CVD process are taken into account as they are not included in the yearly OPEX cost estimation.

Payback period (PBP) helps determine the time, in years, to recover the initial investment from the annual cash flows generated from the sale of the final product. The formula for payback period is as shown in Eq. 7.4. This study evaluates a simple payback period (Towler & Sinnott, 2012) which is based on the assumption that the TCI for the plant construction is completed in year zero itself. The average annual cash flow is calculated based on yearly tax-deducted cash flows over the assumed 20-year plant operational life. PBP is favoured to be as low as possible as it would reflect the faster recoupment of the money invested which would increase investor confidence and allow faster debt repayment.

$$PBP = \frac{\text{TCI}}{\text{Average Annual Cash Flow}} \tag{7.4}$$

The NPV and PBP for the two processes are shown in Fig. 7.13, which are calculated from their cash flow spreadsheet in Appendix F. The CVD process has the highest NPV of 0.76 Billion (B) EUR and the lowest PBP of 1.25 years, compared to the 0.53B EUR NPV and 1.62 years PBP of the electrochemical process. The factors attributing to the better economic performance of the CVD process over the electrochemical process, with regards to NPV and PBP are perceived to be:

- ≈ 20M EUR higher OPEX of the electrochemical process
- ≈ 16M EUR higher sales revenue of the CVD process

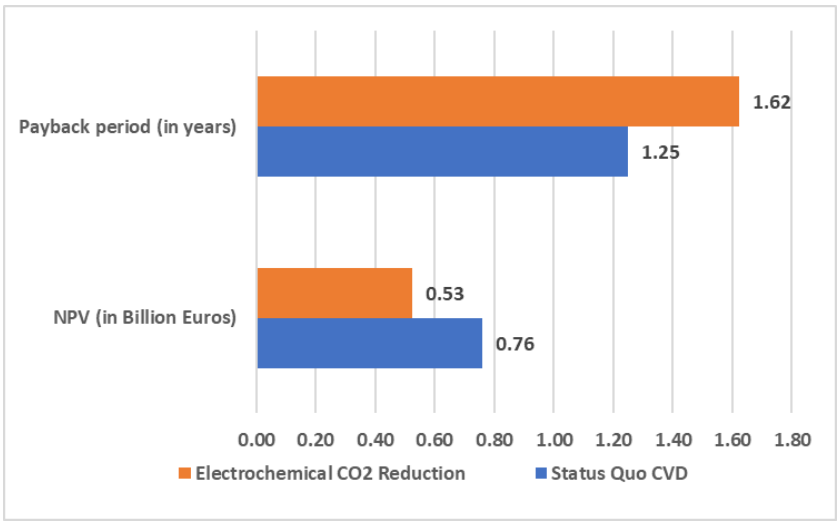

Figure 7.13: NPV and Payback period results of the two processes

The CVD processes modelled by A. E. Agboola et al. (2007) are shown to have high NPVs

of up to 0.75B EUR based on a 10-year plant operational life consideration. This is because the cost of SWCNT considered by A. E. Agboola et al. (2007) is an exceptionally high figure of 82.8 EUR/kg, which is understandable given the 2005 temporal scope and price superiority of SWCNT over MWCNT. However, for a 10-year operational life consideration, the calculated NPV of 0.75B EUR is very high compared to the 20-year operational life based 0.76B EUR NPV of this study's CVD process. This makes the economic assessment performed by A. E. Agboola et al. (2007) seem unrealistic.

The positive NPVs of >500M EUR and PBPs of less than 2 years make both the modelled processes of this study seem financially very attractive. However, it is important to note that these high NPVs and low PBPs are primarily based on the inherent modelling considerations that -

- both processes will consistently produce 5000 tonnes of high-quality MWCNT
- the market for the produced MWCNT exists with a retail price of 36.8 EUR/kg
- the OPEX and replacement costs (≈ 90M EUR) calculated are less than half the sales revenue (≈ 180M)

These considerations were taken during the research due to the lack of plant-level data which renders a more realistic NPV and PBP estimation difficult and thus adds uncertainty to these results. Such profitable NPV and PBP estimates would also be associated with high global interest in MWCNT production through either of the processes, however, that is not the case in actuality. Firstly, this could be because of the lack of technical expertise to overcome the high technological complexity associated with the large-scale production of the nanometer-sized MWCNT. Secondly, the high temperatures involved in these two processes also make the production of MWCNT risky and unfavourable. Thirdly, the 20,000 tonnes market demand for MWCNT (Modekwe et al., 2020) is low compared to that of other carbon-based commodities, such as methanol with a global demand of 75M tonnes (Methanol Institute, 2023), thus making MWCNT production economically unattractive. Given that CNT has only been officially discovered in 1991 (J. Chen et al., 2021), its growth mechanism is still yet to be fully understood (Kumar, 2011) and its applications are still yet to reach maturity. With growing research and understanding of CNT, improved risk tolerance through safety improvements and advances in its large-scale applications, such as in concrete (Dimov et al., 2018; Manchester, n.d.), the three mentioned drawbacks could be overcome to realise large-scale profitable production of MWCNT. The interest in such large production of MWCNT can be observed to be picking up with planned capacity increases of several thousand tons by leading companies such as LG Chem for satisfying demand from battery applications (Businesswire, 2023). Moreover, China specifically is reported to have a considerably large number of MWCNT manufacturers (Modekwe et al., 2020), indicating an increasing interest in MWCNT production.

7.3. Environmental Assessment

A motivation for modelling commercial scale, industrial flue gas CO_2-based MWCNT production from the electrochemical process is the anticipation of realising enhanced environmental performance over the conventional fossil CH_4-based CVD production of MWCNT. Based on the 'gate-to-gate' scope established earlier in Section 2.4, the GHG emissions directly resulting from the two processes, which are known as scope 1 emissions, can be evaluated. Further, the considerable quantity of externally sourced energy used in the two processes makes it

interesting to capture the GHG emissions associated with it, which form the scope 2 emissions. The combined assessment of such scope 1 and scope 2 emissions resulting from the two processes (Bhatia et al., 2004) can help evaluate their environmental performance with respect to the climate change impact contribution of these emissions. Further, the net avoided emissions from using the industrial flue gas based CO_2 for the electrochemical process can shed light on the avoided climate change impact on a Scope 1 and Scope 2 level.

In order to evaluate these impacts, this study performs an attributional life cycle assessment (LCA) of the CVD and electrochemical processes at a simplified level of sophistication (Guinée, 2002). Attributional LCA involves the evaluation of the life cycle impacts associated with a set demand of the product unit being assessed (ISO, 2014), which is applicable to this study for assessing the impacts of commercial scale MWCNT production. The free CMLCA software v6.1 from Leiden University is used to perform this LCA. The lifecycle inventory (LCI) database corresponding to Ecoinvent v3.4 (Ecoinvent, 2017) is integrated into the CMLCA software which includes pre-defined data on the environmental impacts associated with various products and services of different geographical origins. The use of LCA in this study thus allows for an environmental assessment of the processes modelled and adds to the credibility of this study.

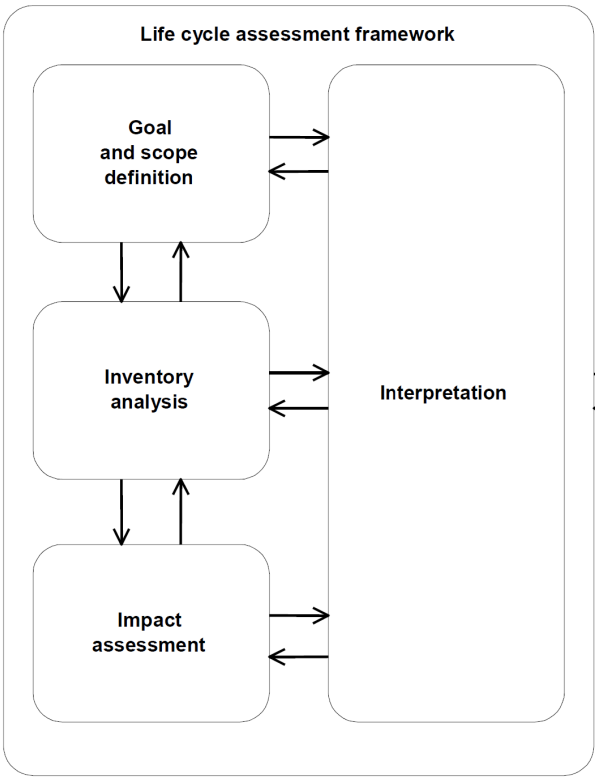

Figure 7.14: LCA framework (ISO, 2014)

The LCA framework elaborated in Guinée (2002) and shown in Fig. 7.14 is followed in this study. The components of the LCA framework in regard to this study, are described below:

1. Goal and Scope Definition: This step elaborates on the goal of the LCA study, the product/service under evaluation, the process boundary scope considered, and the study's

geographic, temporal, and technological scope. The products/services, which are compared, are defined by their reference flows. These reference flows constitute the function and functional unit of the respective product/service.

The *goal* of this LCA is to compare the environmental performance of 'gate to gate' MWCNT production through status quo CVD and electrochemical CO_2 reduction processes, with respect to their climate change impacts. The goal also additionally includes the estimation of the avoided climate change impacts from using waste CO_2 in the electrochemical process.

The 'gate-to-gate' *scope* of this LCA additionally includes the utilities involved in the two processes. Such a 'gate to gate' scope is used to ascertain the impacts of the processes at Scope 1 and Scope 2 levels along with the avoided impacts from using waste CO_2. The data associated with the two processes is mostly based on sources with the geographical scope of the Netherlands and its nearest vicinity. Data from 2022-2023 was used when possible and when not possible, the most recent data was applied. The technology maturity of the CVD process considered is higher than that of the electrochemical process. It is also important to note that this study restrictively performs the LCA considering the whole process as a single process unit instead of employing multiple process units. The end objective of identifying scope 1, scope 2 and avoided impacts deems such a LCA fit for this study.

The *function* of the two processes being compared in this LCA involves the production of small-diameter MWCNT. The *functional unit* of this LCA study is considered to be 5000 tons of small-diameter MWCNT based on the commercial scale Aspen modelling of the two processes. Based on the two *alternative* processes of status quo CVD and electrochemical CO_2 reduction compared in this study, the LCA *reference flows* can be generalised as '5000 tons of small diameter MWCNT production from one of the two processes.

2. Inventory Analysis: In this step, the flow diagrams for the two product systems associated with the previously defined reference flows are created, as shown in Fig. 7.15 and 7.16. The flow diagrams are shown to define the system boundary that demarcate the various feed and waste streams as cutoffs whose pre-processing and post-processing steps are not considered in the LCA in accordance with the 'gate to gate' scope. The foreground process units involve the MWCNT production processes modelled in this study, whereas the background process units involve those that are already defined in the LCI database, such as those supplying steam-based heat and electricity for use in the foreground process units. The economic flows shown in the flow diagrams represent the products, services and wastes circulating into, within or out of the system. These flow diagrams do not display the inflow of environmental resources and outflow of environmental emissions, however, they are taken into account in the LCA. These flow diagrams of the two product systems are accordingly replicated in the CMLCA software using the mass and energy balance data generated from the Aspen process models, as described in Section 6. The main objective of the inventory analysis step is to ascertain the environmental flows associated with these two product systems.

It is important to note that the background processes are based on the 2017 LCI database integrated into the CMLCA software, which forms a limitation of this study. This database does

not comprise any data for the chilled water utility, for which reason such utility is disregarded in the LCA product systems. Also, the varieties of steam generated from the process units are considered as cutoffs and not as co-products, to ensure attribution of environmental impacts mainly to the saleable commodities of MWCNT and the H_2 generated.

The CVD process LCA flow diagram shown in Fig. 7.15 considers the 7 input economic flows based on the feed streams of the CVD process, electricity from the Netherlands market background process, the waste liquids generated as one waste stream, the reference flow of the MWCNT product stream and the co-product stream of H_2. Since the low-pressure steam is both consumed and generated by the CVD process, an associated background process for it is disregarded in the process diagram. The CVD process unit is modelled as a multifunctional process, wherein the environmental emissions associated with the two products generated from this process are economically allocated between them based on their respective unit prices (Section 7.2.2). The unit process data used for the CVD foreground process unit can be referred to from Appendix D 7

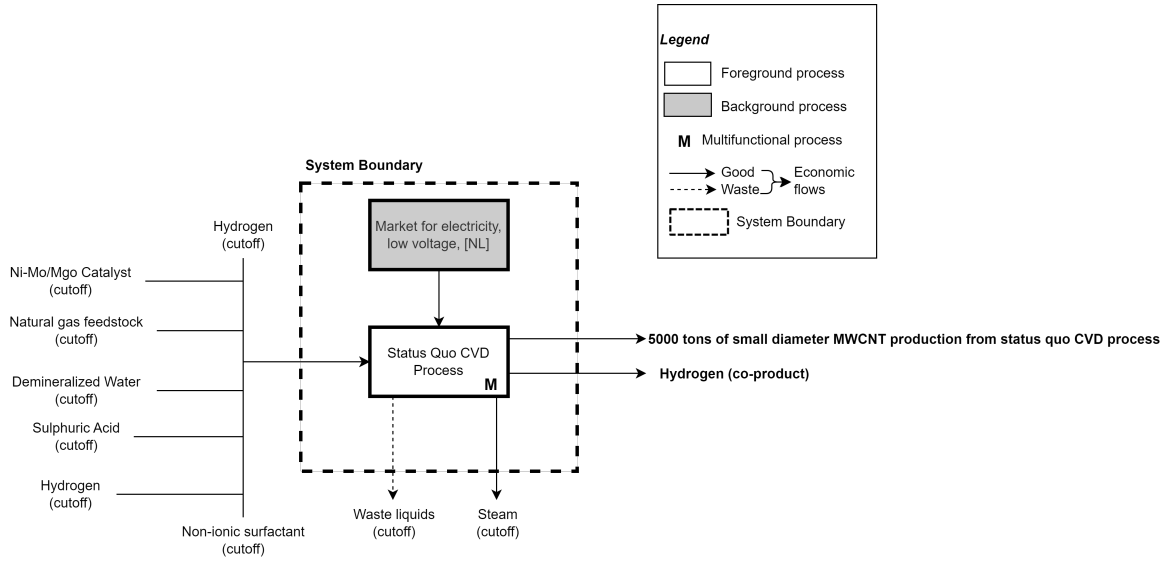

Figure 7.15: CVD LCA flow diagram

The electrochemical process LCA flow diagram shown in Fig. 7.16 considers 4 input economic flows based on the feed streams of the electrochemical process, low carbon renewable electric energy from a Netherlands(NL) based wind electricity production background process, steam-based heat energy from a European (RER) region based process, the waste liquids generated as one waste stream and the reference flow of the MWCNT product stream. The unit process data for the electrochemical foreground process unit can be referred to from Appendix D 8.

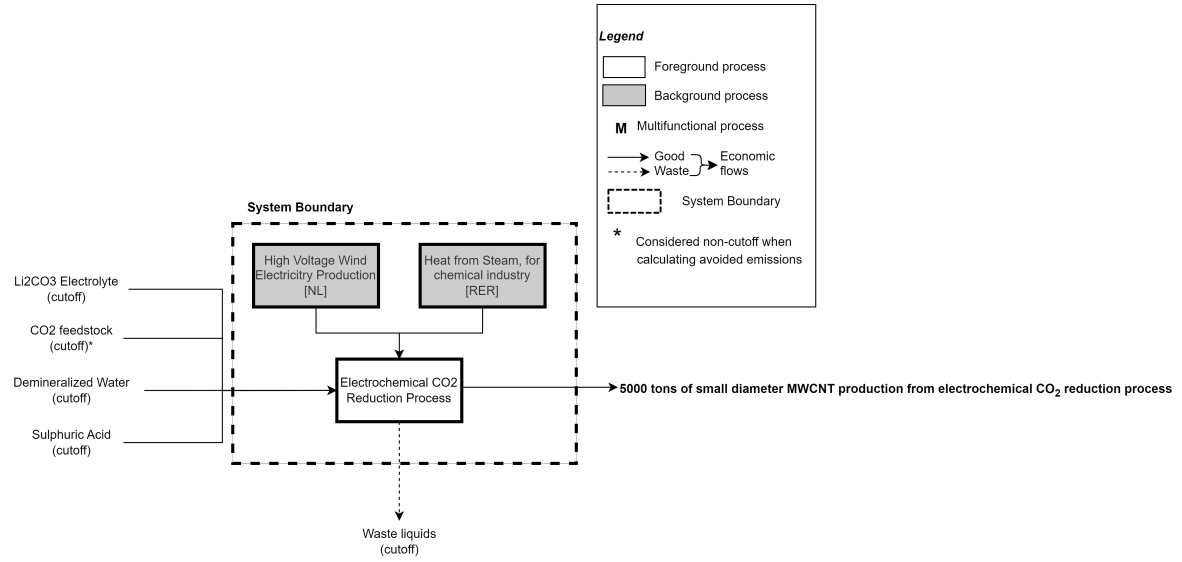

Figure 7.16: Electrochemical CO_2 reduction LCA flow diagram

Three LCA models were created on the CMLCA software for comparing the two product systems discussed based on their absolute scope 1 emission impact, absolute scope 1 + scope 2 emission impact, and net scope 1 + scope 2 emission impact considering the avoided CO_2emissions. The LCA model for the net scope 2 emission impact specifically involves considering the input CO_2 feedstock as an environmental CO_2 flow of fossil origin instead of a cutoff, which allows for the net reduction of the overall scope 2 GHG emissions. The resulting inventory of environmental flows generated from the three LCA models of the CVD-based product system and electrochemical process-based product system can be referred to from Appendix D 9 and D 10 respectively.

3. Impact Assessment and Interpretation: Impact assessment involves measuring the environmental impacts generated by the environmental flows by categorizing them into relevant impact categories and standardising them to a single reference unit that best represents the impact category. This study evaluates the results of the 'Climate Change' impact category that characterizes the environmental flows of mainly CH_4, CO_2 and CO to the reference unit of kg CO_2 equivalent (eq). based on their 100-year global warming potential. The CML 2001 characterization factors are used for standardizing these environmental flows, as shown in Fig. 7.17. Interpretation entails the examination of the impact assessment results to make sense of any underlying implications and assess these results for completeness and consistency.

Environmental flow	Characterisation factor	Unit
Carbon dioxide	1	kg CO2 eq/kg
Carbon monoxide	1.57	kg CO2 eq/kg
Methane, fossil	25	kg CO2 eq/kg

Figure 7.17: GWP Characterisation factors applicable for GHG environmental flows of the two processes

The climate change impacts calculated from the three LCA models are shown in Fig. 7.18. The CVD process is shown to have a high scope 1 climate change impact of 73.9M tonnes(t) CO_2 eq which is two orders of magnitude higher than that of the 2.2 Mt CO_2 eq scope 1 climate

change impact of the electrochemical process. The scope 2 impacts, indicated in red, are found to be ≈ 8.5Mt CO_2 eq for both processes. The CVD scope 2 impact from externally sourced energy is an order of magnitude smaller than the comparable scope 1 impact because of the modelling considerations of high heat integration and fired heat utilities within the processes. The case is however not the same for the electrochemical process, whose high electrical energy requirements are externally sourced leading to a scope 2 impact that is ≈ 4 times higher than the scope 1 impact. This scope 2 impacts could be significantly higher if gird-electricity from the Netherlands energy market is used instead of renewable wind energy as a considerable proportion of the grid electricity is fossil-based. The 10.7Mt CO_2 eq from the combined scope 1 and scope 2 impacts of the electrochemical process are reduced to -9.6Mt CO_2 eq, when the avoided CO_2 emissions from the flue gas feed stream are taken into account. This results in a net avoided impact of 20.3Mt CO_2 eq, highlighted in green, which indicates the huge upside of reduced environmental impact achieved from the use of waste CO_2 streams.

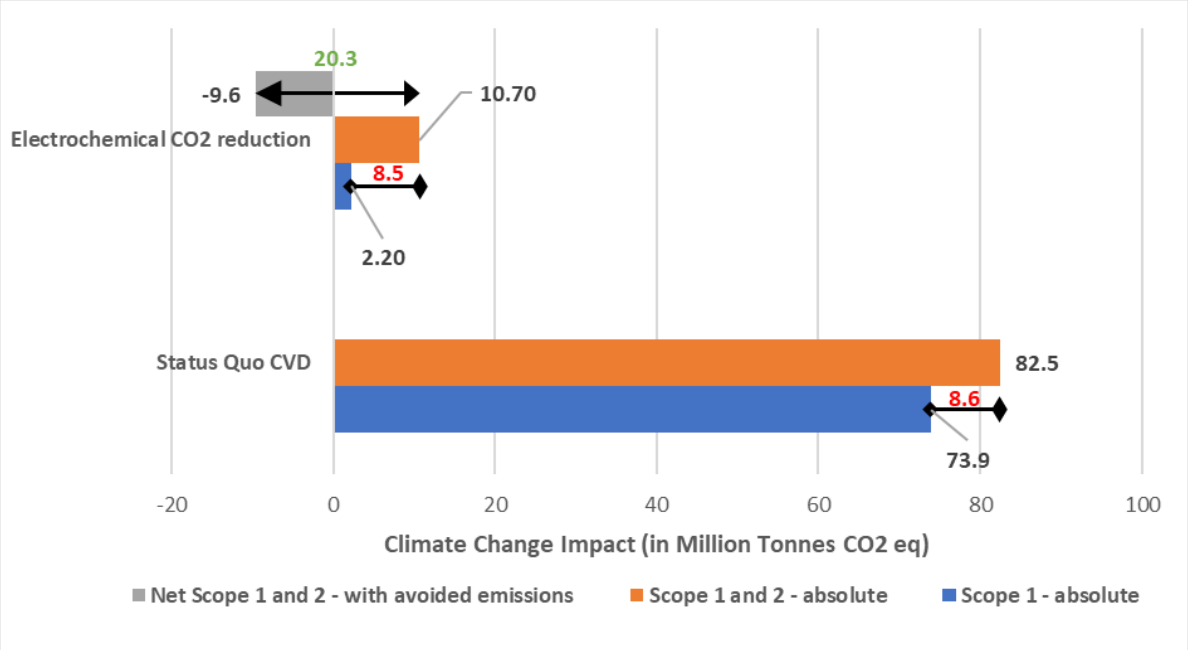

Figure 7.18: Climate change impacts from the GHG emissions of the two processes

The scope 1 climate change impact contribution by GHG emissions for the two processes is shown in Fig. 7.19 below. The CVD process impacts are majorly driven byCH_4 emission, which contributes 81.3%, followed by CO_2 which contributes the rest 18.7%. The high impact of methane emission is due to its purge from the recycle stream in considerable quantities as well as its high characterisation factor of 25kg CO_2 eq/kg. Although $CO_2$is emitted in significantly high quantities mostly from the amorphous carbon oxidation process unit, its low characterisation factor of 1 kg CO_2 eq/kg leads to its lower impact. The electrochemical process impacts are more or less equally driven by the CO_2 and CH_4 emissions which have impact contributions of 52.6% and 47% respectively. These emissions mostly originate from a small proportion of the input PORTHOS stream that is not utilised in the electrolyser process unit and released into the atmosphere. The CH_4 emission, although much lower in magnitude than CO_2, contributes greatly due to its high characterisation factor as mentioned earlier. CO only contributes a minor 0.4% impact due to its substantially low presence as an impurity in

the PORTHOS input stream coupled with its low characterisation factor of 1.57 kg CO_2 eq/kg.

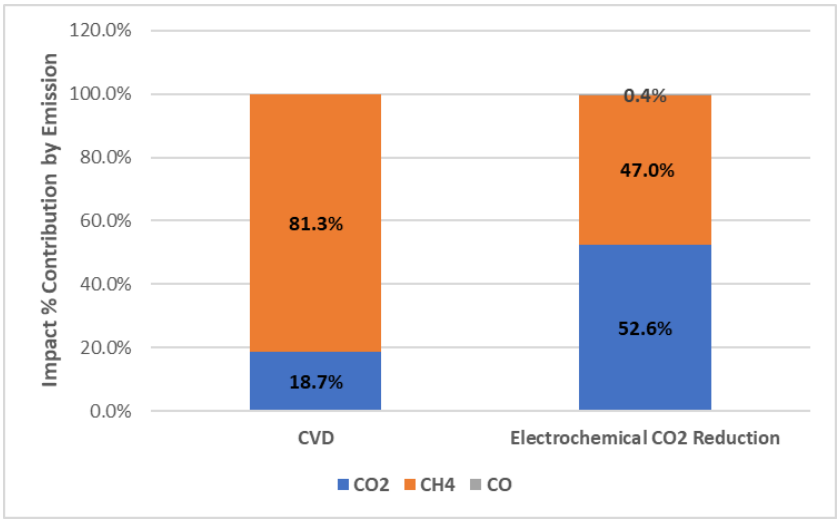

Figure 7.19: Scope 1 climate change impact contribution by GHG emissions

The combined scope 1 and scope 2 climate change impacts by GHG emissions are shown in Fig. 7.20. The impact contribution by emission can be observed to change considerably with more impact being attributed to CO_2 emissions compared to that attributed to Scope 1CO_2 emissions. This is because the Scope 2 emissions stemming from external energy use mainly constitute CO_2 emissions. Other GHG emissions such as C_2H_6, N_2O, etc., also form part of the environmental flows of foreground MWCNT production process units and the background electric and steam utility process units. These emissions, due to their small magnitudes, jointly contribute only 0.6% and 2.2% to the climate change impacts of CVD and electrochemical processes respectively.

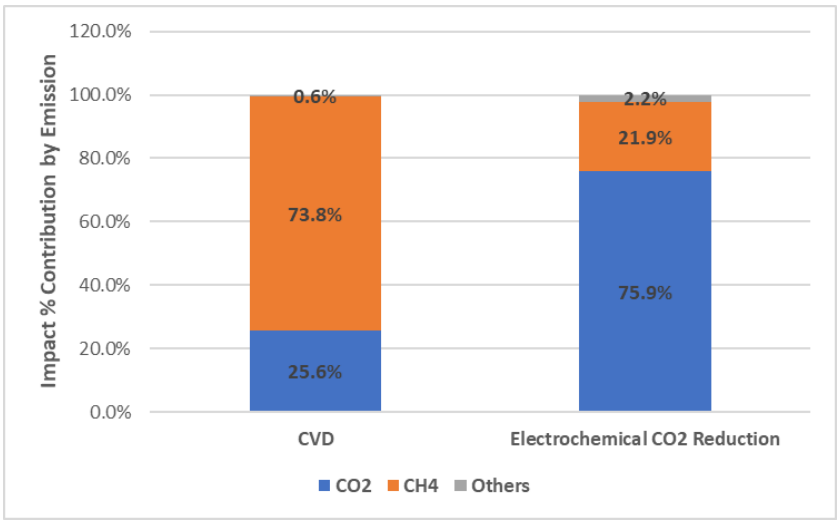

Figure 7.20: Scope 1 and 2 climate change impact contribution by GHG emissions

The contribution of different GHG emissions to the net scope 1 and scope 2 climate change impact of -9.6 Mt CO_2 eq for the electrochemical process is shown in Fig. 7.21 The input CO_2 flow, which was factored into the LCA model as fossil-based environmental flows, results in a

climate change impact decrease of 12.2 Mt CO_2 eq. The methane emissions resulting from the background utility processes and the impurities of PORTHOS stream result in 2.3 Mt CO_2 eq. GHG emissions, apart from CH_4 and CO_2, contribute a minor impact of 0.2%. The net scope 1 and scope 2 climate change impact assessment can also be performed for the CVD process by using a waste/renewable source of methane such as biomethane. The use of such biomethane could also similarly help realise significant avoided climate change impacts from CVD-based MWCNT production.

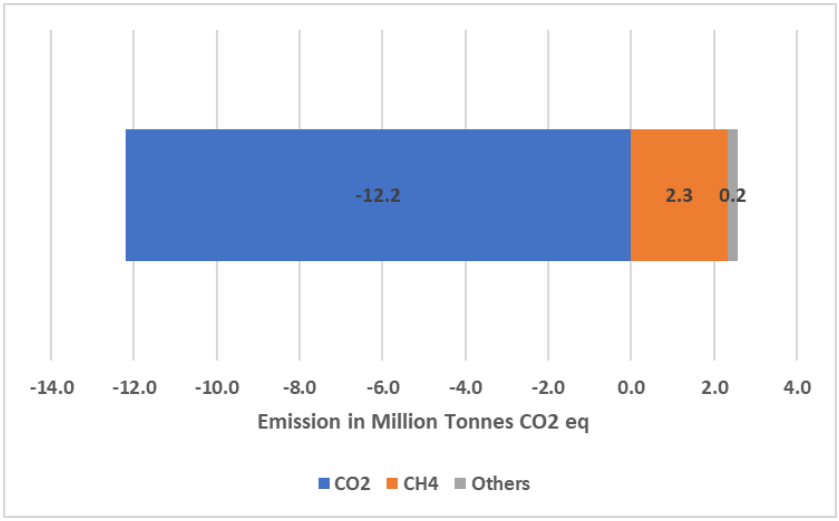

Figure 7.21: Net scope 1 and 2 climate change impact by GHG emissions for the electrochemical process

In regard to the completeness of this study's comparative LCA of the two processes, relevant information from the two corresponding Aspen process simulations was used. Any lack of data and assumptions are accordingly stated during process modelling in Chapter 5. The LCA assessment was also found to be consistent with the goal and scope of this study which involved comparatively assessing scope 1, scope 2 and avoided climate change impacts of the two processes in accordance with the earlier established geographical and temporal scope. The processes compared are, however, not consistent with respect to their technological maturities. The electrochemical process with lower technological maturity involved the use of lab-scale process data which adds greater uncertainty to its impact assessment compared to that of the CVD process which is based on commercial-scale process data.

7.4. Discussion on Overall Research

This research is guided by the MDM described in Fig. 3.1, wherein it focuses on the product technical system of sustainable CNM production and its comparative performance against the status quo CNM production. The use of such MDM helps provide a systems perspective by linking the impacts of the product-technical system to the impacts at higher levels of the product-service system, socio-technical system and societal system through a bottom-up approach. In the case of this study, the realization of sustainable CNM production could be linked to achieving industrial symbiosis of CO_2 gases at the product-service system level, which in turn could be linked to reduced GHG emissions at the socio-technical system level, which in turn could be finally linked to reduced global warming and climate change at a societal system level. At the product technical system, MDM's 4 cyclic steps (Fig. 3.1) of reflection,

analysis, synthesis, and experience provide a sequential framework for answering the research questions of this study in a holistic manner.

The reflection and analysis step helped delve deeper into the status quo CVD processes of fossil-based CNM production and novel processes of CO_2 based CNM production and furthermore helped understand various aspects such as their drawbacks and advantages. This reflection and analysis step however majorly focused on the novel CO_2 based processes and the status quo CVD process coverage could have been more exhaustive with the inclusion of more recent studies. This is recognised as a limitation.

The synthesis step involved the development of a framework for the selection of comparable status quo CVD process and electrochemical CO_2 reduction process for MWCNT production. This framework could be applied directly or adapted accordingly for use in studies that seek to select comparable processes for other types of CNM such as graphene. The case studies of the two selected processes helped develop a greater understanding of their working principles, which were further used to develop process designs with essential unit operations. The Netherlands scope selected is ideal and relevant for this study given the industrial symbiosis potential associated with using the PORTHOS CO_2 stream for the electrochemical CO_2 reduction process plant. This study does not however explore the industrial symbiosis potential for the CVD process with biomethane use. This is a drawback, given the high quantities of biomethane that could be potentially valorised from sources such as biomass waste and cattle manure generated in the Netherlands, which is known to be agriculturally intensive (Bos et al., 2013). The processing of the input carbon precursors is not explored in great detail as the process designs in this study were designed considering a gate-to-gate scope.

The process designs are then accordingly simulated in Aspen Plus based on data obtained from the literature associated with the two selected processes. This data however corresponds to a much lower scale of MWCNT production compared to the 5000-tonne commercial scale considered in this study. The data from the literature could be easily scaled and used in Aspen Plus process simulations, as Aspen Plus automatically sizes the equipment needed based on the scaled data. Aspen Plus enables quick identification of the equipment needed and technical constraints of various process units, thus allowing for a realistic depiction of the processes. The mass and energy balance data obtained from the intermediate versions of the process models allowed for improvements in energy and resource use.

The Aspen Plus simulation of the CVD process involved the assumption of ambient pressure operating conditions, based on Douven et al. (2012). However, at such a large scale of 5000 tonnes of annual MWCNT production, higher operating pressure could be required to maintain mass flows between process units and to fasten the reactions happening in various process units, thus indicating a limitation. The inclusion of the recycle stream in the process model causes the dilution of CH_4 and H_2 components to a combined $\approx$ 50 mol.% in the main input stream of the CVD process unit. The remaining stream components involve majorly N_2 and small amounts of C_2H_6, C_3H_8 and CO_2, which accumulate over time in a steady state process. These remaining stream components are assumed to be inert in this process, however, they could have significant impacts on the MWCNT formation which forms a limitation of this process. Further,

the equipment is evaluated to accommodate the flow of these assumed inert flows which do not play any role in the CVD process, thus leading to higher than necessary equipment costs and resulting in another limitation. Only 20% of the carbon formed from the CVD process is assumed to be amorphous carbon and the rest 80% is assumed to be MWCNT based on A. E. Agboola et al. (2007) which may not be the case in reality, and thus forms a serious limitation. The PSA system involved adaptations of the original system from Burgers (2020) to higher temperature and greater purification conditions, which may not be possible in actuality and thus forms a limitation of this study. Further, the relevant equipment for the PSA process is not available on Aspen Plus which creates uncertainty for its cost evaluation and thus adds to the limitation of the PSA system. The relevant equipment for the froth flotation process unit is also not available on Aspen Plus. Further, the data applicable for the separation of high quantities of MWCNT from froth flotation was lacking and resulted in the consideration of a high quantity of surfactant, thus adding another limitation to this process. The cyclone equipment used in the process is assumed to be 100% efficient in separating the gases from solids which may not be the case in reality and thus forms a limitation. The high-speed disk centrifuge considered in this process only separates particles up to 500 mm in size, which is a limitation as Aspen Plus does not provide another alternative that can filter nm-sized particles of MWCNT.

The learnings from the design and simulation of the CVD process aided in the ex-ante process design and simulation of the electrochemical CO_2 reduction process. The large-scale simulation of the status quo CVD process was based primarily on the conceptual process design of SWCNT production from the peer-reviewed study by A. E. Agboola et al. (2007). The same, however, was not possible for the electrochemical CO_2 reduction process which was mostly based on assumptions from lab scale data provided by Douglas et al. (2018), Douglas et al. (2017) and a non-peer-reviewed study by Srininvasan (2018). Hence, there is considerable uncertainty associated with the large-scale electrochemical process simulation due to the lack of reliable data, which forms a limitation. One of the greatest limitations of this process is the inability to model the electrolyser in the Aspen process simulation. Due to this, the Fe cathode particles that are scraped off the cathode while collecting the MWCNT, could not be reflected in the simulation, thus leading to 100% purified MWCNT as the final product. In order to be comparable to such MWCNT, the CVD process was also modelled to produce 100% pure MWCNT. Such MWCNT are not representative of the reference MWCNT with trace impurities of transition metal, as defined in Section 4.1 , thus forming a limitation for both processes. Also, other types of CNM are assumed to be absent and only MWCNT is assumed to form on the cathodes. This may not be the case in actuality and would thus impose a serious limitation on this study. The technical data on RotoDynamic heater incorporated for supplying the heating needs of this process is inadequate leading to grave assumptions on its costs and efficiency, thus becoming a limitation for the electrochemical process simulation. The yearly replacement of the steel cathode, five-year replacement of the Ni-anode, and the Li_2CO_3 electrolyte losses in the electrolyser process unit highlight the considerable loss of critical resources resulting from such process, which forms a material use limitation of this process. Additionally, the CVD process limitations associated with the use of centrifuge and cyclone equipment are also applicable to the electrochemical process.

The final experience step of the MDM involved the technical, economic and environmental

comparison of the two simulated processes based on the data obtained from their mass and energy balances. The EE technical indicator compares the heat and electric utility efficiencies to one another, which may not be appropriate given that heat and electricity are two different types of energy sources. An exergy analysis is better suited for such a comparison, however, such an analysis could not be performed in this study, thus forming a limitation. Some of the feedstock prices used in this study were obtained from the Alibaba website(Alibaba, 2023) which may not reflect the actual cost of the feedstocks and thus forms a limitation for calculating the OPEX and subsequently the NPV and PBP. The attractive NPV and PBP values obtained were attributed to three modelling considerations. A sensitivity analysis to ascertain how sensitive these NPV and PBP values were to the changes in the modelling considerations could not be performed, which forms a limitation. Such sensitivity analysis could also help ascertain the minimum market cost of CNM to achieve a positive/zero NPV.

The environmental performance of the two processes is determined in this study using the LCA tool, which is a fundamental approach of Industrial Ecology to ascertain environmental impact assessment. LCA was performed in this study to primarily ascertain the scope 1 and 2 emissions of the climate change impact category, which clearly shows the electrochemical process to perform better than the CVD process. However, the evaluation of scope 3 emissions with additional impact categories, such as depletion of abiotic resources, could have different conclusions given the significant material use limitation associated with the electrochemical process, thus forming a limitation of this LCA. The electrochemical process has a high electricity consumption of 270 GWh/yr for heating the process to a high temperature of 750°C and for driving electric CO_2 disassociation. The environmental assessment was performed considering the use of renewable wind energy from the Netherlands for satisfying the large energy requirement which however could affect its availability for other essential requirements such as powering homes. This in turn could have negative externalities of high renewable electricity prices and increased usage of cheaper fossil-based sources for other essential requirements, thus resulting in a serious limitation. Therefore a sensitivity analysis to ascertain the impacts of considering electricity from the Netherlands energy grid instead could be insightful. Further, a sensitivity analysis involving the use of biomethane in the CVD process could indicate potential improvements in the environmental performance of the CVD process.

From the results of this study, it is observed that CO_2 utilisation through electrochemical CO_2 reduction process for MWCNT production has favourable NPV and PBP estimates, which indicate profitability, and avoided climate change impacts at the scope 1 and scope 2 level, which indicate environmental sustainability. This profitable and environmentally sustainable consumption of industrial CO_2 emissions as a raw material can potentially have the negative externality of allowing companies to delay their decarbonization efforts, through end-of-pipe carbon capture and utilisation and continue indiscriminate use of fossil fuels. However, if such negative externalities are prevented, CO_2 utilisation for MWCNT production can help pay for the carbon capture efforts which generate the initial spark of motivation for industries to captureCO_2 from their flue gases. Given the pace at which climate change impacts are worsening across the world, rapid progress must be achieved to reduce the industrial CO_2 emissions. The CO_2 utilisation for MWCNT production can help achieve this rapid progress and thus create value for the captured carbon. The industrial symbiosis potential of PORTHOS

CO_2 stream can be valorized this way instead of it being transported to the seabeds for storage. Further, the utilisation of CO_2 captured from the atmosphere for MWCNT production could potentially help achieve net negative emissions based on the final application of MWCNT and in conformance to the negative emission qualifications discussed by (Eleanor Tanzer & Ramírez, 2019). One such application could be its large-scale utilisation in concrete structures, which could essentially imply the storage of CO_2 in the form of MWCNT throughout the long life of the concrete structure. The realisation of net negative emissions can make this CO_2 utilisation process technology Paris compatible, as defined by de Kleijne et al. (2022), and thus accelerate large scaleCO_2 removal from the atmosphere for decelerating and potentially reversing climate change.

7.5. Recommendations

Several limitations of this study have been outlined in Section7.4 . The following recommendations are made to further improve the study and overcome some of these limitations:

1. Addressing the lack of data through interviews with relevant professionals in the industry for data collection
2. Optimisation of heat integration for efficient use of energy
3. Modification of the CVD process simulation to suit the requirements of the PSA system, as stated by Burgers (2020)
4. Use of MATLAB for more detailed modelling of the electrolyser and linking the same to Aspen Plus process simulation of electrochemical CO_2 reduction process
5. Exergy analysis for comparison of energy types
6. Sensitivity analysis of NPV and PBP estimations
7. Consideration of scope 3 emissions and other impact categories in the LCA
8. Sensitivity analysis for LCA of the electrochemical process considering the use of electricity from the electricity grid mix of Netherlands
9. Sensitivity analysis for LCA of CVD process considering the substitution of fossil-based natural gas with biomethane

Further research avenues that can build upon the results and insights generated in this study and bring greater value are recommended below:

1. Case study for the implementation of an electrochemical CO_2 reduction plant for sustainable and profitable MWCNT production within the Port of Rotterdam region using PORTHOS CO_2 stream
2. TEEA study of atmospheric CO_2 capture and conversion to CNM and its potential to achieve net negative emissions through various applications

8

Conclusion

The primary objective of this study is to address the lack of understanding of the commercial-scale implementation of novel CO_2 based CNM production and its comparison with status quo CNM production processes using unsustainable fossil resources. The study uses a multilevel design model to frame this primary objective from the perspective of the product technical system level. This objective is further expanded to the higher system levels which highlight its overarching implications for facilitating industrial symbiosis, GHG emission reduction, and global warming reduction.

Based on this objective, the main research question of this study was framed as : *"How to assess ex-ante CO_2 based CNM production, considering its technical, economical, and environmental aspects for its commercial implementation, and how does it compare against the status quo CNM production?"*

To answer this main research question, first, a literature review is performed on the status quo commercial-scale CNM production processes and the lab-scale CO_2 based processes. In regards to the status quo processes, the literature review yielded mainly CVD processes of CNT and graphene production. With respect to the lab scale CO_2 based processes, the literature review involved categorising the identified processes into four different approaches based on their working principles. Following such literature review, a framework is developed to select one process each from the status quo CVD processes and the novel CO_2 based processes, which produced comparable CNM. This framework is applied to the processes obtained from the literature review, which led to the selection of a methane-based CVD process and an electrochemical CO_2 reduction process for small-diameter MWCNT production. These selected processes were designed and simulated in Aspen Plus at a commercial-scale production level of 5000-tonnes per operating year. The mass balance, energy balance, and equipment cost data obtained from the simulations of the processes were used to assess the technical, economic, and environmental indicators of the ex-ante CO_2 based production process and the status quo CVD production process. The "How to assess" part of the main research question is now clearly answered by the research explained thus far.

Category	Performance Indicator	Status Quo CVD	Electrochemical CO2 reduction	Unit
Technical performance	RI	2.2	4.1	t_precursor/t_MWCNT
	Electric Utility EE	11	194.1	GJ/t
	Hear Utility EE	-6.5	0.7	GJ/t
	Overall EE	4.5	194.8	GJ/t
Economic Performance	TCI	125.6	118.7	Million Euros
	OPEX	66.7	87.6	Million Euros
	NPV	0.76	0.53	Billion Euros
	PBP	1.62	1.25	Years
Environmental Performance (Climate Change)	Scope 1 impact - absolute	73.9	2.2	Million Tonnes CO2 eq
	Scope 2 impact - absolute	8.6	8.5	Million Tonnes CO2 eq
	Scope 1 and 2 impact - net	92.5	-9.6	Million Tonnes CO2 eq
	Avoided Impact	none	-20.3	Million Tonnes CO2 eq

Figure 8.1: Performance indicator comparison

In regard to the "how does it compare" part of the main research question, the comparative technical, economic, and environmental indicators of both processes are summarised in Fig. 8.1. It can be observed that the CVD process performs better than the electrochemical process in most technical and economic performance indicators except TCI. However, the electrochemical process performs significantly better than the CVD process on all the climate change-based environmental performance indicators.

Further advancements in the technical and economic performance of the electrochemical process could help it realistically outperform the status quo CVD process. Ultimately, the techno-economic and environmental viability of such CO_2 based process for MWCNT production can help valorise the CO_2 streams and drive its large-scale removal mainly from the industrial flue gas emissions and potentially from the atmosphere, thereby helping decrease global warming and decelerate climate change.

References

Access Intelligence. (2023). The Chemical Engineering Plant Cost Index. Retrieved July 29, 2023, from https://www.chemengonline.com/pci-home/

Agboola, A. (2005). Development and model formulation of scalable carbon nanotube processes: HiPCO and CoMoCAT process models. *LSU Master's Theses*. https://doi.org/10.31390/gradschool_theses.1635

Agboola, A. E., Pike, R. W., Hertwig, T. A., & Lou, H. H. (2007). Conceptual design of carbon nanotube processes. *Clean Technologies and Environmental Policy*, *9*(4), 289–311. https://doi.org/10.1007/s10098-006-0083-2

Alibaba. (2023). Industrial Grade Multi Walled Carbon Nanotubes Powder Price Mwcnts - Buy Multi Walled Carbon Nanotubes Powder,Carbon Nanotubes Powder,Carbon Nanotubes Product on Alibaba.com. Retrieved August 8, 2023, from https://www.alibaba.com/product-detail/Industrial-Grade-Multi-Walled-Carbon-Nanotubes_1600261135010.html

Azevedo, M., Magdalena Baczyńska, Ken Hoffman, & Aleksandra Krauze. (2022). How lithium mining is fueling the EV revolution | McKinsey. Retrieved June 20, 2023, from https://www.mckinsey.com/industries/metals-and-mining/our-insights/lithium-mining-how-new-production-technologies-could-fuel-the-global-ev-revolution

Azonano. (2020). Using Waste to Cost-Effectively Produce Graphene [Section: Nanotechnology Article]. Retrieved May 19, 2023, from https://www.azonano.com/article.aspx?ArticleID=5589

Baik, S., Park, J. H., & Lee, J. W. (2020). One-pot conversion of carbon dioxide to CNT-grafted graphene bifunctional for sulfur cathode and thin interlayer of Li–S battery. *Electrochimica Acta*, *330*, 135264. https://doi.org/10.1016/j.electacta.2019.135264

Bhatia, P., Ranganathan, J., & Development (WBCSD), W. B. C. f. S. (2004). *The Greenhouse Gas Protocol*. Retrieved July 30, 2023, from https://www.wri.org/research/greenhouse-gas-protocol-0

Bleu, Y., Bourquard, F., Tite, T., Loir, A., Maddi, C., Donnet, C., & Garrelie, F. (2018). Review of Graphene Growth From a Solid Carbon Source by Pulsed Laser Deposition (PLD. *Frontiers in Chemistry*, *6*. https://doi.org/10.3389/fchem.2018.00572

Bos, J. F. F. P., Smit, A. (L., & Schröder, J. J. (2013). Is agricultural intensification in The Netherlands running up to its limits? *NJAS - Wageningen Journal of Life Sciences*, *66*, 65–73. https://doi.org/10.1016/j.njas.2013.06.001

Bromberg, L., Nitzsche, M. P., & Hatton, T. A. (2022). Capture and electrochemical conversion of CO2 in molten alkali metal borate–carbonate blends [Publisher: The Royal Society of Chemistry]. *Nanoscale*, *14*(36), 13141–13154. https://doi.org/10.1039/D2NR03355K

Bronikowski, M. J., Willis, P. A., Colbert, D. T., Smith, K. A., & Smalley, R. E. (2001). Gas-phase production of carbon single-walled nanotubes from carbon monoxide via the HiPco process: A parametric study. *Journal of Vacuum Science & Technology A*, *19*(4), 1800–1805. https://doi.org/10.1116/1.1380721

Burgers, I. (2020). Novel Technology for Hydrogen Separation from Natural Gas using Pressure Swing Adsorption. Retrieved July 10, 2023, from https://repository.tudelft.nl/islandora/object/uuid%3Aa1ff79ef-2d91-4b57-a7e2-dcedeae2f8c3

Businesswire. (2023). Global Market for Carbon Nanotubes 2023-2033: Production Capacities to More than Double by 2025 Due to the Explosion in Demand from EV Battery Market - ResearchAndMarkets.com. Retrieved August 9, 2023, from https://www.businesswire.com/news/home/20230531005634/en/Global-Market-for-Carbon-Nanotubes-2023-2033-Production-Capacities-to-More-than-Double-by-2025-Due-to-the-Explosion-in-Demand-from-EV-Battery-Market---ResearchAndMarkets.com

Carlsson, J.-O., & Martin, P. M. (2010). Chapter 7 - Chemical Vapor Deposition. In P. M. Martin (Ed.), *Handbook of Deposition Technologies for Films and Coatings (Third Edition)* (pp. 314–363). William Andrew Publishing. https://doi.org/10.1016/B978-0-8155-2031-3.00007-7

Chakrabarti, A., Lu, J., Skrabutenas, J. C., Xu, T., Xiao, Z., Maguire, J. A., & Hosmane, N. S. (2011). Conversion of carbon dioxide to few-layer graphene [Publisher: The Royal Society of Chemistry]. *Journal of Materials Chemistry*, *21*(26), 9491–9493. https://doi.org/10.1039/C1JM11227A

Chang, L., Stacchiola, D. J., & Hu, Y. H. (2017). Direct conversion of CO2 to meso/macro-porous frameworks of surface-microporous graphene for efficient asymmetrical supercapacitors [Publisher: The Royal Society of Chemistry]. *Journal of Materials Chemistry A*, *5*(44), 23252–23258. https://doi.org/10.1039/C7TA07003A

Chemanalyst. (2021). Netherlands Carbon Nanotubes Market Analysis. Retrieved August 8, 2023, from https://secure.livechatinc.com/

Chemanalyst. (2023). H2 Price Trend and Forecast. Retrieved August 8, 2023, from https://secure.livechatinc.com/

Chen, J., Wei, S., & Xie, H. (2021). A Brief Introduction of Carbon Nanotubes: History, Synthesis, and Properties [Publisher: IOP Publishing]. *Journal of Physics: Conference Series*, *1948*(1), 012184. https://doi.org/10.1088/1742-6596/1948/1/012184

Chen, Y., Wang, M., Lu, S., Tu, J., & Jiao, S. (2020). Electrochemical graphitization conversion of CO2 through soluble NaVO3 homogeneous catalyst in carbonate molten salt. *Electrochimica Acta*, *331*, 135461. https://doi.org/10.1016/j.electacta.2019.135461

Chiang, I. W., Brinson, B. E., Huang, A. Y., Willis, P. A., Bronikowski, M. J., Margrave, J. L., Smalley, R. E., & Hauge, R. H. (2001). Purification and Characterization of Single-Wall Carbon Nanotubes (SWNTs) Obtained from the Gas-Phase Decomposition of CO (HiPco Process) [Publisher: American Chemical Society]. *The Journal of Physical Chemistry B*, *105*(35), 8297–8301. https://doi.org/10.1021/jp0114891

Choudhary, N., Hwang, S., & Choi, W. (2014). Carbon Nanomaterials: A Review. In B. Bhushan, D. Luo, S. R. Schricker, W. Sigmund, & S. Zauscher (Eds.), *Handbook of Nanomaterials Properties* (pp. 709–769). Springer. https://doi.org/10.1007/978-3-642-31107-9_37

Chungchamroenkit, P., Yanatatsaneejit, U., Kitiyanan, B., Scamehorn, J. F., & Resasco, D. E. (2004). Separation of Carbon Black from Silica by Froth Flotation Technique as an Approach for Single-Walled Carbon Nanotubes Purification.

Church, J. A., White, N. J., Aarup, T., Wilson, W. S., Woodworth, P. L., Domingues, C. M., Hunter, J. R., & Lambeck, K. (2008). Understanding global sea levels: Past, present and future. *Sustainability Science*, *3*(1), 9–22. https://doi.org/10.1007/s11625-008-0042-4

Coolbrook. (n.d.). Technology & Offering. Retrieved July 11, 2023, from https://coolbrook.com/technology/

Cunning, B. V., Pyle, D. S., Merritt, C. R., Brown, C. L., Webb, C. J., & Gray, E. M. A. (2014). Hydrogen adsorption characteristics of magnesium combustion derived graphene at 77 and 293 K. *International Journal of Hydrogen Energy*, *39*(12), 6783–6788. https://doi.org/10.1016/j.ijhydene.2014.02.054

de Kleijne, K., Hanssen, S. V., van Dinteren, L., Huijbregts, M. A. J., van Zelm, R., & de Coninck, H. (2022). Limits to Paris compatibility of CO2 capture and utilization. *One Earth*, *5*(2), 168–185. https://doi.org/10.1016/j.oneear.2022.01.006

Deng, B., Liu, Z., & Peng, H. (2019). Toward Mass Production of CVD Graphene Films [_eprint: https://onlinelibrary.wiley.com/doi/pdf/10.1002/adma.201800996]. *Advanced Materials*, *31*(9), 1800996. https://doi.org/10.1002/adma.201800996

Dimov, D., Amit, I., Gorrie, O., Barnes, M., Townsend, N., Neves, A., Withers, F., Russo, S., & Craciun, M. (2018). Ultrahigh Performance Nanoengineered Graphene-Concrete Composites for Multifunctional Applications. *Advanced Functional Materials*, *28*(23), 1705183. https://doi.org/10.1002/adfm.201705183

Douglas, A., & Pint, C. (2017). Review—Electrochemical Growth of Carbon Nanotubes and Graphene from Ambient Carbon Dioxide: Synergy with Conventional Gas-Phase Growth Mechanisms. *ECS Journal of Solid State Science and Technology*, *6*(6), 3084–3089. https://doi.org/10.1149/2.0131706jss

Douglas, A., Carter, R., Li, M., & Pint, C. L. (2018). Toward Small-Diameter Carbon Nanotubes Synthesized from Captured Carbon Dioxide: Critical Role of Catalyst Coarsening [Publisher: American Chemical Society]. *ACS Applied Materials & Interfaces*, *10*(22), 19010–19018. https://doi.org/10.1021/acsami.8b02834

Douglas, A., Carter, R., Muralidharan, N., Oakes, L., & Pint, C. L. (2017). Iron catalyzed growth of crystalline multi-walled carbon nanotubes from ambient carbon dioxide mediated by molten carbonates. *Carbon*, *116*, 572–578. https://doi.org/10.1016/j.carbon.2017.02.032

Douven, S., Pirard, S. L., Chan, F.-Y., Pirard, R., Heyen, G., & Pirard, J.-P. (2012). Large-scale synthesis of multi-walled carbon nanotubes in a continuous inclined mobile-bed rotating reactor by the catalytic chemical vapour deposition process using methane as carbon source. *Chemical Engineering Journal*, *188*, 113–125. https://doi.org/10.1016/j.cej.2012.01.110

Ecoinvent. (2017). Ecoinvent v3.4 - ecoinvent. Retrieved July 30, 2023, from https://ecoinvent.org/the-ecoinvent-database/data-releases/ecoinvent-3-4/

Eleanor Tanzer, S., & Ramírez, A. (2019). When are negative emissions negative emissions? [Publisher: Royal Society of Chemistry]. *Energy & Environmental Science*, *12*(4), 1210–1218. https://doi.org/10.1039/C8EE03338B

Esrafilzadeh, D., Zavabeti, A., Jalili, R., Atkin, P., Choi, J., Carey, B. J., Brkljača, R., O'Mullane, A. P., Dickey, M. D., Officer, D. L., MacFarlane, D. R., Daeneke, T., & Kalantar-Zadeh, K. (2019). Room temperature CO2 reduction to solid carbon species on liquid metals featuring atomically thin ceria interfaces [Number: 1 Publisher: Nature Publishing Group]. *Nature Communications*, *10*(1), 865. https://doi.org/10.1038/s41467-019-08824-8

Eurostat. (2023). Estimated hourly labour costs. Retrieved August 2, 2023, from https://ec.europa.eu/eurostat/statistics-explained/index.php?title=File:Estimated_hourly_labour_costs,_2022_(EUR).png

Faber, G., Mangin, C., & Sick, V. (2021). Life Cycle and Techno-Economic Assessment Templates for Emerging Carbon Management Technologies. *Frontiers in Sustainability*, *2*. Retrieved March 21, 2023, from https://www.frontiersin.org/articles/10.3389/frsus.2021.764057

Farmand, M., Jahanpeyma, F., Gholaminejad, A., Azimzadeh, M., Malaei, F., & Shoaie, N. (2022). Carbon nanostructures: A comprehensive review of potential applications and toxic effects. *3 Biotech*, *12*(8), 159. https://doi.org/10.1007/s13205-022-03175-6

Fortune Business Insights. (2022). Graphene Market Size, Growth, Share | Research Report [2029]. Retrieved June 6, 2023, from https://www.fortunebusinessinsights.com/graphene-market-102930

Gasunie. (2023). Hydrogen quality for the Dutch network. Retrieved August 8, 2023, from https://www.gasunie.nl/en/expertise/hydrogen/hydrogen-and-industry/hydrogen-quality-for-the-dutch-network

Giannakopoulou, T., Todorova, N., Plakantonaki, N., Vagenas, M., Papailias, I., Sakellis, E., & Trapalis, C. (2022). CO2 metallothermic conversion to valuable nanocarbons by mixed Mg/Ca reductant. *Journal of CO2 Utilization*, *65*, 102200. https://doi.org/10.1016/j.jcou.2022.102200

Global Market Insights. (2023). Carbon Nanotubes Market Share & Size | Forecast Report – 2032. Retrieved June 6, 2023, from https://www.gminsights.com/industry-analysis/carbon-nanotubes-market

Gong, P., Tang, C., Wang, B., Xiao, T., Zhu, H., Li, Q., & Sun, Z. (2022). Precise CO2 Reduction for Bilayer Graphene [Publisher: American Chemical Society]. *ACS Central Science*, *8*(3), 394–401. https://doi.org/10.1021/acscentsci.1c01578

Guinée, J. B. (2002). *Handbook on Life Cycle Assessment: Operational Guide to the ISO Standards* [Google-Books-ID: Q1VYuV5vc8UC]. Springer Science & Business Media.

Hong, G., Diao, S., Antaris, A. L., & Dai, H. (2015). Carbon Nanomaterials for Biological Imaging and Nanomedicinal Therapy [Publisher: American Chemical Society]. *Chemical Reviews*, *115*(19), 10816–10906. https://doi.org/10.1021/acs.chemrev.5b00008

Hong, W. (2022). A techno-economic review on carbon capture, utilisation and storage systems for achieving a net-zero CO2 emissions future. *Carbon Capture Science & Technology*, *3*, 100044. https://doi.org/10.1016/j.ccst.2022.100044

Hu, L., Song, Y., Ge, J., Zhu, J., Han, Z., & Jiao, S. (2017). Electrochemical deposition of carbon nanotubes from CO2 in CaCl2–NaCl-based melts [Publisher: The Royal Society of Chemistry]. *Journal of Materials Chemistry A*, *5*(13), 6219–6225. https://doi.org/10.1039/C7TA00258K

Hu, L., Song, Y., Jiao, S., Liu, Y., Ge, J., Jiao, H., Zhu, J., Wang, J., Zhu, H., & Fray, D. J. (2016). Direct Conversion of Greenhouse Gas CO2 into Graphene via Molten Salts Electrolysis [Publisher: John Wiley & Sons, Ltd]. *ChemSusChem*, *9*(6), 588–594. https://doi.org/10.1002/cssc.201501591

Hu, L., Yang, W., Yang, Z., & Xu, J. (2019). Fabrication of graphite via electrochemical conversion of CO2 in a CaCl2 based molten salt at a relatively low temperature [Publisher: The Royal Society of Chemistry]. *RSC Advances*, *9*(15), 8585–8593. https://doi.org/10.1039/C8RA10560J

Huntsman. (n.d.). Surfonic-L-24-7.-TDS..pdf. Retrieved July 10, 2023, from https://monsonco.com/wp-content/uploads/2019/08/Surfonic-L-24-7.-TDS..pdf

IEA. (2019). Putting CO2 to Use – Analysis. Retrieved July 1, 2023, from https://www.iea.org/reports/putting-co2-to-use

IEA. (2021). Is carbon capture too expensive? – Analysis. Retrieved May 21, 2023, from https://www.iea.org/commentaries/is-carbon-capture-too-expensive

Ijije, H. V., Sun, C., & Chen, G. Z. (2014). Indirect electrochemical reduction of carbon dioxide to carbon nanopowders in molten alkali carbonates: Process variables and product properties. *Carbon*, *73*, 163–174. https://doi.org/10.1016/j.carbon.2014.02.052

ISO. (2014). ISO 14040:2006. Retrieved July 30, 2023, from https://www.iso.org/standard/37456.html

Jain, N., Gupta, E., & Kanu, N. (2021). Plethora of Carbon Nanotubes Applications in Various Fields – A State-of-the-Art-Review. *Smart Science*, *10*(1), 1–24. https://doi.org/10.1080/23080477.2021.1940752

Jiang, M., Li, Z., Yu, Y., Wu, H., Li, W., Ji, D., Liu, Y., He, Z., & Zhang, Z. (2017). Efficient Conversion of Greenhouse Gas of CO2 into Carbon Products with Desirable Structures via Molten Carbonates Electrolysis [Publisher: IOP Publishing]. *Journal of The Electrochemical Society*, *164*(14), D1022. https://doi.org/10.1149/2.1561714jes

Jo, C., Mun, Y., Lee, J., Lim, E., Kim, S., & Lee, J. (2019). Carbon dioxide to solid carbon at the surface of iron nanoparticle: Hollow nanocarbons for sodium ion battery anode application. *Journal of CO2 Utilization*, *34*, 588–595. https://doi.org/10.1016/j.jcou.2019.08.003

Joore, P., & Brezet, H. (2015). A Multilevel Design Model: The mutual relationship between product-service system development and societal change processes. *Journal of Cleaner Production*, *97*, 92–105. https://doi.org/10.1016/j.jclepro.2014.06.043

Kamkeng, A., Wang, M., Hu, J., Du, W., & Qian, F. (2021). Transformation technologies for CO2 utilisation: Current status, challenges and future prospects. *Chemical Engineering Journal*, *409*, 128138. https://doi.org/10.1016/j.cej.2020.128138

Kim, G. M., Choi, W. Y., Park, J. H., Jeong, S. J., Hong, J.-E., Jung, W., & Lee, J. W. (2020). Electrically Conductive Oxidation-Resistant Boron-Coated Carbon Nanotubes Derived from Atmospheric CO2 for Use at High Temperature [Publisher: American Chemical Society]. *ACS Applied Nano Materials*, *3*(9), 8592–8597. https://doi.org/10.1021/acsanm.0c01909

Kim, G. M., Lim, W.-G., Kang, D., Park, J. H., Lee, H., Lee, J., & Lee, J. W. (2020). Transformation of carbon dioxide into carbon nanotubes for enhanced ion transport and energy storage [Publisher: The Royal Society of Chemistry]. *Nanoscale*, *12*(14), 7822–7833. https://doi.org/10.1039/C9NR10552B

Kirchherr, J., Reike, D., & Hekkert, M. (2017). Conceptualizing the circular economy: An analysis of 114 definitions. *Resources, Conservation and Recycling*, *127*, 221–232. https://doi.org/10.1016/j.resconrec.2017.09.005

Kumar, M. (2011). Carbon Nanotube Synthesis and Growth Mechanism. In *Carbon Nanotubes - Synthesis, Characterization, Applications*. IntechOpen. https://doi.org/10.5772/19331

Kumar, M., & Ando, Y. (2010). Chemical Vapor Deposition of Carbon Nanotubes: A Review on Growth Mechanism and Mass Production. *Journal of Nanoscience and Nanotechnology*, *10*(6), 3739–3758. https://doi.org/10.1166/jnn.2010.2939

Lertrojanachusit, N., Pornsunthorntawee, O., Kitiyanan, B., Chavadej, J., & Chavadej, S. (2013). Separation and purification of carbon nanotubes using froth flotation with three

sequential pretreatment steps of catalyst oxidation, catalyst removal, and silica dissolution [_eprint: https://onlinelibrary.wiley.com/doi/pdf/10.1002/apj.1727]. *Asia-Pacific Journal of Chemical Engineering*, *8*(6), 830–842. https://doi.org/10.1002/apj.1727

Li, C., Zhang, X., Wang, K., Su, F., Chen, C.-M., Liu, F., Wu, Z.-S., & Ma, Y. (2021). Recent advances in carbon nanostructures prepared from carbon dioxide for high-performance supercapacitors. *Journal of Energy Chemistry*, *54*, 352–367. https://doi.org/10.1016/j.jechem.2020.05.058

Li, C., Zhang, X., Wang, K., Sun, X., Liu, G., Li, J., Tian, H., Li, J., & Ma, Y. (2017). Scalable Self-Propagating High-Temperature Synthesis of Graphene for Supercapacitors with Superior Power Density and Cyclic Stability [_eprint: https://onlinelibrary.wiley.com/doi/pdf/10.1002/adma.201604690]. *Advanced Materials*, *29*(7), 1604690. https://doi.org/10.1002/adma.201604690

Li, X., Shi, H., Wang, X., Hu, X., Xu, C., & Shao, W. (2022a). Direct synthesis and modification of graphene in Mg melt by converting CO2: A novel route to achieve high strength and stiffness in graphene/Mg composites. *Carbon*, *186*, 632–643. https://doi.org/10.1016/j.carbon.2021.10.017

Li, X., Shi, H., Wang, X., Hu, X., Xu, C., & Shao, W. (2022b). Direct synthesis of graphene by blowing CO2 bubble in Mg melt for the seawater/oil pollution. *Journal of Alloys and Compounds*, *921*, 165938. https://doi.org/10.1016/j.jallcom.2022.165938

Li, Z., Yu, Y., Li, W., Wang, G., Peng, L., Li, J., Gu, D., Yuan, D., & Wu, H. (2018). Carbon dioxide electrolysis and carbon deposition in alkaline-earth-carbonate-included molten salts electrolyzer [Publisher: The Royal Society of Chemistry]. *New Journal of Chemistry*, *42*(19), 15663–15670. https://doi.org/10.1039/C8NJ02965B

Liu, S., Jin, Y., Bae, J.-S., Chen, Z., Dong, P., Zhao, S., & Li, R. (2020). CO2 derived nanoporous carbons for carbon capture. *Microporous and Mesoporous Materials*, *305*, 110356. https://doi.org/10.1016/j.micromeso.2020.110356

Liu, X., Licht, G., Wang, X., & Licht, S. (2022). Controlled Growth of Unusual Nanocarbon Allotropes by Molten Electrolysis of CO2 [Number: 2 Publisher: Multidisciplinary Digital Publishing Institute]. *Catalysts*, *12*(2), 125. https://doi.org/10.3390/catal12020125

LM Plus. (n.d.). Developing Unique Liquid Metal Based Technology. Retrieved December 21, 2022, from https://lmplus.com.au/

Luo, B., Liu, H., Jiang, L., Jiang, L., Geng, D., Wu, B., Hu, W., Liu, Y., & Yu, G. (2013). Synthesis and morphology transformation of single-crystal graphene domains based on activated carbon dioxide by chemical vapor deposition [Publisher: The Royal Society of Chemistry]. *Journal of Materials Chemistry C*, *1*(17), 2990–2995. https://doi.org/10.1039/C3TC30124A

Made-in-China. (2023). Lithium Ion Battery Material Multi Walled Carbon Nanotubes. Retrieved August 9, 2023, from https://f69fe4bdad5cc81f.en.made-in-china.com/product/HQMRPYeKhhVk/China-Lithium-Ion-Battery-Material-Multi-Walled-Carbon-Nanotubes.html

Maduraiveeran, G., & Jin, W. (2021). Carbon nanomaterials: Synthesis, properties and applications in electrochemical sensors and energy conversion systems. *Materials Science and Engineering: B*, *272*, 115341. https://doi.org/10.1016/j.mseb.2021.115341

Manchester, U. (n.d.). Applications - Graphene. https://www.graphene.manchester.ac.uk/learn/applications/

Mason, H. (2020). Graphene 101: Forms, properties and applications. Retrieved July 7, 2023, from https://www.compositesworld.com/articles/graphene-101-forms-properties-and-applications

Methanex. (2023). Methanol Pricing. Retrieved May 21, 2023, from https://www.methanex.com/about-methanol/pricing/

Methanol Institute. (2023). The Methanol Industry. Retrieved August 9, 2023, from https://www.methanol.org/the-methanol-industry/

Modekwe, H. U., Olaitan Ayeleru, O., Onu, M. A., Tobias, N. T., Mamo, M. A., Moothi, K., Daramolad, M. O., & Olubambi, P. A. (2020). The Current Market for Carbon Nanotube Materials and Products. In J. Abraham, S. Thomas, & N. Kalarikkal (Eds.), *Handbook of Carbon Nanotubes* (pp. 1–15). Springer International Publishing. https://doi.org/10.1007/978-3-319-70614-6_73-1

Molina-Jirón, C., Chellali, M. R., Kumar, C. N. S., Kübel, C., Velasco, L., Hahn, H., Moreno-Pineda, E., & Ruben, M. (2019). Direct Conversion of CO2 to Multi-Layer Graphene using Cu–Pd Alloys [_eprint: https://onlinelibrary.wiley.com/doi/pdf/10.1002/cssc.201901404]. *ChemSusChem*, *12*(15), 3509–3514. https://doi.org/10.1002/cssc.201901404

Mortazavi, S. Z., Novinrooz, A. J., Reyhani, A., & Mirershadi, S. (2010). Effects of acid treatment duration and sulfuric acid molarity on purification of multi-walled carbon nanotubes. *Central European Journal of Physics*, *8*(6), 940–946. https://doi.org/10.2478/s11534-010-0017-9

Mubarak, N. M., Abdullah, E. C., Jayakumar, N. S., & Sahu, J. N. (2014). An overview on methods for the production of carbon nanotubes. *Journal of Industrial and Engineering Chemistry*, *20*(4), 1186–1197. https://doi.org/10.1016/j.jiec.2013.09.001

Mutlu, Ö. Ç., & Zeng, T. (2020). Challenges and Opportunities of Modeling Biomass Gasification in Aspen Plus: A Review [_eprint: https://onlinelibrary.wiley.com/doi/pdf/10.1002/ceat.202000068]. *Chemical Engineering & Technology*, *43*(9), 1674–1689. https://doi.org/10.1002/ceat.202000068

NANOCYL. (n.d.). NANOCYL NC700. Retrieved July 7, 2023, from https://www.nanocyl.com/product/

Nganglumpoon, R., Watmanee, S., Teerawatananond, T., Pinthong, P., Poolboon, K., Hongrutai, N., Tungasmita, D. N., Tungasmita, S., Boonyongmaneerat, Y., Jantaping, N., Wannapaiboon, S., Praserthdam, P., Morikawa, Y., Goodwin, J. G., & Panpranot, J. (2022). Growing 3D-nanostructured carbon allotropes from CO2 at room temperature under the dynamic CO2 electrochemical reduction environment. *Carbon*, *187*, 241–255. https://doi.org/10.1016/j.carbon.2021.11.011

NOGEPA. (2008). *Potential for CO2 storage in depleted gas fields on the Netherlands Continental Shelf* (tech. rep.). Netherlands Oil, Gas Exploration, and Production Association. Retrieved June 28, 2023, from https://www.nlog.nl/sites/default/files/f353faea-f50f-4102-9803-fe16ce7062a0_dhv%20tno%20ccs%20offshore%20final%2030-06-08.pdf

Nyári, J., Magdeldin, M., Larmi, M., Järvinen, M., & Santasalo-Aarnio, A. (2020). Techno-economic barriers of an industrial-scale methanol CCU-plant. *Journal of CO2 Utilization*, *39*, 101166. https://doi.org/10.1016/j.jcou.2020.101166

OCSiAl. (2014). OCSiAl's world first: Capability for unlimited, low-cost production of Single Wall Carbon Nano. Retrieved May 19, 2023, from http://ocsial.com/news/-ocsials-

world-first-capability-for-unlimited-low-cost-production-of-single-wall-carbon-nanotubes-announced-at-institute-of-materials-/

Park, J. H., Yang, J., Kim, D., Gim, H., Choi, W. Y., & Lee, J. W. (2022). Review of recent technologies for transforming carbon dioxide to carbon materials. *Chemical Engineering Journal*, *427*, 130980. https://doi.org/10.1016/j.cej.2021.130980

Parry, E. J. (2007). The Greatest Threat To Global Security: Climate Change Is Not Merely An Environmental Problem [Publisher: United Nations]. Retrieved December 19, 2022, from https://www.un.org/en/chronicle/article/greatest-threat-global-security-climate-change-not-merely-environmental-problem

Patnaik, P. (2003). *Handbook of inorganic chemicals*. McGraw-Hill.

Peters, M. S., Timmerhaus, K. D., & West, R. E. (2003). *Plant Design and Economics for Chemical Engineers* [Google-Books-ID: yNZTAAAAMAAJ]. McGraw-Hill Education.

Pinthong, P., Phupaichitkun, S., Watmanee, S., Nganglumpoon, R., Tungasmita, D. N., Tungasmita, S., Boonyongmaneerat, Y., Promphet, N., Rodthongkum, N., & Panpranot, J. (2022). Room Temperature Nanographene Production via CO2 Electrochemical Reduction on the Electrodeposited Bi on Sn Substrate [Number: 19 Publisher: Multidisciplinary Digital Publishing Institute]. *Nanomaterials*, *12*(19), 3389. https://doi.org/10.3390/nano12193389

Pirard, S. L., Douven, S., & Pirard, J.-P. (2017). Large-scale industrial manufacturing of carbon nanotubes in a continuous inclined mobile-bed rotating reactor via the catalytic chemical vapor deposition process. *Frontiers of Chemical Science and Engineering*, *11*(2), 280–289. https://doi.org/10.1007/s11705-017-1635-1

Poh, H. L., Sofer, Z., Luxa, J., & Pumera, M. (2014). Transition Metal-Depleted Graphenes for Electrochemical Applications via Reduction of CO2 by Lithium [_eprint: https://onlinelibrary.wiley.com/doi/pdf/10.1002/smll.201303002]. *Small*, *10*(8), 1529–1535. https://doi.org/10.1002/smll.201303002

Pornsunthorntawee, O., Chuaybumrung, S., Kitiyanan, B., & Chavadej, S. (2011). Purification of Single-Walled Carbon Nanotubes (SWNTs) by Acid Leaching, NaOH Dissolution, and Froth Flotation [Publisher: Taylor & Francis _eprint: https://doi.org/10.1080/01496395.2011.585626]. *Separation Science and Technology*, *46*(13), 2056–2065. https://doi.org/10.1080/01496395.2011.585626

Porthos. (2021). CO2-specifications.pdf. Retrieved July 8, 2023, from https://www.porthosco2.nl/wp-content/uploads/2021/09/CO2-specifications.pdf

Porthos. (2023). Porthos. Retrieved June 28, 2023, from https://www.porthosco2.nl/en/project/

PWC. (2023). Netherlands - Corporate - Taxes on corporate income. Retrieved July 30, 2023, from https://taxsummaries.pwc.com/netherlands/corporate/taxes-on-corporate-income

Rafique, M. M. A., & Iqbal, J. (2011). Production of Carbon Nanotubes by Different Routes-A Review. *Journal of Encapsulation and Adsorption Sciences*, *01*(02), 29–34. https://doi.org/10.4236/jeas.2011.12004

Ratso, S., Walke, P. R., Mikli, V., Ločs, J., Šmits, K., Vītola, V., Šutka, A., & Kruusenberg, I. (2021). CO2 turned into a nitrogen doped carbon catalyst for fuel cells and metal–air battery applications [Publisher: The Royal Society of Chemistry]. *Green Chemistry*, *23*(12), 4435–4445. https://doi.org/10.1039/D1GC00659B

Remmel, A.-L., Ratso, S., Divitini, G., Danilson, M., Mikli, V., Uibu, M., Aruväli, J., & Kruusenberg, I. (2022). Nickel and Nitrogen-Doped Bifunctional ORR and HER Electrocatalysts

Derived from CO2 [Publisher: American Chemical Society]. *ACS Sustainable Chemistry & Engineering*, *10*(1), 134–145. https://doi.org/10.1021/acssuschemeng.1c05250

Ren, J., Johnson, M., Singhal, R., & Licht, S. (2017). Transformation of the greenhouse gas CO2 by molten electrolysis into a wide controlled selection of carbon nanotubes. *Journal of CO2 Utilization*, *18*, 335–344. https://doi.org/10.1016/j.jcou.2017.02.005

Resasco, D., Alvarez, W., Pompeo, F., Balzano, L., Herrera, J., Kitiyanan, B., & Borgna, A. (2002). A Scalable Process for Production of Single-walled Carbon Nanotubes (SWNTs) by Catalytic Disproportionation of CO on a Solid Catalyst. *Journal of Nanoparticle Research*, *4*(1), 131–136. https://doi.org/10.1023/A:1020174126542

Ritchie, H. (2020). Emissions by sector. Our World in Data. https://ourworldindata.org/emissions-by-sector#citation

Ruthven, D. M., Farooq, S., & Knaebel, K. S. (1993). Pressure Swing Adsorption | Wiley. Retrieved July 10, 2023, from https://www.wiley.com/en-nl/Pressure+Swing+Adsorption-p-9780471188186

Saconsint, S., Sae-tang, N., Srifa, A., Koo-Amornpattana, W., Assabumrungrat, S., Fukuhara, C., & Ratchahat, S. (2022). Development of high-performance nickel-based catalysts for production of hydrogen and carbon nanotubes from biogas [Number: 1 Publisher: Nature Publishing Group]. *Scientific Reports*, *12*(1), 15195. https://doi.org/10.1038/s41598-022-19638-y

Salomon's Metlanen B.V. (n.d.). Inconel Alloy 600. Retrieved August 2, 2023, from https://salomons-metalen.nl/datasheets/Alloy_600.pdf

Seekaew, Y., Tammanoon, N., Tuantranont, A., Lomas, T., Wisitsoraat, A., & Wongchoosuk, C. (2022). Conversion of Carbon Dioxide into Chemical Vapor Deposited Graphene with Controllable Number of Layers via Hydrogen Plasma Pre-Treatment [Number: 8 Publisher: Multidisciplinary Digital Publishing Institute]. *Membranes*, *12*(8), 796. https://doi.org/10.3390/membranes12080796

SkyNano. (n.d.). Home. Retrieved July 8, 2023, from https://www.skynanotechnologies.com

Spek, M. v. d., Ramirez, A., & Faaij, A. (2017). Challenges and uncertainties of ex ante techno-economic analysis of low TRL CO2 capture technology: Lessons from a case study of an NGCC with exhaust gas recycle and electric swing adsorption. *Applied Energy*, *208*, 920–934. https://doi.org/10.1016/j.apenergy.2017.09.058

Srininvasan, P. (2018). Carbon Budget and Cost Analysis of C2CNT: A Carbon Dioxide to Solid Carbon Conversion Process - ProQuest. Retrieved June 28, 2023, from https://www.proquest.com/openview/175d6fd919610c020f52e2108380c8a3/1?cbl=18750&pq-origsite=gscholar&parentSessionId=sbyxxkOdpXSFhr7k%2BtjucfgvZUqu9%2BiCaZ50qo5UNWQ%3D

Tang, J., Tang, J., Mayyas, M., Ghasemian, M., Sun, J., Rahim, M., Yang, J., Han, J., Lawes, D., Jalili, R., Daeneke, T., Saborio, M., Cao, Z., Echeverria, C., Allioux, F., Zavabeti, A., Hamilton, J., Mitchell, V., O'Mullane, A., & Kalantar-Zadeh, K. (2021). Liquid-Metal-Enabled Mechanical-Energy-Induced CO 2 Conversion. *Advanced Materials*, *34*(1), 2105789. https://doi.org/10.1002/adma.202105789

Terrones, M. (2003). Science and Technology of the Twenty-First Century: Synthesis, Properties, and Applications of Carbon Nanotubes [_eprint: https://doi.org/10.1146/annurev.matsci.33.012802.100255]. *Annual Review of Materials Research*, *33*(1), 419–501. https://doi.org/10.1146/annurev.matsci.33.012802.100255

Thomassen, G., Dael, M. V., Passel, S. V., & You, F. (2019). How to assess the potential of emerging green technologies? Towards a prospective environmental and techno-economic assessment framework [Publisher: The Royal Society of Chemistry]. *Green Chemistry*, *21*(18), 4868–4886. https://doi.org/10.1039/C9GC02223F

Towler, G., & Sinnott, R. K. (2012). *Chemical Engineering Design: Principles, Practice and Economics of Plant and Process Design* [Google-Books-ID: m6mLiGEGI7UC]. Elsevier.

TU Delft. (2022). RELEASE. Retrieved March 21, 2023, from https://www.tudelft.nl/innovatie-impact/innovation-projects/projects-2022/release

United Nations. (n.d.). Causes and Effects of Climate Change [Publisher: United Nations]. Retrieved December 19, 2022, from https://www.un.org/en/climatechange/science/causes-effects-climate-change

UpCatalyst. (n.d.). Technology. Retrieved December 19, 2022, from https://upcatalyst.com/technology/

Wang, C., Li, F., Qu, H., Wang, Y., Yi, X., Qiu, Y., Zou, Z., Luo, Y., & Yu, B. (2015). Fabrication of three dimensional carbon nanotube foam by direct conversion carbon dioxide and its application in supercapacitor. *Electrochimica Acta*, *158*, 35–41. https://doi.org/10.1016/j.electacta.2015.01.112

Wang, J., Ma, R., Zhou, Z., Liu, G., & Liu, Q. (2015). Magnesiothermic synthesis of sulfur-doped graphene as an efficient metal-free electrocatalyst for oxygen reduction [Number: 1 Publisher: Nature Publishing Group]. *Scientific Reports*, *5*(1), 9304. https://doi.org/10.1038/srep09304

Wang, P., Wang, M., & Lu, J. (2021). Electrochemical conversion of CO2 into value-added carbon with desirable structures via molten carbonates electrolysis [Publisher: The Royal Society of Chemistry]. *RSC Advances*, *11*(46), 28535–28541. https://doi.org/10.1039/D1RA03890G

Wang, X., & Song, C. (2020). Carbon Capture From Flue Gas and the Atmosphere: A Perspective. *Frontiers in Energy Research*, *8*. Retrieved October 9, 2022, from https://www.frontiersin.org/articles/10.3389/fenrg.2020.560849

Wang, X., Liu, X., Licht, G., & Licht, S. (2020). Calcium metaborate induced thin walled carbon nanotube syntheses from CO2 by molten carbonate electrolysis [Number: 1 Publisher: Nature Publishing Group]. *Scientific Reports*, *10*(1), 15146. https://doi.org/10.1038/s41598-020-71644-0

Wei, F., Zhang, Q., Qian, W.-Z., Yu, H., Wang, Y., Luo, G.-H., Xu, G.-H., & Wang, D.-Z. (2008). The mass production of carbon nanotubes using a nano-agglomerate fluidized bed reactor: A multiscale space–time analysis. *Powder Technology*, *183*(1), 10–20. https://doi.org/10.1016/j.powtec.2007.11.025

Wei, S., Shi, H., Li, X., Hu, X., Xu, C., & Wang, X. (2022). A green and efficient method for preparing graphene using CO2@Mg in-situ reaction and its application in high-performance lithium-ion batteries. *Journal of Alloys and Compounds*, *902*, 163700. https://doi.org/10.1016/j.jallcom.2022.163700

Wei, W., Stacchiola, D. J., & Hu, Y. H. (2017). 3D graphene from CO2 and K as an excellent counter electrode for dye-sensitized solar cells [_eprint: https://onlinelibrary.wiley.com/doi/pdf/10.1002/er.3815]. *International Journal of Energy Research*, *41*(15), 2502–2508. https://doi.org/10.1002/er.3815

Wei, W., Sun, K., & Hu, Y. H. (2014). Synthesis of 3D cauliflower-fungus-like graphene from CO2 as a highly efficient counter electrode material for dye-sensitized solar cells [Publisher: The Royal Society of Chemistry]. *Journal of Materials Chemistry A*, *2*(40), 16842–16846. https://doi.org/10.1039/C4TA03909B

Wei, W., Sun, K., & Hu, Y. H. (2016). Direct conversion of CO2 to 3D graphene and its excellent performance for dye-sensitized solar cells with 10% efficiency [Publisher: The Royal Society of Chemistry]. *Journal of Materials Chemistry A*, *4*(31), 12054–12057. https://doi.org/10.1039/C6TA04008J

Wei, W., Sun, K., & Hu, Y. H. (2017). Synthesis of Mesochannel Carbon Nanowall Material from CO2 and Its Excellent Performance for Perovskite Solar Cells [Publisher: American Chemical Society]. *Industrial & Engineering Chemistry Research*, *56*(7), 1803–1809. https://doi.org/10.1021/acs.iecr.6b04768

Wickramasinghe, S., Wang, J., Morsi, B., & Li, B. (2021). Carbon Dioxide Conversion to Nanomaterials: Methods, Applications, and Challenges. *Energy & Fuels*, *35*(15), 11820–11834. https://doi.org/10.1021/acs.energyfuels.1c01533

Xing, Z., Luo, X., Qi, Y., Stickle, W. F., Amine, K., Lu, J., & Ji, X. (2016). Nitrogen-Doped Nanoporous Graphenic Carbon: An Efficient Conducting Support for O2 Cathode [_eprint: https://onlinelibrary.wiley.com/doi/pdf/10.1002/cnma.201600112]. *ChemNanoMat*, *2*(7), 692–697. https://doi.org/10.1002/cnma.201600112

Xing, Z., Wang, B., Gao, W., Pan, C., Halsted, J. K., Chong, E. S., Lu, J., Wang, X., Luo, W., Chang, C.-H., Wen, Y., Ma, S., Amine, K., & Ji, X. (2015). Reducing CO2 to dense nanoporous graphene by Mg/Zn for high power electrochemical capacitors. *Nano Energy*, *11*, 600–610. https://doi.org/10.1016/j.nanoen.2014.11.011

Xu, C., Chen, P., Liu, K., Gao, X., & Du, L. (2019). CO2 Conversion into N-Doped Carbon Nanomesh Sheets [Publisher: American Chemical Society]. *ACS Applied Nano Materials*, *2*(5), 2991–2998. https://doi.org/10.1021/acsanm.9b00377

Xu, C., Chen, S., Du, L., Li, C., Gao, X., Liu, J., Qu, L., & Chen, P. (2018). Scalable Conversion of CO2 to N-Doped Carbon Foam for Efficient Oxygen Reduction Reaction and Lithium Storage [Publisher: American Chemical Society]. *ACS Sustainable Chemistry & Engineering*, *6*(3), 3358–3366. https://doi.org/10.1021/acssuschemeng.7b03542

Yianatos, J., Bergh, L., Tello, K., Díaz, F., & Villanueva, A. (2008). Froth mean residence time measurement in industrial flotation cells. *Minerals Engineering*, *21*(12), 982–988. https://doi.org/10.1016/j.mineng.2008.05.004

Zhou, J., Jiang, S., Li, Y., Pan, Z., Qian, Y., Zhao, Y., Lin, N., & Qian, Y. (2020). Chemical fixation of CO2 on activated Si: Producing graphitic carbon-stabilized Si particles for Li-storage. *Energy Storage Materials*, *31*, 36–43. https://doi.org/10.1016/j.ensm.2020.06.006

Zhu, Z. (2017). An Overview of Carbon Nanotubes and Graphene for Biosensing Applications. *Nano-Micro Letters*, *9*(3), 25. https://doi.org/10.1007/s40820-017-0128-6

Zimmermann, A. W., Buchner, G. A., & Schomäcker, R. (2021). Apples and Apples: A Shortcut Assessment Framework for Early-Stage Carbon Capture and Utilization Technologies Based on Efficiency, Feasibility, and Risk [_eprint: https://onlinelibrary.wiley.com/doi/pdf/10.1002/ente.202000691]. *Energy Technology*, *9*(2), 2000691. https://doi.org/10.1002/ente.202000691

Zimmermann, A. W., Wunderlich, J., Müller, L., Buchner, G. A., Marxen, A., Michailos, S., Armstrong, K., Naims, H., McCord, S., Styring, P., Sick, V., & Schomäcker, R. (2020).

Techno-Economic Assessment Guidelines for CO2 Utilization. *Frontiers in Energy Research*, *8*. Retrieved March 15, 2023, from https://www.frontiersin.org/articles/10.3389/fenrg.2020.00005

Zuraiqi, K., Zavabeti, A., Clarke-Hannaford, J., Murdoch, B. J., Shah, K., Spencer, M. J. S., McConville, C. F., Daeneke, T., & Chiang, K. (2022). Direct conversion of CO2 to solid carbon by Ga-based liquid metals [Publisher: The Royal Society of Chemistry]. *Energy & Environmental Science*, *15*(2), 595–600. https://doi.org/10.1039/D1EE03283F

A

CO_2 to CNM processes

Check the supplementary spreadsheet file at : https://drive.google.com/drive/folders/1SMQeQ7t-LTmpRzafImeQ5o6cBtVwEQxW

Study Title	Research group	Author	Type	Material Produced & Quality	Temperature
Capture and electrochemical conversion of CO2 in molten alkali metal borate–carbonate blend		Bromberg et al. , 2022	Electrochemical	Multiwall Carbon nanotube (10-16 graphene layers, diameter ~15.5nm)	550–600 °C
Electrochemical graphitization conversion of CO2 through soluble NaVO3 homogeneous catalyst in		Chen et al.,2020	Electrochemical	CNT (diameter 100-200nm) with 3-10 layers, and carbon sheets of 7 layers	800°C
Iron catalyzed growth of crystalline multi-walled carbon nanotubes from ambient carbon dioxide	Douglas and Pint	Douglas et al., 2017b	Electrochemical	Multiwalled CNT (diameter - 27.5nm)	750°C
Toward Small-Diameter Carbon Nanotubes Synthesized from Captured Carbon Dioxide: Critical	Douglas and Pint	Douglas et al., 2018	Electrochemical	MWCNT (~33/23nm median diameters, 10nm smallest diameter)	750C
Electrochemical Deposition of Carbon Prepared on Cu and Ni Cathodes in CaCl2-LiCl Melts		Ge et al., 2017	Electrochemical	quasi-spherical carbon, carbon tubes, large carbon plates, multi walled	600°C
Electrochemical deposition of carbon nanotubes from CO2 in CaCl2–NaCl-based melts	Liwen Hu group	Hu et al.,2017	Electrochemical	Quasi spheres, carbon nanosheets/graphitsheets, hollow multi walled CNTs	650°C, 750°C
Fabrication of graphite via electrochemical conversion of CO2 in a CaCl2 based molten salt at a	Liwen Hu group	Hu et al.,2019	Electrochemical	Graphite nanostructures and Multi Walled CNT	725°C
Carbon nanotube wools made directly from CO2 by molten electrolysis: Value driven pathways to	Licht group	Johnson et al., 2017	Electrochemical	Long, wool like CNT(95% purity and 0.4–1.2 mm long,0.5 to 1.5 µm diameter	770°C
Carbon Nanotubes Produced from Ambient Carbon Dioxide for Environmentally Sustainable	Licht group	Licht et al.,2016	Electrochemical	straight CNT(diameter 50-400 nm) and tangled CNT (50-350nm) and CNF	750°C
Controlled Transition Metal Nucleated Growth of Carbon Nanotubes by Molten Electrolysis of CO2	Licht group	Liu et al., 2022a	Electrochemical	CNT as straight, curled or thin from 10 to 100 µm, 25-98% purity	770°C
Controlled Growth of Unusual Nanocarbon Allotropes by Molten Electrolysis of CO2	Licht group	Liu et al., 2022b	Electrochemical	regular CNT, nano-bamboo,,graphitic carbon, conical carbon nanofiber,	770°C
Efficient Conversion of Greenhouse Gas of CO2 into Carbon Products with Desirable Structures via	Zhida Li and	M. Jiang et al., 2017	Electrochemical	MWCNT (100-500nm), honeycomb like carbon and carbon spheres	750°C
Electrochemical conversion of CO2 into value-added carbon with desirable structures via molten		P. Wang et al., 2022	Electrochemical	CNT, Carbon Spheres, Honeycomb carbon	500-800
Nickel and Nitrogen-Doped Bifunctional ORR and HER Electrocatalysts Derived from CO2	Ivar kruusenberg	Remmel et al., 2022	Electrochemical	Bamboo shaped Ni and N doped CNTs	540°C
Transformation of the greenhouse gas CO2 by molten electrolysis into a wide controlled selection	Licht group	Ren et al., 2017	Electrochemical	Boron doped MWCNT (150 nm to 1.5 µm)	770°C
Calcium metaborate induced thin walled carbon nanotube syntheses from CO2 by molten	Licht group	X. Wang et al., 2020	Electrochemical	thin walled uniforms CNT (22-42nm diameter) having ~25 concentric	770°C
CO2 Utilization by Electrolytic Splitting to Carbon Nanotubes in Non-Lithiated, Cost-Effective,	Licht group	X. Wang et al., 2022	Electrochemical	80-90% Multi walled CNT, Carbon nano onions and carbon platelets	700-800°C
A novel route to synthesize carbon spheres and carbon nanotubes from carbon dioxide in a	Zhida Li and	Z. Li et al., 2017	Electrochemical	CNTs(50-200 nm diameter) and Carbon spheres	750°C
Carbon Nanotubes Synthesis from CO2 Based on the Molten Salts Electrochemistry: Effect of	Zhida Li and	Z. Li et al., 2019	Electrochemical	hollow multi walled CNT(~300 layers) thicker diameter(200-400nm)	750°C

Figure A.1: Snapshot of the compiled CNT-producing molten salt based electrochemical processes from the excel spreadsheet

B

CVD Modelling Data

Check the supplementary spreadsheet file at : https://drive.google.com/drive/folders/1SMQeQ7t-LTmpRzafImeQ5o6cBtVwEQxW

ID	File Name	Description	Related Source
B1	Operating Conditions	Data from various sources used throughout the process for various process untis are calculated and complied	Mainly Douven et al, 2012
B2	Calculations	The calculations for some of the process unit data and the scaling factors are inclcuded in this sheet	Based on operating conditions data
B3	Equipment Sizing	Equipment sizing calculations that are incorporated into the Aspen Economic Energy Analyzer for equpment calculations	Based on operating conditions data
B4	Equipment Costs	Equipment costs as obtained from Aspen and from other sources for modelling the various equipment considered in this process	APEA
B5	Capex & Opex	Total CAPEX, OPEX and NPV value calculations for the study	APEA and Aspen
B6	Mass Balance	Mass Balance calculated based on the total inflows and outflows of the model based on data retrieved from Aspen	Aspen
B7	Energy Balance and Utilities	Energy Balance and total net utilites required calculated based on the energy flows between various equipment used in the model	Aspen
B8	Streams	Stream Data complied from the aspen model	Aspen

Figure B.1: Appendix B Spreadsheet file contents

C

Electrochemical CO_2 Reduction Modelling Data

Check the supplementary spreadsheet file at : https://drive.google.com/drive/folders/1SMQeQ7t-LTmpRzafImeQ5o6cBtVwEQxW

ID	File Name	Description	Related Source
C1	C2CNT model	Data from the scaled up version of molten salt based CO2 electrochemical reduction process by Stuart Licht's research	Sriniνasan (2008)
C2	Operational Data	Data from the electrochemical molten salt processes that yielded thin diameter MWCNT comparable to the status quo. The data from this process was also scaled to the	Douglas (2018) and Douglas (2017)
C3	Modelling Conditions	The complete modelling condition with respect to the materials and energy used for modelling the process on	Data from C1 and C2
C4	Equipment Costs	Equipment costs as obtained from Aspen and from other sources for modelling the various equipment considered in	APEA
C5	Capex & Opex	Total CAPEX, OPEX and NPV value calculations for the study	APEA and Aspen
C6	Mass Balance	Mass Balance calculated based on the total inflows and outflows of the model based on data retrieved from Aspen	Aspen
C7	Energy Balance and Utilities	Energy Balance and total net utilites required calculated based on the energy flows between various equipment used	Aspen
C8	Stream Data	Stream data compiled from the aspen model	Aspen

Figure C.1: Appendix C spreadsheet file contents

D

Results and Graphing Calculations

Check the supplementary spreadsheet file at : https://drive.google.com/drive/folders/1SMQeQ7t-LTmpRzafImeQ5o6cBtVwEQxW

ID	File Name	Description	Related Source
D1	CVD Energy by Equipment type	Energy consumption by equipments of various types	Appendix B
D2	CO2 Energy by equipment type	Energy consumption by equipments of various types	Appendix C
D3	Resource Efficiency	Primary feedstocks consumed per unit final product produced	Appendix B and Appendix C
D4	Energy Efficiency	Energy consumed per unit product produced	Appendix B and Appendix C
D5	Equipment Cost by type	Equipment cost breakdown of both the processes	Appendix B and Appendix C
D6	Operational Costs	Operational cost breakdown	Appendix B and Appendix C
D7	LCA CVD Documentation	Documentation of the LCA for CVD process along with the comparison with results CO2 based process	LCA files
D8	LCA CO2 based Documentation	Documentation of the LCA for CO2 based process	LCA files
D9	LCA CVD Inventory results	The inventory results from the LCA files of CVD process	LCA files
D10	LCA CO2 based Inventory Results	The inventory results from the LCA files of CO2 based process	LCA files

Figure D.1: Appendix D spreadsheet file contents

E

Process Stream Mass Compositions

	Units	FS-AIR1	FS-AIR2	FS-CA	FS-CAT	FS-CH4	FS-DW	FS-H2SO4	FS-HYD	FS-NG	FS-NISUR	PS-CNT	PS-H2REC	WS-ACID	WS-AIR	WS-CO2AR	WS-DW	WS-FLUG	WS-H2	WS-H2O	WS-PURGE
Total Mass Flows	**kg/hr**	**1976**	**1**	**13115**	**122**	**1947**	**302**	**652**	**25**	**600**	**2617**	**625**	**283**	**2658**	**34**	**2132**	**917**	**13715**	**0**	**85**	**907**
METHANE	kg/hr	0	0	0	0	1373	0	0	0	423	0	0	0	0	0	0	0	0	0	0	329
H2	kg/hr	0	0	0	0	0	0	0	25	0	0	0	283	0	0	0	0	0	0	0	4
C	kg/hr	0	0	0	0	0	0	0	0	0	0	625	0	0	0	0	0	0	0	0	0
ETHANE	kg/hr	0	0	0	0	95	0	0	0	29	0	0	0	0	0	0	0	0	0	0	95
PROPANE	kg/hr	0	0	0	0	9	0	0	0	3	0	0	0	0	0	0	0	0	0	0	9
CO2	kg/hr	0	0	0	0	46	0	0	0	14	0	0	0	0	0	573	0	1269	0	0	46
O2	kg/hr	460	0	3055	0	0	0	0	0	0	0	0	0	0	0	44	0	1248	0	0	0
N2	kg/hr	1516	1	10060	0	424	0	0	0	131	0	0	0	0	1	1516	0	10191	0	0	424
MGO	kg/hr	0	0	0	85	0	0	0	0	0	0	0	0	0	0	0	0	0	0	0	0
NI	kg/hr	0	0	0	18	0	0	0	0	0	0	0	0	0	15	0	0	0	0	0	0
MO	kg/hr	0	0	0	18	0	0	0	0	0	0	0	0	0	18	0	0	0	0	0	0
CO	kg/hr	0	0	0	0	0	0	0	0	0	0	0	0	0	0	0	0	0	0	0	0
AC	kg/hr	0	0	0	0	0	0	0	0	0	0	0	0	0	0	0	0	0	0	0	0
H2O	kg/hr	0	0	0	0	0	0	437	0	0	2011	0	0	2362	0	0	99	1007	0	25	0
H2SO4	kg/hr	0	0	0	0	0	0	215	0	0	0	0	0	1	0	0	0	0	0	0	0
MGSO4	kg/hr	0	0	0	0	0	0	0	0	0	0	0	0	255	0	0	0	0	0	0	0
NISO4	kg/hr	0	0	0	0	0	0	0	0	0	0	0	0	10	0	0	0	0	0	0	0
DW	kg/hr	0	0	0	0	0	302	0	0	0	0	0	0	0	0	0	242	0	0	60	0
SURF	kg/hr	0	0	0	0	0	0	0	0	0	606	0	0	30	0	0	576	0	0	0	0
PG	kg/hr	0	0	0	0	0	0	0	0	0	0	0	0	0	0	0	0	0	0	0	0
N2O	kg/hr	0	0	0	0	0	0	0	0	0	0	0	0	0	0	0	0	0	0	0	0
NO2	kg/hr	0	0	0	0	0	0	0	0	0	0	0	0	0	0	0	0	0	0	0	0
NO	kg/hr	0	0	0	0	0	0	0	0	0	0	0	0	0	0	0	0	0	0	0	0

Figure E.1: Composition of feed streams, product streams and waste streams - Status Quo CVD process

	Units	FS-ACID1	FS-CO2	FS-DI	FS-ELEC2	FS-H2O	PS-CNTFP	WS-ACID1	WS-DW	WS-GAS	WS-H2O	WS-O	WS-VAPOF
Mass Flows	kg/hr	127.0	2610.0	312.0	31.3	5500.0	625.4	112.7	277.8	17.4	5500.0	1984.6	62.4
CO2	kg/hr	0.0	2546.1	0.0	0.0	0.0	0.0	1.6	0.4	16.6	0.0	254.6	0.0
H2O	kg/hr	85.2	0.1	0.0	0.0	5500.0	0.0	73.6	18.4	0.8	5500.0	0.1	0.0
H2	kg/hr	0.0	0.9	0.0	0.0	0.0	0.0	0.0	0.0	0.0	0.0	0.9	0.0
N2	kg/hr	0.0	40.8	0.0	0.0	0.0	0.0	0.0	0.0	0.0	0.0	40.8	0.0
AR	kg/hr	0.0	9.7	0.0	0.0	0.0	0.0	0.0	0.0	0.0	0.0	9.7	0.0
CH4	kg/hr	0.0	9.7	0.0	0.0	0.0	0.0	0.0	0.0	0.0	0.0	9.7	0.0
CO	kg/hr	0.0	1.3	0.0	0.0	0.0	0.0	0.0	0.0	0.0	0.0	1.3	0.0
O2	kg/hr	0.0	0.1	0.0	0.0	0.0	0.0	0.0	0.0	0.0	0.0	1666.2	0.0
ETHANOL	kg/hr	0.0	0.1	0.0	0.0	0.0	0.0	0.0	0.0	0.0	0.0	0.1	0.0
METHANO	kg/hr	0.0	1.2	0.0	0.0	0.0	0.0	0.0	0.0	0.0	0.0	1.2	0.0
C	kg/hr	0.0	0.0	0.0	0.0	0.0	625.4	0.0	0.0	0.0	0.0	0.0	0.0
H2SO4	kg/hr	41.8	0.0	0.0	0.0	0.0	0.0	0.2	0.1	0.0	0.0	0.0	0.0
LI2CO3	kg/hr	0.0	0.0	0.0	31.3	0.0	0.0	0.0	0.0	0.0	0.0	0.0	0.0
LI2SO4	kg/hr	0.0	0.0	0.0	0.0	0.0	0.0	37.2	9.3	0.0	0.0	0.0	0.0
DW	kg/hr	0.0	0.0	312.0	0.0	0.0	0.0	0.0	249.6	0.0	0.0	0.0	62.4
PG	kg/hr	0.0	0.0	0.0	0.0	0.0	0.0	0.0	0.0	0.0	0.0	0.0	0.0

Figure E.2: Composition of feed streams, product streams and waste streams - Electrochemcial CO_2 Reduction process

F

Discounted Cash Flow spreadsheets

Year	0.00	1.00	2.00	3.00	4.00	5.00	6.00	7.00	8.00	9.00	10.00	11.00	12.00	13.00	14.00	15.00	16.00	17.00	18.00	19.00	20.00
Fixed Capital Investment (Euros)	106431098.91																				
Total Capital Investment (Euros)	125588696.72																				
Total Operational Costs (Euros)		66682057.84	66682057.84	66682057.84	66682057.84	66682057.84	66682057.84	66682057.84	66682057.84	66682057.84	66682057.84	66682057.84	66682057.84	66682057.84	66682057.84	66682057.84	66682057.84	66682057.84	66682057.84	66682057.84	66682057.84
Additional Replacement Costs (Euros): CVD Reactor replacement assumed every 10 years	0.00	0.00	0.00	0.00	0.00	0.00	0.00	0.00	0.00	0.00	13391920.41	0.00	0.00	0.00	0.00	0.00	0.00	0.00	0.00	0.00	13391920.41
Total Revenue (Euros)		199820792.35	199820792.35	199820792.35	199820792.35	199820792.35	199820792.35	199820792.35	199820792.35	199820792.35	199820792.35	199820792.35	199820792.35	199820792.35	199820792.35	199820792.35	199820792.35	199820792.35	199820792.35	199820792.35	199820792.35
Gross Profit(Euros)	0.00	133138734.50	133138734.50	133138734.50	133138734.50	133138734.50	133138734.50	133138734.50	133138734.50	133138734.50	119746814.09	133138734.50	133138734.50	133138734.50	133138734.50	133138734.50	133138734.50	133138734.50	133138734.50	133138734.50	119746814.09
MACRS Depreciation Rate (%)		20.00%	32.00%	19.20%	11.52%	11.52%	5.76%	0%	0%	0%	0%	0%	0%	0%	0%	0%	0%	0%	0%	0%	0%
Depreciation Charge (Euros)	0.00	21286219.78	34057951.65	20434770.99	12260862.59	12260862.59	6130431.30	0.00	0.00	0.00	0.00	0.00	0.00	0.00	0.00	0.00	0.00	0.00	0.00	0.00	0.00
Taxable Income (Euros)	0.00	111852514.72	99080782.85	112703963.51	120877871.91	120877871.91	127008303.21	133138734.50	133138734.50	133138734.50	119746814.09	133138734.50	133138734.50	133138734.50	133138734.50	133138734.50	133138734.50	133138734.50	133138734.50	133138734.50	119746814.09
Tax Rate (%)	25.80%	25.80%	25.80%	25.80%	25.80%	25.80%	25.80%	25.80%	25.80%	25.80%	25.80%	25.80%	25.80%	25.80%	25.80%	25.80%	25.80%	25.80%	25.80%	25.80%	25.80%
Taxes Paid (Euros)	0.00	0.00	28857948.80	25562841.98	29077622.59	31186490.95	31186490.95	32768142.23	34349793.50	34349793.50	34349793.50	30894678.04	34349793.50	34349793.50	34349793.50	34349793.50	34349793.50	34349793.50	34349793.50	34349793.50	34349793.50
Cash Flow (Euros)	-125588696.72	133138734.50	104280785.71	107575892.53	104061111.92	101952243.55	101952243.55	100370592.28	98788941.00	98788941.00	85397020.59	102244056.47	98788941.00	98788941.00	98788941.00	98788941.00	98788941.00	98788941.00	98788941.00	98788941.00	85397020.59
Discount Factor	1.00	0.91	0.83	0.75	0.68	0.62	0.56	0.51	0.47	0.42	0.39	0.35	0.32	0.29	0.26	0.24	0.22	0.20	0.18	0.16	0.15
Present Value of Cash flow (Euros)	-125588696.72	121035213.19	86182467.53	80823360.28	71075139.62	63304321.95	57549383.60	51505984.26	46085770.06	41896154.60	32924248.23	35835918.05	31477201.05	28615637.32	26014215.75	23649287.04	21499351.86	19544865.32	17768059.39	16152781.26	12693722.96
Net Present Value - NPV (Euros)	**760044386.58**																				
NPV (in Billion Euros)	**0.76**																				
Average Annual Cash Flow (after tax) in Euros	**100712955.6**																				
Payback period (after tax) in years	**1.25**																				

Figure F.1: Discounted cash flow spreadsheet of status quo CVD process

Year	0.00	1.00	2.00	3.00	4.00	5.00	6.00	7.00	8.00	9.00	10.00	11.00	12.00	13.00	14.00	15.00	16.00	17.00	18.00	19.00	20.00
Fixed Capital Investment (Euros)	100692068.59																				
Total Capital Investment (Euros)	118816640.93																				
Total Operational Costs (Euros)	0.00	87592209.66	87592209.66	87592209.66	87592209.66	87592209.66	87592209.66	87592209.66	87592209.66	87592209.66	87592209.66	87592209.66	87592209.66	87592209.66	87592209.66	87592209.66	87592209.66	87592209.66	87592209.66	87592209.66	87592209.66
Replacement Costs (Euros): Annual Cathode replacement 5 year Anode replacement		38298.00	38298.00	38298.00	38298.00	5010955.20	38298.00	38298.00	38298.00	38298.00	5010955.2	38298.00	38298.00	38298.00	38298.00	5010955.20	38298.00	38298.00	38298.00	38298.00	5010955.20
Total Revenue (Euros)	0.00	184000000.00	184000000.00	184000000.00	184000000.00	184000000.00	184000000.00	184000000.00	184000000.00	184000000.00	184000000.00	184000000.00	184000000.00	184000000.00	184000000.00	184000000.00	184000000.00	184000000.00	184000000.00	184000000.00	184000000.00
Gross Profit(Euros)	0.00	96369492.34	96369492.34	96369492.34	96369492.34	91396835.14	96369492.34	96369492.34	96369492.34	96369492.34	91396835.14	96369492.34	96369492.34	96369492.34	96369492.34	91396835.14	96369492.34	96369492.34	96369492.34	96369492.34	91396835.14
MACRS Depreciation Rate (%)		20.00%	32.00%	19.20%	11.52%	11.52%	5.76%	0%	0%	0%	0%	0%	0%	0%	0%	0%	0%	0%	0%	0%	0%
Depreciation Charge (Euros)	0.00	20138413.72	32221461.95	19332877.17	11599726.30	11599726.30	5799863.15	0.00	0.00	0.00	0.00	0.00	0.00	0.00	0.00	0.00	0.00	0.00	0.00	0.00	0.00
Taxable Income (Euros)	0.00	76231078.62	64148030.39	77036615.17	84769766.03	79797108.83	90569629.19	96369492.34	96369492.34	96369492.34	91396835.14	96369492.34	96369492.34	96369492.34	96369492.34	91396835.14	96369492.34	96369492.34	96369492.34	96369492.34	91396835.14
Tax Rate (%)	25.80%	25.80%	25.80%	25.80%	25.80%	25.80%	25.80%	25.80%	25.80%	25.80%	25.80%	25.80%	25.80%	25.80%	25.80%	25.80%	25.80%	25.80%	25.80%	25.80%	25.80%
Taxes Paid (Euros)	0.00	0.00	19667618.28	16550191.84	19875446.71	21870599.64	20587654.08	23366964.33	24863329.02	24863329.02	24863329.02	23580383.47	24863329.02	24863329.02	24863329.02	24863329.02	23580383.47	24863329.02	24863329.02	24863329.02	24863329.02
Cash Flow (Euros)	-118816640.93	96369492.34	76701874.05	79819300.50	76494045.62	69526235.50	75781838.26	73002528.01	71506163.31	71506163.31	66533506.11	72789108.87	71506163.31	71506163.31	71506163.31	66533506.11	72789108.87	71506163.31	71506163.31	71506163.31	66533506.11
Discount Factor	1.00	0.91	0.83	0.75	0.68	0.62	0.56	0.51	0.47	0.42	0.39	0.35	0.32	0.29	0.26	0.24	0.22	0.20	0.18	0.16	0.15
Present Value of Cash flow (Euros)	-118816640.93	87608629.40	63389978.56	59969421.86	52246462.42	43170322.13	42776872.07	37461839.90	33358152.92	30325593.56	25651546.80	25512138.61	22784067.29	20712788.44	18829807.68	15927592.38	15841030.86	14147113.21	12861012.00	11691829.10	9889781.73
Net Present Value - NPV (Euros)	**525339339.97**																				
NPV (in Billion Euros)	**0.53**																				
Average Annual Cash Flow (after tax) in Euros	**73246167.84**																				
Payback period (after tax) in years	**1.62**																				

Figure F.2: Discounted cash flow spreadsheet of electrochemical CO_2 reduction process